Mathematical modeling of MHC Class II mediated immune responses in tissues

by

Wen Zhou

A dissertation submitted to the graduate faculty

in partial fulfillment of the requirements for the degree of

DOCTOR OF PHILOSOPHY

Major: Applied Mathematics

Program of Study Committee:
Bo Su, Co-major Professor
Paul Sacks, Co-major Professor
Douglas Jones
Gary Lieberman
Steven Hou

Iowa State University

Ames, Iowa

2010

DEDICATION

To my parents, my wife Linxing, and our beloved daughter Michelle.

TABLE OF CONTENTS

LIST OF TABLES

LIST OF FIGURES

ABSTRACT

In this thesis, we developed a spatial-temporal mathematical model to capture fundamental aspects of MHC Class II mediated immune responses, which plays an essential role in protecting the host from a broad range of pathogens. To capture its essential mechanisms, we have considered terms that broadly describe intercellular communication, cell movement, and effector function (activation or inhibition). By defining the pathogen based on the associated antigens±Pathogen Associated Molecular Patterns (PAMPs), a framework to model phenotypic characteristics of pathogens is introduced. It includes the initial dose, distribution at infection site, secretion rate of associated soluble antigens, replication rate of particulate antigens, resistance of an antigen to be effectively processed by immune agents and capacity of intracellular antigens.

The model can account for antigen recognition, an innate immune response, an adaptive immune response, and the elimination of antigen and subsequent resolution of the immune response against an acute infection or equilibrium of the immune response to the presence of persistent antigen (chronic infection). The model is robust to variation in pathogen loads and types. We demonstrate, using numerical simulations that the model can successfully respond to broad classes of pathogens. Challenged by the *in silico* pathogens, our model mimics different immunobiological scenarios: a highly skewed T_H1 response is generated against some virtual pathogens (e.g. those modeled after *Mycobacterium tuberculosis*, *Leishmania major* etc.) and granuloma formation is observed, other virtual pathogens lead to an unskewed or mixed response (e.g. such as *Leishmania mexicana* etc.) and some virtual pathogens lead to a T_H1 to T_H2 switch (modeled after *M. avium paratuberculosis*), and a T_H2 responses is generated against sole extracellular pathogens (e.g. parasitic worms such as *nippostrongylus*

etc.).

Based on the model, we propose testable predictions and hypothesis to explain the critical immunobiological phenomena, such as T_H1 and T_H2 switch in mycobacteria infections.

CHAPTER 1. Introduction

1.1 General biological background on the human immune system

The purpose of the immune system is to defend the host from diseases under continual bombardment of microorganisms. The immune system is commonly visualized as a network that involves different players interacting with each other. The actions executed by the immune agents against foreign pathogens are defined as the immune responses. The immune system can be categorized into a physical barrier, innate immune system and adaptive immune system, according to the order of the line of defense. Each subsystem consists of certain immune agents and generates corresponding responses.

Skin and mucous membranes (mucosal epithelia) form the physical barrier, as the first defense line, which covers an area of approximately 400 m^2 and commits to prevent physical invasion [78]. Innate immunity serves as the next line of defense against the pathogens breaching the physical barrier. It has two constituents: the complement system, composed of twenty different proteins, and professional phagocytes (e.g., macrophages and neutrophils). During innate immune responses, the system eliminates foreign invaders indiscriminately in a very efficient way; in the meanwhile, cytokines (like chemokines) are released by phagocytes to recruit and guide the responsive cells, such as T cells and antigen presenting cells, in reinforcing the system.

In contrast to the innate immunity, the adaptive immune system is mediated by lymphocytes bearing highly diverse antigen-specific receptors, so that it can adapt to protect the system against any foreign antigens. Activated by antigen presenting cells (APCs), lymphocytes proliferate and differentiate quickly. The mature antigen-specific lymphocytes regulate the immune systems at both the infection site and lymphoid organs by releasing certain cy-

tokines (such as IL-2, IL-4, etc. [78]). Not only can the adaptive immune response promote pathogen elimination, it also generates memory lymphocytes and antibodies to offer a more rapid and efficient response upon any reinfection.

The central concept of the adaptive immune system is antigen recognition and presentation. T cells (also called T lymphocytes) and B-cells (also called B lymphocytes) are the manager cells of the adaptive immune system; they manage the system to fight against the identified pathogens in an efficient way. To identify the pathogens, T cells and B cells recognize antigens using different molecules to recognize the associated antigens. B cells fulfill the recognition of free antigens by B cell receptors related to the immunoglobulins (BCR). In contrast, T cell receptors (TCR) only recognize antigens displayed on APCs' surfaces, those peptides are delivered to the cell surface by host-cell glycoproteins, the major histocompatibility complex (MHC molecules). According to the structural and functional differences, the two classes of MHC molecules are classified: MHC Class I and MHC Class II. MHC Class II binds to peptides derived from proteins degraded in endocytic vesicles. In other words, MHC Class II molecules function as billboards used to advertise what is happening outside of the cells. MHC Class II is inspected by helper T cells, which are usually referred to as $CD4^+$ T cells. $CD4^+$ T cells are specialized in activating other immune effector cells, for example, they "help" B cells and macrophages. T cells, therefore, are crucial for both the humoral and cell-mediated adaptive immunities. The functions of $CD4^+$ T cells are related to all infectious diseases, such as tuberculosis [78]. $CD4^+$ T cells also play a central role in defending the host against viruses and building up immunological memory [78]. Thus, deeper understandings of the mechanics of the MHC Class II mediated immune responses are crucial in understanding how $CD4^+$ T cells function in adaptive immune responses, such as the differentiation of $CD4^+$ to the subsets of T_H1 and T_H2 [32, 91, 113, 208]. Understanding of MHC Class II mediated immune responses also offers opportunities to better understand the immunobiological phenomena, for example, the switch of immune responses in *M. avium paratuberculosis* infections [65, 187, 200]. Furthermore, exploration of MHC Class II mediate immune responses also provides new perspectives on designing vaccines for tuberculosis, or on designing treatments against

infectious diseases, like AIDS [156, 157, 159, 170].

1.2 Abstract of MHC Class II mediated immune responses

MHC Class II mediated immune responses towards a pathogen are a complex adaptive system that can be readily summarized conceptually through decomposition into the initiation, effector function, regulation and resolution [78, 183, 204]. Once initiated, a successful immune response must be used to balance the pro-inflammatory destructive actions of the immune effector cells with the protection of organ function. This balance becomes particularly critical when battling pathogens that manage to persist, despite the recognition by and stimulation of the immune system (chronic infections). The immune response continues until the foreign antigen is eliminated, contained, or tolerated; alternatively, the host may become overwhelmed.

Initial phagocyte activation leads to the accumulation of chemokines. Directed by the gradient of chemokine, the attraction of immune cells can, in turn, induce the adaptive immune response through the antigen presentation by APC and the activation of helper T cells ($CD4^+$ T cells). Both dendritic cells (DCs) and B cells can act as APCs, even though they function in different manners. For example, DCs transport between the infection sites and the lymphoid organs (lymph nodes) as biological sensors. In contrast, as alternative APCs, B cells dwell in the lymph nodes to detect the presence of antigens by immunoglobulins. Through the recognition of foreign antigens, different immune functions can be combined with the single mission of protecting the host. It is clear that helper T cells ($CD4^+$ T cells) promote cell-mediated immunity that is primarily defined by macrophage activation, and/or B cell response that is characterized by high antibody production. Their helper functions are defined by the $CD4^+$ secreting cytokines. In the process, a third subset of T cells, regulatory T cells, manage an alternative regulatory pathway to limit the immune response and avoid unlimited inflammation during chronic infection.

Particularly, in the MHC Class II mediated immune responses, the means to T cell skewing remain open to debate [203], with many theories proposed. These theories range from DC subtypes [78] to stochastic-instructive mechanisms [78] to spatial influences [78] to some that

propose that the $CD4^+$ T cell function is determined primarily by the characteristics of the antigen itself [205, 206]. Although the exact mechanisms of T cell skewing remains unknown, the T cell effector response is still believed to be critically important in determining downstream immune functions. The cross-regulation of helper T cell differentiation further our understanding of the dynamics of $CD4^+$ T cell differentiation [52, 53, 54]. In summary, the maturation of the adaptive immune response to any particular pathogen is subject to antigen recognition via T cell-APCs interaction. This macrophage response is directed, in part, by T cell effector functions and B cell-antibody dynamics.

1.3 Mathematical modeling on the immune system

1.3.1 Brief history

A large number of immunological discoveries on the course of infectious diseases have emerged since the late 1960s. Fundamental results relate to the mechanisms of pathogen-immune system interactions at different levels of considerations [78]. These results, followed by newer immunological phenomena, stimulate the application of mathematical models to study immune responses.

Early studies primarily focused on the idiotypic networks of B cells and their antibodies. The work of Hege and Cole [70] described the dynamics of the number of antibodies with respect to the population of plasma cells by differential equations. This study is considered to be one of the first in the field of mathematical immunology. In 1970, Jilek [84, 85, 86, 87] proposed the first series of probabilistic models to study the interaction of antigens with B cells and the subsequent clonal formation by the Monte-Carlo method. Clonal selection and humoral immunity against both monovalent and multivalent antigens were studied by Bell [14, 15, 16, 17] using a discrete predator-prey model in the 1970s. In 1975, some efforts [24] were devoted to modeling the humoral immune reaction to study the heterogeneity of immunocompetent cell populations as functions of antibody affinity and time. Motivated by Jerne [79, 80], Richter [168] and Hoffmann [74] original models of immune systems from the point of view of the network in 1975. In 1977, Waltman [199] incorporated the concept

of threshold switching of B-lymphocytes in the model. At the same time, De Lisi published several papers [36, 37, 38, 39, 40] on the mechanisms of tumor growth in an organism resembling in essence of Bell's original model. Marchuk [115], in 1975, constructed a nonlinear delay differential equations model to study infectious disease by including the damage of target organs, instead of solely humoral immunity. Early partial differential equation models and pioneering works on optimal control problems in immune responses were studied by Perelson [153, 154]. Modeling immune responses in terms of catastrophe theory, on the other hand, is suggested and systematically formulated by Merrill [127, 128].

Along with the discovery and further understanding of T cells, the mathematical modeling of immune systems significantly increased, especially in the 1980s. Large numbers of models were proposed to study immunoregulation, the dynamics of idiotypic immune networks, the spatial organization of immune processes, and immune responses against infectious diseases [111, 114, 132, 145, 155, 157]. Since the beginning of the 1990s, more sophisticated mathematical models were presented; this diversity in models has been rising significantly.

Two complementary conceptions exist: the clonal theory of Brunet [25] and the network theory of Jerne [79]. Particularly, clonal theory visualizes the immune system as a set of large numbers of independent clones of particles interacting with antigens selectively. Based on these two conceptions, in the last 20 years, people have used discrete models, or agent-based models, on the basis of cellular automata, probabilistic models, ordinary differential equations, differential algebraic equations, delay differential equations, integro-differential equations and partial differential equations. These models are used to reveal the mechanism of immune system mathematically.

Considering that the primary goal of the immune system is the defense of the host against infections, the mathematical modeling of immune responses during infectious disease and the study of the mechanisms of viral and bacterial infections became the focus of the attention of both theoretical and experimental immunology in the last few decades. Besides the already mentioned difficulty of understanding the switch of T_H1 and T_H2 immunity during infections caused by mycobacteria, modeling immune responses during infectious disease faces many

conceptual difficulties [41, 62, 91, 102, 113, 151, 204, 208]. Nevertheless, many important works of modeling immune responses against certain type of pathogens have made significant progress since the 1980s, these include: the temporal dynamics of the immune system against HIV infections [143, 144, 156, 158]; the immune response against hepatitis B studied by [116, 152], against influenza as modeled by [22], against bacterial infections modeled by [93] and against parasitic infections by [1, 71]. Furthermore, granuloma formation and macrophage dynamics in tuberculosis were studied by [120, 149] and [119, 201], where the capacity of antigens in the infected immune cells was studied. Meanwhile, functions and cross-regulations of helper T cells were studied by computational models [12, 52] and analyzed systematically in [52, 53, 54]. The activation of B cells and its interaction with antibody dynamics were studied by [96, 154, 179]. The variable dynamics of vaccinations for infectious diseases were studied by [182]. Other mechanisms of immune responses in different contexts are studied by many authors such as [55, 61, 97, 117, 145] and [159, 157] (with the references therein).

1.3.2 Modeling principles and methodologies

As discussed previously, understanding the adaptive immunity is the key to revealing the mechanism of an immune response against all infectious diseases and certain types of cancer. More study on the dynamics of MHC Class II mediated immune response is key to understanding adaptive immunity. Our goal is to build a mathematical model identifying a minimal set of key immune factors that would recapitulate the pattern of MHC Class II mediated immunity to diverse pathogens, and use the model to provide testable hypotheses that could explaine immunobiological phenomena. To institute a simplistic model, we begin with the hypothesis that immune regulations are chemical threshold dependent [190] and the following four principles [90, 190, 207]:

1) The system is not reactive to the self via clonal deletion of self-reactive T and B cells,

2) The antigen load drives the immune activation through threshold functions,

3) The activation of T cells only happens in the confines of the secondary lymph nodes, and

4) The T_H1 v.s. T_H2 bifurcation is determined by the defined characteristics of the antigen that determines APC function.

Essential factors include: antigens (particulate, soluble, intracellular), immune cells, chemokines, and cytokines. The model consists of a system of partial differential equations used to model the behavior of most of the immune cells, antigens and chemicals; ODEs are used to model B cells, as we assume that they primarily dwell in the lymph nodes; and typical delay terms are used to model the proliferation of the helper T cells.

The MHC Class II mediated immune response follows a pattern of engagement with a foreign antigen: recognition, initiation, effector response, and resolution or converge to a new equilibrium.

The antigens to which the immune system responds are highly variable and determined by the type of pathogen that infects the host. However, in our desire to conceptually define the immune response in broad terms, we, in turn, have to define the pathogens and associated antigens broadly, with either soluble or insoluble antigens that exist either extracellularly or intracellularly. We have, therefore, introduced a generic intracellular antigen and a soluble antigen as variations to the particulate antigen (the insoluble antigen). In the model, soluble and particulate antigens, as well as secondary signals (such as pathogen associated molecular patterns or PAMPs), diffuse from the pathogen source. Intracellular antigens are then created as a result of the failure of processing/killing the engulfed antigens in the macrophages. The abundance of responsive neutrophils enables their rapid deployment and the early domination of the infection site, where they quickly reduce the amount of particulate antigen and establish an initial gradient of chemokine [141]. This provides a site of initiation for both innate immunity via neutrophils and macrophages and the opportunity to link to the adaptive immune response via APCs. Dendritic cells, one type of APCs in our model, uptake a variety of antigen information and activate upon antigen recognition, undergoes maturation, and migrates away from the chemokine source to the lymph nodes. In contrast, soluble antigens bypass the innate immune response, diffuse to the secondary lymphoid organ through the lymph and are directly recognized as foreign substances via the interaction with an antigen-specific B cell.

For simplicity, we model that antigen specific CD4$^+$ T cells activated through the innate immunity link via dendritic cells (DCs with particulate antigen peptide presented) are biased towards a T_H1 type immune response. In contrast once B cells are directly activated by the recognition of antigen, they activate CD4$^+$ T cells biased towards becoming T_H2 cells; so do the dendritic cells matured through recognizing immune complexes [18, 64]. Activated CD4$^+$ T cells, in turn, become sensitive to the chemokine gradient and migrate to the pathogen source [103, 125], they also fulfill their duty to promote B cell activation in the lymph nodes through co-stimulatory receptors [78, 183]. B cells, once activated, remain in the secondary lymphoid organ as either short-lived plasma B cells, the antibody producer, or as long-lived memory B cells [49]. Additionally, the present model mimics scenarios that the T cells provide cross-regulation during ongoing T cell activation [6, 20, 78].

Classically activated macrophages process additional particulate antigens and limit neutrophil-induced damage by blocking further neutrophil recruitment [7, 67]. Activated macrophages are less reckless than neutrophils, but they contribute to the pro-inflammatory environment that can damage the host in the long-run. To limit the damage, regulatory T cells are recruited to the site of the infection, where they produce inhibitory cytokines that can block the activation of macrophages and limit macrophage-induced tissue damage [6, 20]. Alternative activated macrophages increase the amount of intracellular antigens as a result of the decrease in immune efficiency, which leads to state transition of the immune system.

The boundary of our symmetric simulation area Ω serves as a surrogate for the lymph nodes. The fundamental equation governing the cell motion in either lymph or blood is the Keller-Segel equations [95]:

$$\begin{cases} \partial_t \rho + \mathrm{div}(\chi_\rho(\nabla c)\rho) = \mathrm{div}(D_\rho \nabla \rho) + R(\rho, c) \\ \partial_t c - \mathrm{div}(D_c \nabla c) = g(\rho, c) \end{cases} \tag{1.1}$$

where $\rho(x,t)$ and $c(x,t)$ are density of organisms and concentration of chemoattractant respectively, and $(x,t) \in \Omega \times [0,\infty)$. In the model, reaction functions $R(\rho, c)$ and $g(\rho, c)$ are employed to model regulation and interactions among immune agents and antigens. Boundary condition will be specified for each immune agent according to its own functional mechanism

in the lymph nodes. Chemicals (proteins), including cytokines, antigens and antibodies, are modeled based on reaction-diffusion equations with the appropriate boundary conditions. To mimic a realistic mechanism of immune cells motion in *vivo*, the highly reticulated random structure of microvasculature must be taken into account. The concept of homogenization is therefore applied to estimate the diffusion and chemotaxis coefficients in the model [191, 193]. The numerical scheme [108] is designed to conduct the *in silico* experiments of the model.

1.4 Thesis Organization

The thesis is organized as follows. Chapter 2 is a detailed description of the MHC Class II mediated immune response model in tissue. In Chapter 3, we briefly discuss the numerical strategy used to solve the model proposed in Chapter 2. In Chapter 4, we conduct a series of numerical experiments to test our model: we justify the biological necessities of regulatory T cells, DCs, B cells and antibodies in the model, explore various phenotypic immune responses against different pathogens, and challenge the immune system by a typical *in silico* pathogen– *Mycobacterium avium subspecies paratuberculosis (Map)* to study the switch between T_H1-mediated and T_H2-mediated immune responses. In Chapter Five, we extend the discussion and summarize the model.

This thesis is primarily based on the published paper [190] and manuscripts under preparation: [90, 108, 207].

CHAPTER 2. The mathematical model

In this chapter, we will discuss our mathematical model of MHC Class mediated immune responses in details. All the state variables, with their biological meanings together, involved in the model are found in Table 2.1.

Table 2.1 State variables of the model

	Biological Meaning
A	particulate antigens± PAMPs
A_s	soluble antigens
A_p	intracellular antigens
IC	immune complexes
T_H1	effector T_H1 cells
T_H2	effector T_H2 cells
T_{reg}	regulatory T cells
DE	immature dendritic cells (DCs)
DA	mature DCs presenting particulate antigens± PAMPs
DF	mature DCs presenting immune complexes
B_a	activated B cells
B_p	plasma B cells
MR	resting macrophages
MA	generic activated macrophages
N	neutrophils
ND	apoptotic neutrophils
CM	cytokine secreted by activated macrophages engulfing apopotic neutrophils
$CT1$	T_H1 cell-released cytokine
$CT2$	T_H2 cell-released cytokine
CT_{reg}	regulatory T cell-released cytokine
CH	generic chemokine
F	generic antibody

Due to the large number of parameters, establishing consistent notation can be challenging. In the equations that follow, we have used α for replication or proliferation, β for secretion, δ

for regulation or modeling associated parameter, γ for activation, λ for uptake (process), μ for death/decay, ϵ for threshold parameters, χ for chemotaxis rate, and D for diffusion rate. $1_{\{\dots\}}$ is indicator function. The parameter subscripts are chosen to indicate which variable is affected by the parameter, so μ_N affects population of neutrophil. When more than one variable can affect another variable via the same mechanism, or when greater clarification is desired, the subscript $X|Y$ indicates variable X is affected via the action of Y. For example, $\lambda_{A|N}$ and $\lambda_{A|MA}$ are the uptake rates of particulate antigen± PAMPs by neutrophil and macrophage, respectively. As convention, the boundary of domain, which is the lymph node in our model, is denoted by $\partial\Omega$.

2.1 Pathogens and antigens

The immune system has developed specific Pattern Recognition Receptors (PRRs) to detect a broad range of ligands, termed Pathogen Associated Molecular Patterns (PAMPS), found on infectious agents [197]. For our broad model, a pathogen is defined as extracellular particulate antigen±PAMPs that is taken up by immune agents and become intracellular antigen, which may or may not secrete soluble antigen.

2.1.1 Particulate antigens

The immune system can recognize the pathogens through associated antigens±PMAPs by PRRs. PRRs are found on cells throughout the immune system but are best described on cells of the innate immune system, including neutrophils, macrophages and dendritic cells [3]. PAMPs include bacterial flagellin, lipopolysaccharide (LPS), bacterial DNA sequences, and double stranded RNA.

The immune system we model is a simplified version triggered only by particulate antigen (e.g. ovalbumin) and PAMP molecules (e.g. LPS). We assume that the particulate antigen and PAMP molecules share similar dynamics, degrading and replicating at the same constant rate μ_A and α_A respectively, diffusing at roughly the same rate D_A, as justified by the Stokes-Einstein equation [68], and consumed largely through the indiscriminate process of pinocytosis

by macrophages, neutrophils, and immature dendritic cells. Henceforth we treat both molecules as one substance, denoted by A, that satisfies the following reaction-diffusion equation, along with initial and boundary conditions.

$$\begin{cases} \dfrac{\partial A}{\partial t} = \overbrace{D_A \Delta A}^{\text{diffusion}} - \overbrace{A\Big(\lambda_{A|MR} MR + \lambda_{A|MA} MA + \lambda_{A|N} N + \lambda_{A|DE} DE + \lambda_{A|F} F\Big)}^{\text{pinocytosis by phagocytes or neutralized / opsonized by antibodies}} \\ \qquad + \underbrace{\alpha_A A}_{\text{replication}} + \underbrace{\Big(\kappa_{A|A_p} + \dfrac{MA \cdot \rho_{A_p|MA}}{\delta_{A_p} + A_p}\big(\mu_{MA} + \mu_{MA|A_p}\big)\Big) A_p}_{\text{from intracellular antigens}} - \underbrace{\mu_A A}_{\text{degradation}} \\ A(x,0) = A_0, \ \dfrac{\partial A}{\partial n}(\cdot, t)\Big|_{\partial\Omega} = 0. \end{cases} \tag{2.1}$$

In the equation (A.1), $\lambda_{A|MR}$, $\lambda_{A|MA}$, $\lambda_{A|N}$ and $\lambda_{A|DE}$ are the rates of antigen±PAMPs uptake through pinocytosis/phagocytosis by resting macrophages (MR), activated macrophages (MA), neutrophils (N) and immature dendritic cells (DE). $\lambda_{A|F}$ is the opsonizing/neutralizing rate of particulate antigen±PAMPs by antibodies. Macrophages engulf the antigen and must process it to achieve a successful immune response; however the probability of success is variable with respect to different pathogens. If the effort of processing an antigen fails, the antigen will become to an intracellular antigens and therefore not be processed by any other immune agents. Some intracellular antigens are released by the macrophage naturally in the rate of $\kappa_{A|A_p}$, which is assumed to be a constant for any particular pathogen based on the assumption that the cellular structure of macrophage is homogeneous compared with the immune system's scale (this number is set to be very small in simulation). Alternatively, intracellular antigens are released due to death of macrophages. In equation (A.1), $\rho_{A_p|MA}$ denotes the capacity of macrophage to hold particulate antigens, which is one of the pathogen characteristics depending on pathogen's pathological and structural attributes.

The initial input of particulate antigens is modeled by a function $A_0(x)$, which depends on the specific pattern of initial infections.

2.1.2 Intracellular antigens

To measure the success rate that macrophages processing antigen, the concept of immune efficiency [188] is needed and is denoted by the generic parameter $p^{\text{eff}}_{A_p|A}(IC, CT2)$ in the model.

Once engulfed by activated macrophages, for any specific type of pathogen, the associated particulate antigens have probability $1 - p^{\text{eff}}_{A_p|A}(IC, CT2)$ to survive in the form of intracellular antigen inside the macrophages. So, $p^{\text{eff}}_{A_p|A} = 1$ is corresponding to an acute infection, while $p^{\text{eff}}_{A_p|A} < 1$ is for chronic infections. The immune efficiency $p^{\text{eff}}_{A_p|A}(IC, CT2)$, which is macrophage-status dependent, is defined later by (2.10).

As a result of high affinity, the motion of intracellular antigen is dominated by the movement of the macrophage as we assume that their own motility is negligible compared with the scale of the macrophages' movement so that the diffusion and chemotaxis rate of intracellular antigen are as same as macrophage's. The third term in equation (2.2) models the production of intracellular antigens following a typical logistic manner due to the volume effect of their host [119, 201], which leads to the necessity to model capacity $\rho_{A_p|MA}$ and it is assumed to be a constant for any particular pathogens [4]. Furthermore, once alternative activation of macrophage is triggered, the replication ability of intracellular antigens will be changed [62, 118], and to capture this the growth rate of intracellular antigen is modeled on the basis of an indicator function in (2.3). The amount of T_H2 type cytokines or immune complexes overwhelming certain threshold is considered as signal to initiate alternative activation [62], and positive modeling parameter n_{A_p} is used to model the subsequent effect of alternative activation of activate macrophage on the self replication of intracellular antigens.

Intracellular antigens decay in the rate of μ_{A_p}. All of the containing intracellular antigens are released once the host activate macrophage is dead either due to natural death or bursting caused by overcrowding of intracellular antigens. Combining these factor, (2.4) is employed to model the lost of intracellular antigens in the system.

$$\begin{cases} \dfrac{\partial A_p}{\partial t} = \overbrace{D_{A_p}\Delta A_p}^{\text{effective diffusion}} - \overbrace{\nabla(\chi_{A_p}(A_p\nabla CH))}^{\text{effective transport}} + \overbrace{\alpha_{A_p}(CT_2, IC)A_p\Big(1 - \dfrac{A_p}{MA\cdot\rho_{A_p|MA}+1}\Big)}^{\text{self replication}} \\ \qquad + \underbrace{(1-p^{\text{eff}}_{A_p|A})(\lambda_{A|MA}A\cdot MA)1_{\{A_p<MA\cdot\rho_{A_p|MA}\}}}_{\text{unsuccessful processing and turn to intracellular antigens}} - \underbrace{f(\mu_{A_p}, MA, \kappa_{A_p|A}, A_p)}_{\text{lost of intracellular antigen}} \\ A_p(x,0) = 0,\ \dfrac{\partial A_p}{\partial n}(\cdot,t)\Big|_{\partial\Omega} = 0 \end{cases} \tag{2.2}$$

where $\int_\Omega u(x,t)dx$ is the total amount of u in Ω, growth and lost rate are modeled as

$$\alpha_{A_p}(CT_2, IC) = \alpha_{A_p} \cdot \left(1 + (n_{A_p} - 1)1_{\left\{\left\{\int_\Omega CT2(x,t)dx > \epsilon_{MA|TH2}\right\} \cup \left\{\int_\Omega IC(x,t)dx > \theta_{IC}\right\}\right\}}\right) \tag{2.3}$$

where α_{A_p} is a positive constant, and

$$f(\mu_{A_p}, MA, \kappa_{A_p|A}) := \mu_{A_p} + \kappa_{A|A_p} + MA\Big(\overbrace{\mu_{MA}\frac{\rho_{A_p|MA}A_p}{\delta_{A_p} + A_p}}^{\text{due to natural death}} + \overbrace{\rho_{A_p|MA}\frac{\mu_{MA|A_p}A_p}{\delta_{A_p} + A_p}}^{\text{due to bursting}}\Big). \tag{2.4}$$

2.1.3 Soluble antigens and immune complexes

In general, when compared with particulate or insoluble antigens, soluble antigens trigger immune responses mediated mainly by antibodies and B cells [78]. In our model, secreted by pathogens whose amount is modeled by total population of particulate antigens and intracellular antigens, soluble antigens rapidly diffuse in the lymph and tissues and quickly reach the lymph nodes. Soluble antigens are not recognized either by the receptors on professional phagocyte or by dendritic cells directly (unless they form immune complexes through binding with antibodies) [78]. However, they are readily recognized by B cell receptors (BCRs) and specific antibodies. Once recognizing free soluble antigens, antibodies bind soluble antigens to form stable immune complexes for the purpose of neutralization or opsonization. The immune complexes diffuse similarly to antibodies and soluble antigens in the tissues, and they are either processed by professional phagocytes to promote chemokines or carried by immature DCs to present MHC Class II to the lymphocytes, such as effector T cells or B cells, in the lymph nodes.

PDEs (2.5) and (2.6) are used to model soluble antigens A_s and immune complexes IC.

$$\begin{cases} \dfrac{\partial A_s}{\partial t} = \overbrace{D_{A_s}\Delta A_s}^{\text{diffusion}} - \overbrace{\mu_{A_s}A_s}^{\text{degradation}} + \overbrace{\beta_{A_s|A}A + \beta_{A_s|A_p}A_p}^{\text{secreted from pathogens}} - \overbrace{\lambda_{A_s|F}A_sF}^{\text{neutralized/opsonized by antibodies}} \\ A_s(\cdot, 0) = 0, \ \dfrac{\partial A_s}{\partial n}(\cdot, t)\Big|_{\partial\Omega} = 0. \end{cases} \tag{2.5}$$

$$
\begin{cases}
\dfrac{\partial IC}{\partial t} = \overbrace{D_{IC}\Delta IC}^{\text{diffusion}} - \overbrace{\mu_{IC} IC}^{\text{degradation}} - \overbrace{(\lambda_{IC|MA} MA + \lambda_{IC|DE} DE + \lambda_{IC|N} N) \cdot IC}^{\text{processed by professional phagocytes or immature DC}} \\
\qquad + \underbrace{(\lambda_{A_s|F} A_s + \lambda_{A|F} A) F}_{\text{formed through binding antibodies}} \\
IC(\cdot, 0) = 0, \ \dfrac{\partial IC}{\partial n}(\cdot, t)\Big|_{\partial\Omega} = 0.
\end{cases}
\tag{2.6}
$$

As we model the lymph node by the boundary of the domain, for simplicity, the boundary condition for antigens and immune complexes are set to satisfy the Neumann boundary condition for balancing flow. The dynamics of the different antigens within the model are summarized in figure 2.1.

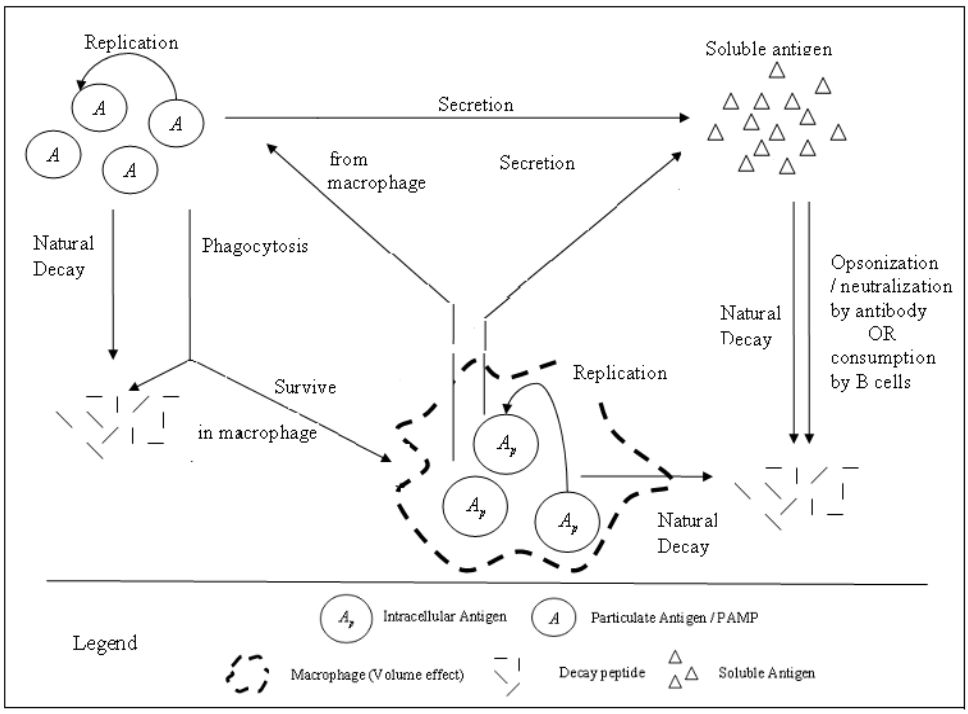

Figure 2.1 Schematic of the dynamics of antigens.

Finally, as a summary, we hypothesize that pathogen characteristics can be used to identify certain pathogens and mimic and approximate their behaviors, and we define pathogen characteristics in our model as following:

Definition 2.1.1. (Pathogen characteristics) The generic parameters: self replication rate α_A (or α_{A_p}), secretion rate of soluble antigen by pathogen $\beta_{A_s|A}$ (or $\alpha_{A_s|A_p}$), survivability during immune responses $1 - p^{\text{eff}}_{A_p|A}$ (complementary to immune efficiency), capacity of intracellular antigens in activated macrophage $\rho_{A_p|MA}$; and initial infection dose, are called pathogen characteristics.

2.2 Professional Phagocytes

Two types of professional phagocytes are studied in our model: neutrophils, denoted by N, are the major component during innate immunity, and macrophages, denoted by MR and MA, are the major professional phagocyte for adaptive immunity, particularly, the MHC Class II mediated immune responses.

2.2.1 Neutrophil

Neutrophils, denoted by N, constitute 40% $\sim$ 70% of the white blood cells in the blood stream [19]. They respond early to threats against the host by detecting changes in the vascular endothelium induced by tissue damage and/or infection [78]. Neutrophils, and other immune cells, initially approach the source of antigen through the microvascular system that extends into the tissue. Once activated by changes in the vascular endothelium, neutrophils exit the microvasculature and move through the tissue by sensing molecules, or chemokines, produced by damaged or infected tissue [7, 78]. This process, termed chemotaxis, plays a significant role in immune cell motion in our model [171].

Neutrophil's movement is governed by Stokes equation in blood vessels and the considerably slower processes of diffusion and chemotaxis in the tissue [34, 83]. We account for movement through the microvasculature using the concept of homogenization [30, 191, 193]. For simplicity, we assume that the microvasculature tubules form a random reticulated structure, densely distributed everywhere and with arbitrary direction (as shown in figure 2.2). With these assumptions, homogenization is applied to the mix of microvasculature and extravasculature tissue to obtain an effective diffusion/chemotaxis process, where the diffusion

coefficient D_N or chemotaxis coefficient χ_N of neutrophils, for example, is substantially larger than diffusion/chemotaxis coefficients measured *in vitro* [133]. Hereafter, the motion of most immune cells in the tissue is justified as effective diffusion or effective chemotaxis.

The movement of most immune cells are similar to neutrophils and therefore, we are going to use Keller-Segel equations [95] coupling with reaction functions to model the mechanism of immune cell during infection and immune response. Their diffusion and chemotaxis coefficients must be interpreted as effective one thereafter.

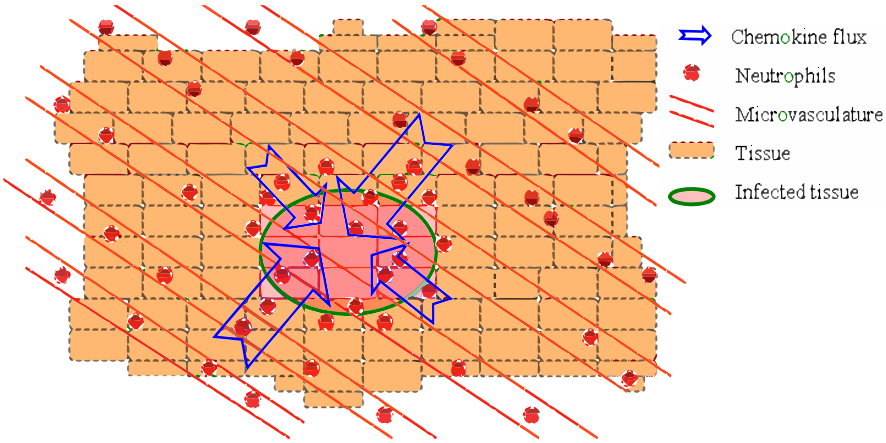

Figure 2.2 Schematic diagram of neutrophil movement in microvascularized tissue. This figure is from the published article [190].

One of the main tasks of neutrophils is to deliver a potent mix of noxious chemicals to the presumed location of the invading pathogens. The delivery is achieved through a process called degranulation, which culminates in the death of the neutrophil [7, 141]. It should not be surprising that such a lethal arsenal is highly regulated, mostly to ensure that the chemicals are released near pathogens. It would be wasteful, not to mention dangerous, to release the chemicals in the absence of pathogen. In our model, we use the successful scavenging of particulate antigens±PAMPs and immune complexes as an indication of the presence of pathogen, so antigen or immune complex uptake at rate $\lambda_{A|N}$ or $\lambda_{IC|N}$ is immediately followed by neutrophil death by degranulation. If neutrophils do not encounter particulate antigens±PAMPs or immune complexes after leaving the microsvasculature, they die through a constitutive pro-

cess of apoptosis at rate μ_N, a programmed cell death that is much cleaner and less destructive to surrounding tissue [78].

Degranulation of neutrophils, no matter how targeted, is nevertheless destructive to surrounding host tissue, so there is heavy incentive to reduce the number of neutrophils as soon as possible. The presence of apoptotic neutrophils, represented by ND in our model, serves as an early indication of the successful clearance of pathogen [7, 141]. Apoptotic cells are cleared through phagocytosis at rate $\lambda_{ND|MA}$ by activated macrophages MA. Upon phagocytosing apoptotic neutrophils, activated macrophages hasten to limit the damage of future degranulation by producing a chemokine CM (see equation (A.9)) that stops the influx of fresh neutrophils into the model area [7, 23], implemented as a on/off boundary condition thresholded at level ϵ_N.

Because we assume a high density of microvasculature everywhere in the tissue, we assume the initial concentration of neutrophils is positive constant N_0 throughout the simulation domain, though initially there are no apoptotic neutrophils. Neutrophils are known to release many self-regulating molecules [44, 150, 202]. Since chemokine CH is predominately produced by neutrophils early in infection (see equation (A.9)), we therefore use CH levels to auto-regulate these cells and introduce the self-regulation term $\delta_{N|CH} CH \cdot N$ in (A.2), involving the generic chemokine CH (more details are in section 2.6.2).

$$\begin{cases} \dfrac{\partial N}{\partial t} = \overbrace{D_N \Delta N}^{\text{effective chemotaxis}} - \overbrace{\nabla(\chi_N (N \cdot \nabla CH))}^{\text{effective chemotaxis}} - \overbrace{\Big(\lambda_{N|A} A + \lambda_{N|IC} IC + \mu_N + \delta_{N|CH} CH\Big) \cdot N}^{\text{degranulation/apoptosis/auto-regulation}} \\ \dfrac{\partial ND}{\partial t} = \underbrace{D_{ND} \Delta ND}_{\text{diffusion}} + \underbrace{\mu_N N}_{\text{transfer from N}} \underbrace{-\lambda_{ND|MA} ND \cdot MA}_{\text{phagocytosis by macrophages}} \underbrace{-\mu_{ND} ND}_{\text{decay}}, \\ N(\cdot, t)\Big|_{\partial\Omega} = N_0 \cdot 1_{\{CM \leq \epsilon_N\}}, \ \dfrac{\partial ND}{\partial n}\Big|_{\partial\Omega} = 0, \ N(x,0) = N_0, \ ND(x,0) = 0. \end{cases} \tag{2.7}$$

In [205, 206], the authors have proposed a postulate that connects the immune responses and antigen's phenotypic features. Furthermore, based on the approach we used to model the regulation of neutrophils recruitment in the tissues, we hypothesize that the activation and deactivation mechanism of immune agents are also chemical threshold dependent [190]:

Hypothesis 2.2.1. The regulation mechanism of activation and deactivation of immune agents

are chemical threshold dependent.

The activation or deactivation of immune agents in our model will be approached by characteristic functions of level sets for certain chemicals in the following sections.

2.2.2 Macrophage

Macrophages are scavengers that clear antigen/PAMP from the site of infection in a highly regulated operation. Regulation is achieved by careful management of the switch of different macrophages states.

Like all of the other immune cells in our model, macrophages are attracted to the source of antigen/PAMP by chemotaxis along a chemokine gradient established by neutrophils. In our model, resting macrophages patrol the tissue through effective diffusion, existing at some steady state level MR_0, representing the balance of macrophage recruitment and death in the tissues at rate μ_{MR} [62, 78].

The activation of macrophages is a process involving many different signals that can lead to different functional outcomes. Innate activation, classical activation, humoral activation and alternative activation are included in our model to capture a broad response from macrophages. The mechanism is summarized as following:

(i) Innate activation is simply the result that once recognized by PRRs, microbial stimuli will induce production of pro-inflammatory cytokines. The resting macrophage is therefore consequently activated [62, 112, 183]

(ii) Classical macrophage activation is mediated by a stimulus such as IFN-γ from effector T_H1 cells. The activation status of resting macrophage (or a macrophage activated only through PRR) is dramatically enhanced [8, 78, 112, 183].

(iii) Humoral macrophage activation is mediated by antibody (F) or complement receptors. These anti-inflammatory signals are secreted during high antibody levels the result of which is that the macrophage undergoes a downregulation [62].

(iv) Alternative activation is mediated by T_H2 type cytokines such as IL-4 or IL-13, and alternative activation will enhance the capacity for pinocytosis and endocytosis, and thus can

inhibit macrophage-mediated killing of pathogens [62, 118, 131]. In other word, not only the efficiency for activation of macrophage becomes lower but also the survival rate of pathogens becomes higher.

(v) In addition, macrophages are activated or de-activated under a competition between effector and regulatory T cells with their corresponding secreted cytokines [196]. Therefore, regulatory T cells play a deactivation role in our model by cytokine secretion.

Thus, in our model, processing the cytokine amount from effector T cells (e.g. IL2, IFN-γ, IL4 etc.) along with information on particulate antigen±PAMP levels in tissues [201], macrophages are activated at a rate (function) $\gamma_{MR}(CT1, CT2, CT_{\text{reg}}, A, F)$. Knowing little about how these cytokine signals are actually interpreted, we model the comprehensive activation rate (function) of macrophage by following indicator functions with threshold mechanism included:

$$C_r = \overbrace{\Big\{ \int_\Omega CT_{\text{reg}}(x,t)dx < \epsilon^1_{MA|T_{\text{reg}}} + \epsilon^2_{MA|T_{\text{reg}}} \int_\Omega A(x,t)dx \Big\}}^{\text{down-regulated by regulatory T cells}}, \tag{2.8a}$$

$$C_1 = \overbrace{\Big\{ \int_\Omega CT1(x,t)dx > \epsilon^1_{MA|T_H1} + \epsilon^2_{MA|T_H1} \int_\Omega A(x,t)dx \Big\}}^{\text{classical activation through IFN-}\gamma\text{ etc.}}, \tag{2.8b}$$

$$C_2 = \overbrace{\Big\{ \int_\Omega CT2(x,t)dx > \epsilon_{MA|T_H2} \Big\}}^{\text{alternative activation}}, \; C_F = \overbrace{\Big\{ \int_\Omega F(x,t)dx > \theta_F \Big\}}^{\text{humoral activation}}, \tag{2.8c}$$

so that the activation rate, as a functions based on chemical threshold [190], is

$$\gamma_{MR}(x,t) := \gamma_{MR}(CT1, CT2, CT_{\text{reg}}, A, F) = \gamma_{MA|MR} \cdot 1_{C_r \cap \left(C_F \cup C_1 \cup C_2\right)} \tag{2.9}$$

which attempts to approach macrophage activation such that the activation occurs when inflammatory signal $CT1$ dominates antigen±PAMPs (set defined as (2.8b)) [190], or, either T_H2 type cytokines or antibodies overcome certain threshold (sets defined as (2.8c)), and antigens, in turn, dominate suppressive signal CT_{reg} (set defined as (2.8a)).

Additionally, during humoral or alternative activation, the amount of immune complex or T_H2 type cytokines (e.g. $IL-4$ and $IL-13$) usually stays large [62, 78, 118]. For simplicity, in our model, we therefore utilize the local amount of immune complexes and T_H2 cytokines

as easily-observable marks to model the subsequent effect of humoral or alternative activation on immune efficiency (see section 2.1.2). Upon activation status, the immune efficiency of macrophage $p^{\text{eff}}_{A_p|A}(IC, CT2)$ is defined as:

$$p^{\text{eff}}_{A_p|A}(IC, CT2) := \left(1 - \delta \cdot 1_{\left\{\{\int_\Omega IC(x,t)dx > \theta_{IC}\} \cup \{\int_\Omega CT2(x,t)dx > \epsilon_{MA|T_H2}\}\right\}}\right) p^{\text{eff}}_{A_p|A} \tag{2.10}$$

where the model-specified constant $p^{\text{eff}}_{A_p|A}$ and parameter $\delta \in (0, 1]$ are used to mimic alternative activation.

Upon activation, macrophages lose access to the microvasculature and are thus less mobile (diffusion rate $D_{MA} < D_{MR}$), but are voracious consumers of antigen/PAMP ($\lambda_{A|MA} > \lambda_{A|MR}$), and acquire additional skills, including the ability to phagocytize apoptotic neutrophils at rate $\lambda_{ND|MA}$ (see equation (A.2) and references[7, 8, 23]) and produce chemokine at rate $\beta_{CH|MA}$ (see equation (A.9) and reference [149]). The macrophage's mechanism is highlighted in the figure 2.3.

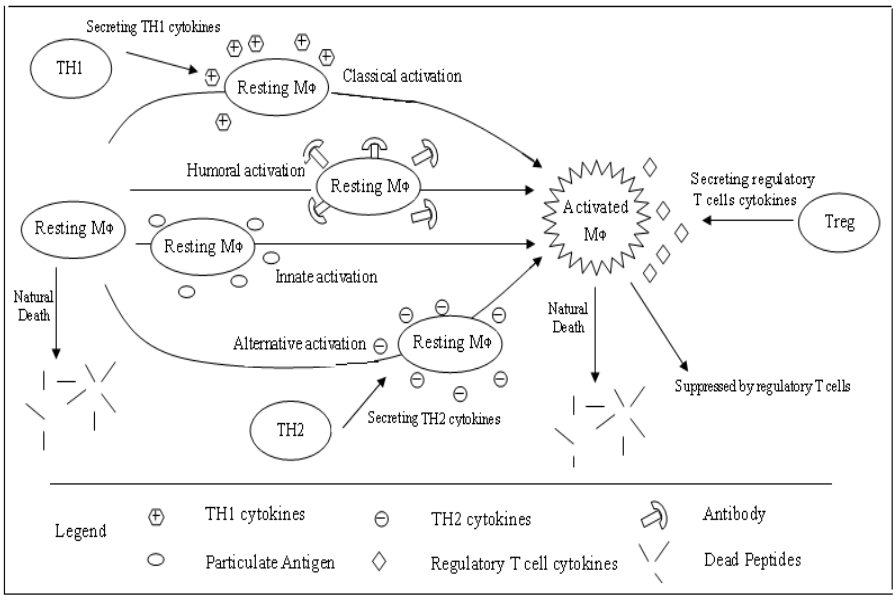

Figure 2.3 Schematic diagram of macrophage response.

Taking into account the natural death of macrophage and its burst due to growth of intra-

cellular antigens, the modeling equations of macrophage are summarized below:

$$\begin{cases} \dfrac{\partial MR}{\partial t} = \overbrace{D_{MR}\Delta MR}^{\text{effective diffusion}} - \overbrace{\nabla(\chi_{MR}(MR\cdot\nabla CH))}^{\text{effective chemotaxis}} - \overbrace{\mu_{MR}MR}^{\text{natural death}} - \overbrace{\lambda_{MR|A}A\cdot MR}^{\text{innate activation}} \\ \qquad - \overbrace{\gamma_{MR}(CT1, CT2, CT_{\text{reg}}, A, F)\cdot MR}^{\text{activation}}, \\ \dfrac{\partial MA}{\partial t} = \underbrace{D_{MA}\Delta MA}_{\text{effective diffusion}} - \underbrace{\nabla(\chi_{MA}(MA\cdot\nabla CH))}_{\text{effective chemotaxis}} - \underbrace{\mu_{MA}MA}_{\text{degradation}} + \underbrace{\lambda_{MR|A}A\cdot MR}_{\text{innate activation}} \\ \qquad + \underbrace{\gamma_{MR}(CT1, CT2, CT_{\text{reg}}, A, F)\cdot MR}_{\text{activation}} - \underbrace{\Big(\dfrac{\mu_{MA|A_p}A_p}{\delta_{A_p}+A_p}\Big)MA}_{\text{burst due to } A_p}, \\ MR(\cdot,t)\Big|_{\partial\Omega} = MR_0, \dfrac{\partial MA}{\partial n}\Big|_{\partial\Omega} = 0,\ MR(x,0) = MR_0,\ MA(x,0) = 0. \end{cases} \tag{2.11}$$

where activation rate $\gamma_{MR}(CT1, CT2, CT_{\text{reg}}, A, F)$ is defined as above in (A.8).

2.3 Dendritic cells

Some time after the innate immune response launches at the infection site, evidence of the infection reaches the lymph nodes via antigen presenting cells (APCs). The adaptive immune response is a carefully orchestrated affair that detects the pathogen with greater sensitivity and, deflecting unwanted damage to the host, directs the inflammatory response more precisely at the pathogen. We consider dendritic cells to be the main antigen presenting cells (APCs), with two phases: immature and mature [101].

Immature dendritic cells, DE in equation (A.3), migrate toward the site of infection following the chemokine gradient established by neutrophils and, later, activated macrophages. They uptake antigens±PAMPs or immune complexes [103, 183], contributing to the processing terms in equation (A.1) and (2.6). Simultaneously, immature dendritic cells undergo antigen±PAMPs or immune complex-induced activation to become mature dendritic cells in a constant rate of γ^1_{DE} or γ^2_{DE}, following the activation, they degrade the engulfed antigen±PAMP or immune complex and present corresponding MHC Class II peptide or antigen bond or immune complexes on their surfaces to fulfill their messenger duty in the lymph node [78, 103]. According to different types of peptide presented on the surface, mature dendritic cells may be categorized into different generic subsets [18]. In our model (A.3), based on the assumption of a single

phenotype of presented peptide on the DC's surface, we use DA, mature dendritic cell with particulate antigen, and DF, mature dendritic cell with immune complex, to approach the differentiation of mature DC. Mature dendritic cells reverse responsiveness to the chemokine gradient and migrate away from the infection site toward the lymph nodes, where they present the MHC Class II to specific lymphocytes. We therefore model the movements of dendritic cells by coupled transport terms in (A.3).

Dendritic cells also experience natural death in the rate of μ_{DE}, μ_{DA} and μ_{DF}, and effective diffusion with diffusion coefficient D_{DE}, D_{DA} or D_{DF}. The model equation of DC are summarized as below:

$$\begin{cases} \dfrac{\partial DE}{\partial t} = \overbrace{D_{DE}\Delta DE}^{\text{effective diffusion}} - \overbrace{\nabla(\chi_{DE}(DE\cdot\nabla CH))}^{\text{effective chemotaxis}} - \overbrace{\mu_{DE}DE}^{\text{natural death}} - \overbrace{DE\cdot\left(\gamma^1_{DE}A+\gamma^2_{DE}IC\right)}^{\text{uptake antigens/immune complexes}} \\ \dfrac{\partial DA}{\partial t} = D_{DA}\Delta DA + \nabla(\chi_{DA}(DA\cdot\nabla CH)) - \mu_{DA}DA + \gamma^1_{DE}DE\cdot A \\ \dfrac{\partial DF}{\partial t} = D_{DF}\Delta DF + \nabla(\chi_{DF}(DF\cdot\nabla CH)) - \mu_{DF}DF + \gamma^2_{DE}DE\cdot IC \\ DE(\cdot,t)\Big|_{\partial\Omega} = DE_0, \dfrac{\partial DA}{\partial n}\Big|_{\partial\Omega} = \dfrac{\partial DF}{\partial n}\Big|_{\partial\Omega} = 0, \\ DE(x,0) = DE_0\cdot 1_{\{x\in\partial\Omega\}}\ , DA(x,0) = DF(x,0) = 0. \end{cases} \tag{2.12}$$

For simplicity, we assume that pathogens rarely damage the bone marrow directly during the MHC Class II mediated immune responses in our model, so that immature DCs in the lymph node have a constant supply from hemopoietic bone marrow progenitor cells. In (A.3), DE_0 is therefore set as a positive constant, which can also be relaxed and adjusted to mimic other type of pathogens that invades the bone marrow.

A schematic diagram of DCs' behavior and interactions with macrophages and effector T cells are sketched in figure 2.4.

2.4 B cells

This iteration of the model does not distinguish between non-specific and antigen-specific B (or T) cells. Therefore any B cell that encounters antigen in the lymph node will become

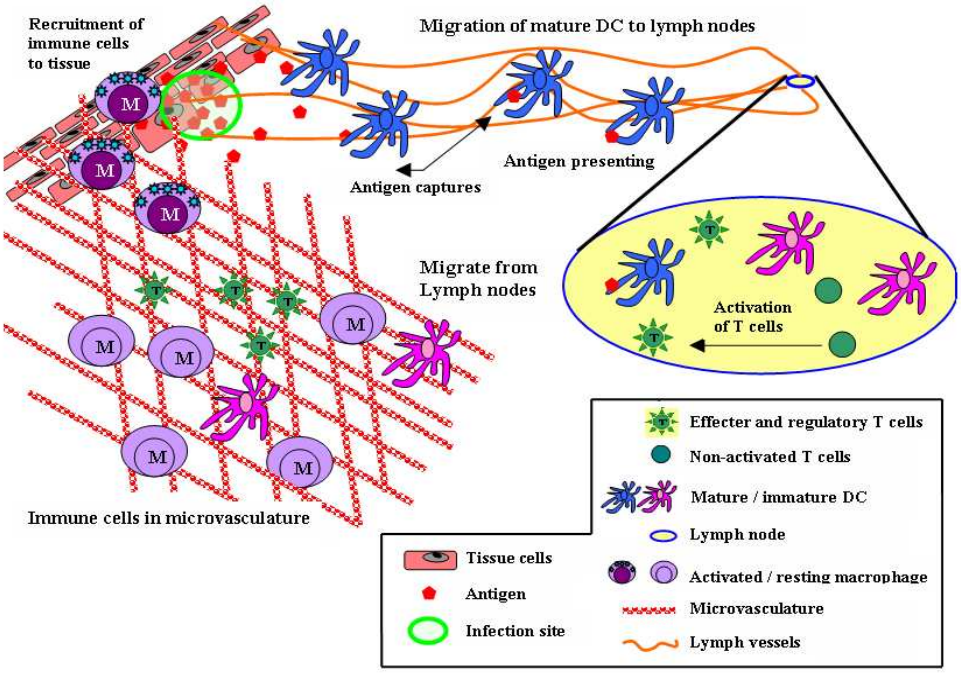

Figure 2.4 Schematic of interactions of DC with other immune agents in immune system in the model. This figure is from the published article [190].

licensed to activate. Once licensed they will act as APCs to present antigen in the context of MHC Class II to effector T cells and become either memory B cells or antibody producing plasma B cells [78, 183]. The licensing, activation, proliferation and function of B cells are primarily limited to the lymph nodes [78, 183, 198] so that in our system the dynamics of B cells occurs primarily in the boundary of the domain.

Crosslinking of B cell receptors (BCRs) is a licensing signal and a consequence of the abundance of the antigens and enables the B cell to become activated, which is dependent upon its interaction with T cells [183]. Though the main source of antigen for interaction with BCRs, in our model, is soluble antigen, particulate antigens can be presented to the B cells in the lymph node as well [18]. Regardless of the source, the amount for either type of antigen needs to exceed a threshold for B cell licensing and is described as threshold functions.

Once the threshold is reached and the B cells are licensed, effector T cell's help is needed for full activation. For simplicity we have modeled that T cells can be directly activated by

licensed B cells through cell-cell contact and this activation leads to a T_H2 response. We also account for the fact that previously activated effector T cells in the lymph nodes can contact licensed B cells and promote antibody production via IFN-γ (T_H1 responses). During the immune response, the number of activated B cells and plasma B cell produced antibodies varies according to the phenotype of immune response. For simplicity, we assume that there is always a constant supply of follicular or memory B cells, whose amount is denoted by constant parameter B_m, circulating in the lymph nodes and being activated by direct encountering with the soluble antigens or immune complexes.

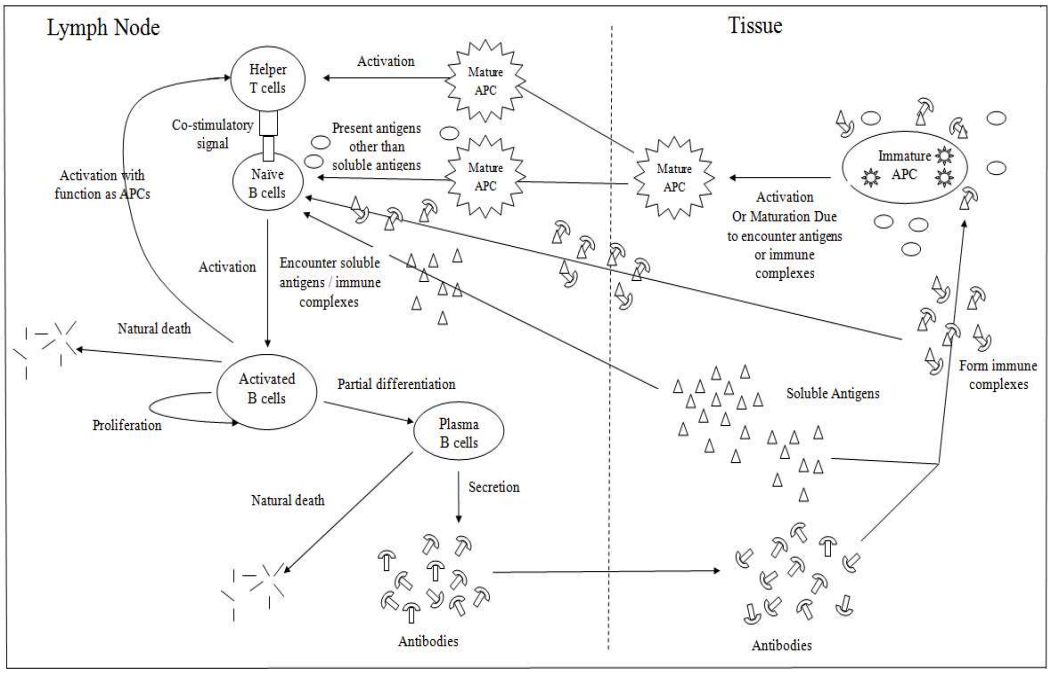

Figure 2.5 Schematic diagram of activation of B cells.

A sufficient amount of antigens presented in the lymph node leads to the rapid proliferation of activated B cells [183], and is approached by replication rate $G(A_s, A, DA, DF, IC)$ in (2.13). Besides natural death, the activated B cells commit to career choice that they differentiate into plasma B cells with a certain rate [26, 27]. To approximate the function of plasma B cells, we model their net effect as a homogeneously distributed antibody-source (ref (2.22)). Our model is biased to short term antibody production and short lived plasma cells and we do not have a

term for long-lived bone marrow resident plasma B cells that produce antibodies for extended periods of time [26, 27]. The mechanisms of B cell activation as described in the model are summarized in schematic diagram in figure 2.5.

As a summary, by defining the replication rate as

$$G(A_s, A, DA, DF, IC) = \left.\frac{A_s + A + p_{B|DE}(DA + DF)\rho_{DE} + IC}{\delta_{B_a} + (A_s + A + p_{B|DE}(DA + DF)\rho_{DE} + IC)}\right|_{\partial\Omega}, \tag{2.13}$$

and the sets of activation as

$$U_X = \{X(\cdot, t)|_{\partial\Omega} > \theta_{B_a|X}\}, \text{ for } X \in \{A_s, IC, A\}, \tag{2.14a}$$

$$U_{DA,DF} = \Big\{\rho_{DE} \cdot \big(DA(\cdot, t) + DF(\cdot, t)\big)|_{\partial\Omega} > \theta_{B_a|DA,DF}\Big\}. \tag{2.14b}$$

the activated B cells in the model are governed by:

$$\begin{cases} \dfrac{dB_a}{dt} = \overbrace{\gamma_{B_a|T_H2} \cdot T_H2(\cdot, t)\Big(A_s(\cdot, t)1_{U_{A_s}} + IC(\cdot, t)1_{U_{IC}} + A(\cdot, t)1_{U_A} + p_{B|DE}\rho_{DE}}^{T_H2 \text{ promotion due to exposure of } T_H2 \text{ cells to free antigens, immune complexes,}} \cdots \\ \overbrace{\big((DA + DF)(\cdot, t)\big) \cdot 1_{U_{DA,DF}}\Big)}^{\text{and DC-bond antigens}}\Big|_{\partial\Omega} + \overbrace{\gamma_{B_a|T_H1} \cdot T_H1(\cdot, t)\Big(A(\cdot, t)1_{U_A} + \cdots}^{\text{co-stimulation of naïve B cells by}} \\ \overbrace{p_{B|DE}\rho_{DE}\big((DA + \cdots + DF)(\cdot, t)\big)1_{U_{DA,DF}}\Big)}^{\text{other effector T cells}}\Big|_{\partial\Omega} - \overbrace{(\mu_{B_a} + \alpha_{B_p|B_a}) \cdot B_a}^{\text{decay and career choice}} \\ + \overbrace{\gamma_{B_m|A_s,IC} \cdot B_m\big(IC(\cdot, t) + A_s(\cdot, t)\big)}^{\text{activation from memory B cells}}\Big|_{\partial\Omega} + \overbrace{\alpha_{B_a} B_a G(A_s, A, DA, DF, IC)}^{\text{proliferation}} \\ B_a(0) = 0, \end{cases} \tag{2.15}$$

The parameter ρ_{DE} in (2.15), (2.13) and (2.14b) is the average number of antigen bonds on the surface of mature DCs, and model specific parameter $p_{B|DE}$ stands for the fraction of available antigen bonds among the total on mature DCs to activate naïver B cells in the lymph node. Modeling equation for plasma B cells is

$$\begin{cases} \dfrac{dB_p}{dt} = \overbrace{\alpha_{B_p|B_a} \cdot B_a}^{\substack{\text{differentiated from} \\ \text{activated B cells}}} - \overbrace{\mu_{Bp} B_p}^{\text{natural death}} \\ B_p(0) = 0 \end{cases} \Rightarrow B_p(t) = \alpha_{B_p|B_a} e^{-\mu_{B_p} t} \int_0^t e^{\mu_{B_p} s} B_a(s) ds \tag{2.16}$$

2.5 Effector T cells and regulatory T cells

It is well known that CD4$^+$ T cells (or called helper T cells, in this model we call it effector T cells) orchestrate the adaptive immune response [78, 183]. Peptides are presented to CD4$^+$ T cells in the context of MHC Class II so that naïve T cells are activated and differentiate into at least two different subsets of effector T cell: T_H1 and T_H2 cells, defined by the cytokines they produce. Though the mechanisms leading to T_H1 and T_H2 cell dichotomy are still far from clear, current knowledge provides information for modeling the behavior of effector T cells based on known functions and interactions.

Once activated by APCs, the common function of all these effector T cell subsets is to reduce antigen load by either supporting macrophage activation through pro-inflammatory signals or supporting B cell production of antibody in the absence of pro-inflammatory signals [203]. In our model, we approach this mechanism as T_H1 cells mainly activate macrophages while T_H2 cells are specialized for the task of stimulating B cells to produce certain classes of antibodies. In contrast, the regulatory T cells [63] function to reduce inflammation.

2.5.1 Effector T cells, their subsets and activation

Naïve T cells continuously recirculate between the vasculature and lymph nodes, where they interact with APCs and scan surface expressed MHC Class II or peptide complexes. If a peptide or MHC Class II matches the T cell receptor there is the opportunity for activation [78]. In our model, all APCs with antigen are themselves "activated" either through the recognition of particulate antigen±PAMP if a DC or through the recognition of their cognate antigen if a B cell. We thus assume that if a T cell contacts an antigen loaded APC the T cell will become activated with certain threshold conditions satisfied (ref. equation (2.20) and (2.21)). T cell activation is limited by the amount of antigen and only modulated by regulatory T cells, which downregulate the ability of naïve T cells to become activated. Activated T cells, in turn, migrate to the site of infection via the microvasculature. We simplify the model by assuming that naïve T cells reside in the lymph node (the boundary) until they are activated by contact with APCs.

It is clear that $T_H1 - T_H2$ phenotypes are acquired upon antigen induced differentiation of naïve T cells [32, 78]. However, definitive factors directing T_H2 development have not been conclusively demonstrated [91, 113, 208]. There have been many ideas put forward, such as results indicating that MHC Class II that interacts strongly with TCR favor promotion of T_H1 phenotype while weak binding favors priming for T_H2 phenotype [161]. Clearly the cytokine milieu during T cell activation has a significant effect on the ultimate T cell phenotype although identifying an initial source of T_H2 cytokines has been particularly inconsistent. Newer theories suggest spatial relationships during cellular division as an important factor determining T_H1 and T_H2 polarization [137, 139]. These inconsistencies make designing a biologically consistent model of T_H1 v.s. T_H2 differentiation difficult, although it is the central theme during the generation of an antigen specific immune response. As T_H2 cells largely support the B cell response, we propose that if a B cell captures its cognate antigen via an antigen specific receptor that it becomes activated (over some threshold) and, in turn, drives any responding antigen specific T cells to become T_H2 cells. This conceptually simple solution can be supported by results from several lines of investigation: for example, the results in [13, 164, 165] reveal that the disruption of T cell-B cell interaction via loss of SAP signaling leads preferentially to a loss of T_H2 T cells much more significantly than any loss of a T_H1 response; in addition, it has recently been shown that B cells are required to generate T_H2 cells after infection *Leishmania mexicana* or *nippostrongylus* [110]. Collectively, these types of results suggest modeling a flow of information from B cells to T cells is consistent with the immune response towards some infections. Furthermore, in our model the T_H2 dependent antibodies function to reduce the soluble antigen providing an efficient feedback response and maintaining the central role that the level of antigen in the lymph node plays in determining the immune response [2].

More generally, in the proposed model, as long as antigens reach the lymph node in the absence of a classically activated mature DC then T cells develop into T_H2 cells by default or B cells activate them to commit to T_H2 cells [13] while DCs with information about particulate antigen±PAMPs are inclined to promote T_H1 responses [18, 113]. Furthermore, signaling by TCRs involves a sufficient activation signal [78]. To model this, indicator functions with

respect to the thresholds are applied: once the population of APCs overcomes some threshold, the activation is exerted (refer to (2.20)). Activation of effector T cells is known to be time-lapse as the receptor engagement requires certain time period [183]. The effect of time-lapse activation of T cells is modeled by incorporating delay terms in (2.20) where τ_0 is the necessary time period to fulfill the activation.

Furthermore, in our model, it is assumed that the MHC Class II on the surface of APCs (either DCs or B cells) is fully occupied with the appropriate peptide and therefore the activation of effector T cells is directly proportional to the amount of mature APCs in the lymph nodes.

Once activated, the effector T cells in our model have no cytotoxic activities, but divide rapidly, secrete cytokines and migrate to the source of infection as determined by the infection-associated chemokine gradient (cell movement is governed by both diffusion and chemotaxis). The T cells continue to secrete cytokines (discussed in section 2.6.2) to upregulate the immune response, via either macrophage activation [58, 78] or B cell-released antibodies [78, 183].

2.5.2 Regulatory T cells

Recently, a subpopulation of T cells that play a significant role in limiting the pro-inflammatory immune response has been discovered. The mechanisms by which these cells, called regulatory T cells, exert their suppressory/regulatory activities is not completely understood, but it may be mediated by both immunosuppressive cytokines, such as TGF-β and IL-10, as well as direct cell-to-cell contact with T effector cells [82, 175, 196].

Less is known about the origins of regulatory T cells, and there may be several different sources depending upon the specific immune response [82, 97, 98, 192, 196]. In our model, they begin life as effector T cells in the lymph node that become activated by signals from the infection site [192]. We assume the activation signal for regulatory T cell commitment originates with the activated effector T cell population itself, which proliferates and secretes positive growth signals, like IL-2 [94, 98], that promote regulatory T cell differentiation and survival [63]. However, immune suppression is only warranted when immune inflammation

exceeds the perceived threat level. The severity of the threat is proportionally related to the total amount of various antigens. To summarize these considerations, we assume that the development of regulatory T cells in the lymph node depends on a threshold mechanism modeled by level sets incorporating the amount of cytokines released by effector T cells and the amount of surrounding antigens in the lymph nodes(refer to equation (A.6) and (2.19)).

Generally, activated regulatory T cells are generated and then migrate to the infection site when cytokine from effector T cells is high and antigen load is low. Cytokines produced by regulatory T cells (section 2.6.2) affect macrophages as discussed in section 2.2.2.

As a summary, in our model:

1. Regulatory T cells suppress primed effector T cells through direct cell contact at a constant rate, and this contributes to effector T cells becoming unresponsive;
2. Regulatory T cells suppress the immune response by secreting undefined negative signals, which we discuss in section 2.6.2 and denote by CT_{reg};
3. Regulatory T cells undergo chemotaxis and diffusion in a manner similar to previously discussed effector T cells. Therefore, the governing equation of regulatory T cell is therefore set up as:

$$\begin{cases} \dfrac{\partial T_{\text{reg}}}{\partial t} = \overbrace{D_{T_{\text{reg}}}\Delta T_{\text{reg}}}^{\text{effective diffusion}} - \overbrace{\nabla(\chi_{T_{\text{reg}}}(T_{\text{reg}} \cdot \nabla CH))}^{\text{effective chemotaxis}} - \overbrace{\mu_{T_{\text{reg}}} T_{\text{reg}}}^{\text{natural death}} \\ T_{\text{reg}}(x,0) = 0 \\ T_{\text{reg}}(\cdot,t)\Big|_{\partial\Omega} = \gamma_{T_{\text{reg}}}(CT1, CT2)\Big((T_H1(\cdot,t) + T_H2(\cdot,t))\Big|_{\partial\Omega}\Big) \end{cases}, \tag{2.17}$$

where the activation function $\gamma_{T_{\text{reg}}}(CT1, CT2)$ is modeled by

$$\gamma_{T_{\text{reg}}}(CT1, CT2) = \gamma_{T_{\text{reg}}} \cdot 1_{\{U_1 \cup U_2\}} \tag{2.18}$$

where the level sets U_1 and U_2 are defined as

$$U_1 = \Big\{CT1(\cdot,t)\big|_{\partial\Omega} > \epsilon^1_{T_{\text{reg}}} + \epsilon^2_{T_{\text{reg}}}\big(A(\cdot,t) + \rho_{DE}DA(\cdot,t)\big)\big|_{\partial\Omega}\Big\}, \tag{2.19a}$$

$$U_2 = \Big\{CT2(\cdot,t)\big|_{\partial\Omega} > \epsilon^1_{T_{\text{reg}}} + \epsilon^2_{T_{\text{reg}}}\big(A_s(\cdot,t) + \rho_{DE}DF(\cdot,t) + IC(\cdot,t)\big)\big|_{\partial\Omega}\Big\}. \tag{2.19b}$$

2.5.3 Regulation of effector T_H1 and T_H2 cells

Both T_H1 and T_H2 cells secrete a large number of cytokines [189]. As phenotypic markers, interleukin-2 (IL-2), and interferon-γ (IFN-γ) are secreted by T_H1 while interleukins 4 and 13 (IL-4 and IL-13) are secreted by T_H2 [78].

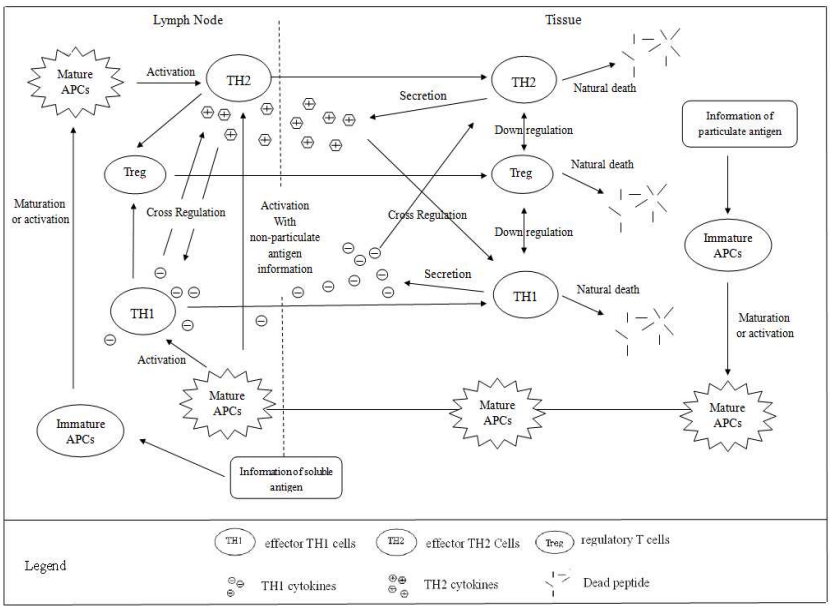

Figure 2.6 Schematic diagram of the dynamics of T cells. Details are included according to discussion in section 2.5.1-2.5.3.

It is known that activated T_H1 and T_H2 cells are cross-suppressive via their cytokines. For example, IFN-γ suppresses proliferation of T_H2 cells [46, 56, 78, 183], while IL-4 suppresses the proliferation of T_H1 cells [47, 48, 78, 135, 136, 162, 183]. This cross-regulation of T_H1 and T_H2 cells is also studied by [52, 53, 54]. In summary, once a cytokine profile is established, a systematic feedback will be established. The terms $-\delta_{T_H2|T_H1}CT1 \cdot T_H2$ and $-\delta_{T_H1|T_H2}CT2 \cdot T_H1$ in model equation (2.20) represent the suppression of T_H1 and T_H2 cells by corresponding cytokines at certain rates. As discussed in section 2.5.2, regulatory T cells suppress the effector T cells through a direct cell-cell contact, so that the terms $-\delta_{T_H1|T_{\text{reg}}}T_H1 \cdot T_{\text{reg}}$ and $-\delta_{T_H2|T_{\text{reg}}}T_H2 \cdot T_{\text{reg}}$ in (2.20) accounts for possible contact-mediated suppression, where regulatory T cells directly abrogate effector T cell function, effectively removing such cells from

the infection site.

The complete schematic of T cell mechanism is highlighted in figure 2.6.

2.5.4 Recruitment and initial distribution of effector and regulatory T cells

The boundary and initial conditions for subsets of T cells are summarized in equations (2.20) and (2.17). Here, the role of the boundary as lymph node is pertinent, and there are no effector T cells until mature APCs start presenting antigen to the naïve T cells in the lymph nodes (boundary), but as long as APCs are mature with antigen or MHC Class II in the lymph node, and the population threshold condition is satisfied and enough time has elapsed, effector T cells appear on the boundary at certain rate per APC.

In a summary, effector T cells are modeled by the following PDEs:

$$
\begin{cases}
\dfrac{\partial T_H1}{\partial t} = \overbrace{D_{T_H1}\Delta T_H1}^{\text{effective diffusion}} - \overbrace{\nabla\cdot(\chi_{T_H1}(T_H1\cdot\nabla CH))}^{\text{effective chemotaxis}} - \overbrace{\delta_{T_H1|T_{\text{reg}}}T_H1\cdot T_{\text{reg}}}^{\substack{\text{down-regulated by}\\ \text{contact with } T_{\text{reg}}}} \\
\qquad - \overbrace{\delta_{T_H1|T_H2}CT2\cdot T_H1}^{\text{crossregulation}} - \overbrace{\mu_{T_H1}T_H1}^{\text{natural death}} \\
\dfrac{\partial T_H2}{\partial t} = \overbrace{D_{T_H2}\Delta T_H2}^{\text{effective diffusion}} - \overbrace{\nabla\cdot(\chi_{T_H2}(T_H2\cdot\nabla CH))}^{\text{effective chemotaxis}} - \delta_{T_H2|T_{\text{reg}}}T_H2\cdot T_{\text{reg}} \\
\qquad - \overbrace{\delta_{T_H2|T_H1}CT1\cdot T_H2}^{\text{crossregulation}} - \overbrace{\mu_{T_H2}T_H2}^{\text{natural death}} \\
T_H1(\cdot,t)\Big|_{\partial\Omega} = \underbrace{\gamma_{T_H1|DA}DA(\cdot,t-\tau_0)|_{\partial\Omega}\cdot K(DA,\theta_{T_H1})}_{\text{activation by mature DC with particulate antigen}} + \underbrace{\gamma_{T_H1|DF}K(DF,\theta_{T_H1})\cdots}_{\text{activation by mature}} \\
\qquad \underbrace{DF(\cdot,t-\tau_0)|_{\partial\Omega}}_{\text{DC with soluble antigen}} \\
T_H2(\cdot,t)\Big|_{\partial\Omega} = \underbrace{\gamma_{T_H2|B_a}B_a(t-\tau_0)\cdot K(Ba,\theta_{T_H2})}_{\substack{\text{activation by APCs that collects antigens}\\ \text{different from particulate antigen (e.g. B cells)}}} + \underbrace{\gamma_{T_H2|DF}K(DF,\theta_{T_H2})\cdots}_{\text{activation by mature}} \\
\qquad \underbrace{DF(\cdot,t-\tau_0)|_{\partial\Omega}}_{\text{DC with soluble antigen}} \\
T_H1(x,0)=0,\ T_H2(x,0)=0,
\end{cases}
\tag{2.20}
$$

where the activation rate (function) of effector T cells $K(x, y, z)$ is defined as

$$K(x, y) = 1_{\left\{x(\cdot, t-\tau_0)|_{\partial\Omega} > y\right\}}. \tag{2.21}$$

2.6 Chemicals

2.6.1 Antibody

There are various types of antibodies with significantly different functions and structures (e.g. IgG1, IgG2, IgE, IgM, IgA etc.). To avoid complexity, we use a generic antibody to capture the diverse but essentially similar effects of different types of antibodies. As a relatively small molecule, once produced by plasma B cells, antibodies diffuse very fast in the tissue up to homogenization [30, 191, 193]. Once encountering their corresponding antigens, antibodies bind them and effectively neutralize them. One aspect of this binding is that immune complexes are generated which may be processed by professional phagocytes. In our model we reconcile the fact that different antibody isotypes have different functions as immune complexes when in contact with phagocytes.

In the model we found that when antibodies are at a low level they reflect the activation of B cells predominantly from T_H1 cells and antibody levels reached relatively high levels only when a T_H2 response is generated. Therefore immune complexes generated under a threshold antibody titer promote classical macrophage activation and DC maturation with subsequent T_H1 skewing. If immune complexes are generated over the threshold they promote alternative macrophage activation, and DCs that acquire immune complexes above the threshold will recycle the immune complex to their surface for B cell recognition once within the lymph node and perpetuate a T_H2 response.The dynamics of antibody is therefore governed by the following reaction diffusion equations, where B_p is defined in (2.16):

$$\begin{cases} \dfrac{\partial F}{\partial t} = \overbrace{D_F \Delta F}^{\text{diffusion}} - \overbrace{(\lambda_{F|A} A + \lambda_{F|A_s} A_s) \cdot F}^{\substack{\text{de-function when} \\ \text{forming immune complex}}} - \overbrace{\mu_F F}^{\text{decay}} + \overbrace{\beta_{F|B_p} B_p}^{\substack{\text{secreted by} \\ \text{plasma B cells}}} \\ F(\cdot, 0) = 0, \ \dfrac{\partial F}{\partial n}(\cdot, t)\Big|_{\partial\Omega} = 0. \end{cases} \tag{2.22}$$

2.6.2 Chemicals messengers by professional phagocytes: chemokines

Chemokines are released by many different types of cells and serve to direct the movement of innate and adaptive immune cells [171, 198]. Although there are many chemokines employed by the immune system, we utilize a single, generic chemokine to drive all forms of chemotaxis in our simple model. In our model, chemotaxis of most immune cells is determined by the concentration gradient of a generic chemokine CH, produced by neutrophils at rate $\beta^i_{CH|N}$ and activated macrophages at rate $\beta^i_{CH|MA}$ $(i = 1, 2)$, in response to encounters of these cells with particulate antigen±PAMP [23, 178] or immune complex [183].

This inflammatory chemokine functions as a chemoattractant for neutrophils and other effector immune cells to the site of infection. The chemokine also decays at rate μ_{CH} and diffuses through the tissue with coefficient D_{CH}. The initial chemokine gradient is established by the rapid arrival of neutrophils to the infection site through effective diffusion via the microvasculature. The governing equation is therefore set as:

$$\begin{cases} \dfrac{\partial CH}{\partial t} = \overbrace{(\beta^1_{CH|MA}MA + \beta^1_{CH|N}N)A}^{\text{in accordance to particulate antigens}} + \overbrace{(\beta^2_{CH|MA}MA + \beta^2_{CH|N}N)IC}^{\text{in accordance to immune complex}} \\ \qquad\qquad - \overbrace{\mu_{CH}CH}^{\text{decay}} + \overbrace{D_{CH}\Delta CH}^{\text{diffusion}}, \\ \dfrac{\partial CH}{\partial n}\Big|_{\partial\Omega} = 0, CH(x, 0) = 0. \end{cases} \tag{2.23}$$

2.6.3 Chemical messengers by T cells and macrophages: cytokines

Cytokines are a family of proteins, peptides or glycoproteins that are used for intercellular communication. They are secreted by specific immune cells and carry local information of secretion cells, and have effects on other cells in distance. They are important in both innate and adaptive immune responses. Cytokines are characterized by considerable abundant in that many appear to share similar functions [78].

In our model, to avoid ambiguity and complexity of the roles of cytokines, we simplify the system with only four major cytokine categories: those produced by effector T cells, such as IL-2 and IFN-γ by T_H1 cells, denoted by $CT1$ that promotes activations of regulatory T cells

and macrophages (refer to (2.8b)), or such as IL-4, IL-5 and IL-13 by T_H2 cells, denoted by $CT2$ that promotes activation of B cells and production of antibodies or induce alternative activation (refer to sections 2.4 and 2.2.2); cytokines produced by regulatory T cells, such as IL-10 and TGF-β, denoted by CT_{reg} that regulates the pro-inflammatory immune responses by blocking activation of macrophages (refer to (2.8a)); and cytokines produced by activated macrophages upon engulfing apoptotic neutrophils, such as IL-1 and TNF-α [8] and denoted by CM in the model which is used to limit the recruitment of neutrophils (refer to equation (A.2)). Cytokines diffuse in the tissue through microvasculature rapidly and decay in certain rates.

The modeling equation of all cytokines are a group of reaction diffusion equations with Neumann boundary condition imposed to capture balance flow in the lymph nodes, and they are summarized as below:

$$\begin{cases} \dfrac{\partial CM}{\partial t} = \overbrace{\beta_{CM} ND \cdot MA}^{\text{secreted by MA when engulfing ND}} - \overbrace{\mu_{CM} CM}^{\text{decay}} + \overbrace{D_{CM} \Delta CM}^{\text{diffusion}}, \\ \dfrac{\partial CT1}{\partial t} = \overbrace{\beta_{CT1} T_H1}^{\text{secreted by } T_H1} - \overbrace{\mu_{CT1} CT1}^{\text{decay}} + \overbrace{D_{CT1} \Delta CT1}^{\text{diffusion}}, \\ \dfrac{\partial CT2}{\partial t} = \overbrace{\beta_{CT2} T_H2}^{\text{secreted by } T_H2} - \overbrace{\mu_{CT2} CT2}^{\text{decay}} + \overbrace{D_{CT2} \Delta CT2}^{\text{diffusion}}, \\ \dfrac{\partial CT_{\text{reg}}}{\partial t} = \overbrace{\beta_{CT_{\text{reg}}} T_{\text{reg}}}^{\text{secreted by } T_{\text{reg}}} - \overbrace{\mu_{CT_{\text{reg}}} CT_{\text{reg}}}^{\text{decay}} + \overbrace{D_{CT_{\text{reg}}} \Delta CT_{\text{reg}}}^{\text{diffusion}}, \\ \dfrac{\partial CT1}{\partial n}\Big|_{\partial\Omega} = \dfrac{\partial CT2}{\partial n}\Big|_{\partial\Omega} = \dfrac{\partial CT_{\text{reg}}}{\partial n}\Big|_{\partial\Omega} = \dfrac{\partial CM}{\partial n}\Big|_{\partial\Omega} = 0, \\ CT_{\text{reg}}(x,0) = CT1(x,0) = CT2(x,0) = CM(x,0) = 0. \end{cases} \tag{2.24}$$

CHAPTER 3. Numerical scheme to the model

The fundamental equation of our model is the Keller-Segel equation [95] modeling chemotaxis

$$\begin{cases} \partial_t \rho + \mathrm{div}(\chi_\rho \cdot \nabla c \rho) = \mathrm{div}(D_\rho \nabla \rho) + R(\rho, c) \\ \partial_t c - \mathrm{div}(D_c \nabla c) = g(\rho, c), \end{cases} \tag{3.1}$$

while equations (A.1)-(2.6), (2.22)-(A.10) are reaction diffusion equations for various antigens, chemokine, and cytokines. The equations involving the dynamics of immune cells, (A.2), (A.7), (A.3), (2.17) and (2.20), are Keller-Segel type equations where the convection term $\mathrm{div}(\chi_\rho(\nabla c)\rho)$ contributes to the chemoattraction effect.

In this section, we briefly discuss a numerical scheme developed to approach a general version of Keller-Segel equation

$$\begin{cases} \partial_t \rho + \mathrm{div}(\chi_\rho(c, |\nabla c|)\nabla c \cdot \rho) = \mathrm{div}(D_\rho(c, |\nabla c|)\nabla \rho) + R(\rho, c) \\ \partial_t c - \mathrm{div}(D_c(c, |\nabla c|)\nabla c) = g(\rho, c) \end{cases}, \tag{3.2}$$

in which the chemotaxis coefficient χ_ρ and diffusion coefficient D_ρ, D_c are dependent on $(c, |\nabla c|)$, the concentration and the magnitude of its gradient. The numerical scheme developed for (3.2) can easily be adapted to (3.1) with constant coefficients in our model.

Numerical computation of chemotaxis equations is a nontrivial mathematical task. Different numerical approaches to simulate equations (3.1) or similar systems have been proposed in [29, 50, 51, 108, 121, 176]. Two issues must be addressed for the numerical simulation of this model: resolution and computing time. Implicit scheme are applied to guarantee unconditional stability of reaction diffusion equations. The time step size is therefore determined solely by the C.F.L. condition for convection-diffusion equations.

3.1 Numerical approach to chemicals c

The equations governing the concentration or antigens and chemicals are reaction-diffusion equations, for which we apply the conservative difference scheme to approximate.

Consider the second equation of (3.2) in 1-dimension,

$$\frac{\partial c}{\partial t} = \frac{\partial}{\partial x}\Big(D_c(c, |c_x|)\frac{\partial c}{\partial x}\Big) + g(\rho, c), \tag{3.3}$$

where the diffusion coefficient $D_c(c, |c_x|)$ is assumed to be smooth and positive in general (it is assumed to be a constant in our immune model). Let $\{x_i\}$ be a uniform partition, $x_i = i\Delta x$ and $x_{i+\frac{1}{2}} = (i + \frac{1}{2})\Delta x$. Let c_i^n denote the numerical approximation of $c(x, t)$ at the point (x_i, t_n). Equation (3.3) can be discretized by

$$\frac{c_i^{n+1} - c_i^n}{\Delta t} - \frac{1}{\Delta x^2}\big[\theta\Delta^+(\Gamma_{i-\frac{1}{2}}\Delta^- c_i^{n+1}) + (1-\theta)\Delta^+(\Gamma_{i-\frac{1}{2}}\Delta^- c_i^n)\big] = g(\rho_i^n, c_i^n) \tag{3.4}$$

where $\Delta^+ a_i = a_{i+1} - a_i$, $\Delta^- a_i = a_i - a_{i-1}$, $c_i^n \approx c(x_i, t_n)$, $\theta = \frac{1}{2}$ or 1, and

$$\Gamma_{i-\frac{1}{2}} = D\bigg(\frac{c_{i-1}^n + c_i^n}{2}, |\frac{c_i^n - c_{i-1}^n}{\Delta x}|, p^{D_c}\bigg). \tag{3.5}$$

Multi dimensional extension of scheme (3.4) on a cartesian grid is straightforward. With the data appropriately stored, conjugate gradient methods can be applied to solve c. In practice, the fully implicit scheme ($\theta = 1$) is used.

3.2 Numerical approach to population of cells ρ

The first equation in (3.2)

$$\partial_t\rho + \mathrm{div}(\chi_\rho(c, |\nabla c|)\nabla c \cdot \rho) = \mathrm{div}(D_\rho(c, |\nabla c|)\nabla\rho) + R(\rho, c), \tag{3.6}$$

which is governing the cell density ρ (in the model, most immune cells like professional phagocytes, DCs and T cells, and chemotaxis and diffusion coefficients are assumed to be constant particularly), is a nonlinear convection-diffusion equation. We use the finite volume MUSCL scheme [105] and an operator splitting to solve (3.6).

(3.6) can be approximated by the following two equations during a time step, for $t \in [0, \Delta t]$,

$$\begin{cases} \widetilde{\rho}_t + \operatorname{div}(\chi_\rho(c, |\nabla c|)\nabla c\widetilde{\rho}) = 0, \\ \widetilde{\rho}(X, 0) = \rho(X, t_n); \end{cases} \tag{3.7}$$

for $t \in [0, \Delta t]$,

$$\begin{cases} \rho_t = \operatorname{div}(D_\rho(c, |\nabla c|)\nabla \rho) + R(\rho, c) \\ \left.\dfrac{\partial \rho}{\partial \vec{n}}\right|_{\partial\Omega} = 0 \ , \ \text{and} \ \ \rho(X, 0) = \widetilde{\rho}(X, \Delta t). \end{cases} \tag{3.8}$$

Partitioning the domain uniformly as before, we approximate (3.7) by the *MUSCL scheme* which is discussed below, and approximate (3.8) by the difference scheme (3.4).

Consider equation (3.7) in 1-dimension (we use ρ instead of $\widetilde{\rho}$ for convenience)

$$\frac{\partial \rho}{\partial t} + \frac{\partial}{\partial x} f(\rho) = 0, \quad f(\rho) = \chi_\rho(c, |c_x|)c_x\rho, \tag{3.9}$$

where $\chi_\rho(c, |c_x|)$ is assumed to be smooth and nonnegative. Integrating over $\left(x_{i-\frac{1}{2}}, x_{i+\frac{1}{2}}\right)$, we have

$$\frac{d}{dt}\left[\frac{1}{\Delta x}\int_{x_{i-\frac{1}{2}}}^{x_{i+\frac{1}{2}}} \rho dx\right] = -\frac{1}{\Delta x}\left[f(\rho(x_{i+\frac{1}{2}}, t)) - f(\rho(x_{i-\frac{1}{2}}, t))\right]. \tag{3.10}$$

We may compute the chemotaxis coefficient $\chi_\rho(c, |c_x|)$ as discussed previously. The above equation can be approximated by a semi-discrete conservative scheme

$$\frac{d}{dt}\bar{\rho}_i = -\frac{1}{\Delta x}(\hat{f}_{i+\frac{1}{2}} - \hat{f}_{i-\frac{1}{2}}), \tag{3.11}$$

where $\bar{\rho}_i$ approximates the cell average of ρ in $(x_{i-\frac{1}{2}}, x_{i+\frac{1}{2}})$ and $\hat{f}_{i+\frac{1}{2}}$ is the numerical flux approximating $f(\rho(x_{i+\frac{1}{2}}, t))$. The *MUSCL scheme* first reconstructs a piecewise linear function $\hat{\rho}$ out of $\{\bar{\rho}_i\}$, such that

$$\hat{\rho}(x) = \bar{\rho}_i + S_i(x - x_i), \ \text{for } x \in (x_{i-\frac{1}{2}}, x_{i+\frac{1}{2}}), \ \text{for all } i,$$

where

$$S_i = \begin{cases} \operatorname{sign}(\Delta^+\bar{\rho}_i)\min\left(\frac{|\Delta^+\bar{\rho}_i|}{\Delta x}, \frac{|\Delta^-\bar{\rho}_i|}{\Delta x}\right), & \text{if } \Delta^+\bar{\rho}_i\Delta^-\bar{\rho}_i > 0, \\ 0, & \text{otherwise}, \end{cases} \tag{3.12}$$

and operators $\Delta^{\pm}$ are defined as before. Then we use the Lax-Friedrich flux (see e.g. [181]) to define

$$\hat{f}_{i+\frac{1}{2}} = \chi_\rho\Big(\frac{c_{i+1}+c_i}{2}, \frac{|c_{i+1}-c_i|}{\Delta x}\Big)\frac{c_{i+1}-c_i}{\Delta x}\frac{1}{2}\Big(\hat{\rho}_{i+\frac{1}{2}-} + \hat{\rho}_{i+\frac{1}{2}+}\Big) + \frac{\alpha}{2}(\hat{\rho}_{i+\frac{1}{2}-} - \hat{\rho}_{i+\frac{1}{2}+}),$$

where $\hat{\rho}_{i+\frac{1}{2}-} = \hat{\rho}\big(x_{i+\frac{1}{2}}-\big)$, α is the maximum convection speed, i.e $\alpha = \sup_x \big|\chi_\rho(c, |\nabla c|)\nabla c\big|$ at the time level t_n. The time is discretized by the forward Euler method (or by the improved Euler method).

Equation (3.8) can be solved as in the previous subsection. The time step size Δt for solving (3.2) or (3.1) is determined by the CFL condition for the hyperbolic part, such that

$$\alpha\frac{\Delta t}{\Delta x} < 1. \tag{3.13}$$

The extension of (3.11) to 2-dimension is through a dimension-by-dimension formulation, see [99]. We partition the numerical domain by a uniform rectangular mesh with mesh size $\Delta x \times \Delta x$, and the cell D_{ij} is centered at $x_{ij} = (x_i, y_j) = (i\Delta x, j\Delta x)$. As before, denote the approximate cell average of ρ on the cell centered at x_{ij} at the time t_n by $\bar{\rho}^n_{ij} \approx \dfrac{1}{|D_{ij}|}\displaystyle\int_{D_{ij}} \rho dx$. The extension of (3.11) to 2-dimension can be written as

$$\frac{d}{dt}\bar{\rho}_{i,j} = -\frac{\Delta t}{\Delta x}\Big((\hat{g}_{i+\frac{1}{2},j} - \hat{g}_{i-\frac{1}{2},j}) + (\hat{\hat{h}}_{i,j+\frac{1}{2}} - \hat{\hat{h}}_{i,j-\frac{1}{2}})\Big), \tag{3.14}$$

where

$$\begin{aligned}
\hat{g}_{i+\frac{1}{2},j} =& \frac{c_{i+1,j}-c_{i,j}}{\Delta x}\chi_\rho\Big(\frac{c_{i+1,j}-c_{i,j}}{\Delta x}, \frac{c_{i+1,j}+c_{i,j}}{2}\Big)\frac{1}{2}(\hat{\rho}_{i+\frac{1}{2}-,j} + \hat{\rho}_{i+\frac{1}{2}+,j}) \\
&+ \frac{\alpha}{2}(\hat{\rho}_{i+\frac{1}{2}-,j} - \hat{\rho}_{i+\frac{1}{2}+,j}), \\
\hat{\hat{h}}_{i,j+\frac{1}{2}} =& \frac{c_{i,j+1}-c_{i,j}}{\Delta x}\chi_\rho\Big(\frac{c_{i,j+1}-c_{i,j}}{\Delta x}, \frac{c_{i,j+1}+c_{i,j}}{2}\Big)\frac{1}{2}(\hat{\hat{\rho}}_{i,j+\frac{1}{2}-} + \hat{\hat{\rho}}_{i,j+\frac{1}{2}+}) \\
&+ \frac{\beta}{2}(\hat{\hat{\rho}}_{i,j+\frac{1}{2}-} - \hat{\hat{\rho}}_{i,j+\frac{1}{2}+}),
\end{aligned} \tag{3.15}$$

α and β are the maximum convection speed along $x-$ and $y-$ directions respectively, $\hat{\rho}$ denotes the (MUSCL) reconstructed piecewise linear polynomial of one variable defined along each horizontal grid lines as discussed above, $\hat{\hat{\rho}}$ denotes the reconstructed piecewise linear polynomial of one variable defined along each vertical grid lines, $\hat{\rho}_{i+\frac{1}{2}-,j} = \hat{\rho}(x_{i+\frac{1}{2},j}-)$. Similarly, Forward Euler or improved Euler time stepping is used to obtain a fully discretized explicit scheme.

Staggered central scheme (the NT scheme [142]) doesn't use any numerical flux function and has higher resolution for piecewise linear reconstruction.

3.3 Numerical Test

In this section, the scheme is tested by both 1-dimensional and 2-dimensional examples.

3.3.1 1-dimensional Keller-Segel equation

The numerical domain is set to be $[-2, 2]$, then we employ uniform partition with $nx = 200$ meshes and $nx = 400$ meshes and $\Delta x = \dfrac{4}{nx}$. The initial condition is set to be

$$c(x,0) = 0, \quad \rho(x,0) = \begin{cases} 10 & |x| < 1 \\ 0 & \text{else} \end{cases} . \tag{3.16}$$

We set $g(\rho, c) = \beta\rho - \alpha c$ and $R(\rho, c) = 0$. The Neumann boundary conditions

$$\frac{\partial \rho}{\partial n}\Big|_{\partial\Omega} = \frac{\partial c}{\partial n}\Big|_{\partial\Omega} = 0$$

are applied in the numerical experiments. Numerically, we test following groups of coefficients:

$$\chi_\rho = 1, D_\rho = 0, D_c = 1, \beta = 1, \alpha = 1; \tag{3.17}$$

$$\chi_\rho = 1, D_\rho = 0.5, D_c = 2, \beta = 3, \alpha = 0.5 \tag{3.18}$$

To check the L^1 stability for scheme, we use numerical integral to check the total mass of ρ on the numerical domain $[-2, 2]$. Positivity is well preserved as well.

Table 3.1 L^1 norm of population ρ (1D)

Mesh	Coefficients	L^1 at $t = 0$	L^1 at $t = 0.6$	L^1 at $t = 1.5$	L^1 at $t = 2.5$
200	(3.17)	20.0002	20.0002	20.0002	20.0002
400	(3.18)	20.0002	20.0002	20.0002	20.0002

3.3.2 2-dimensional Keller-Segel equation

For 2-dimensional simulation, we first remark that in [31], the authors conjectured that the solution of Keller-Segel equation (3.1) has two possible features, which are related to the chemotactic collapse and blowing up of ρ:

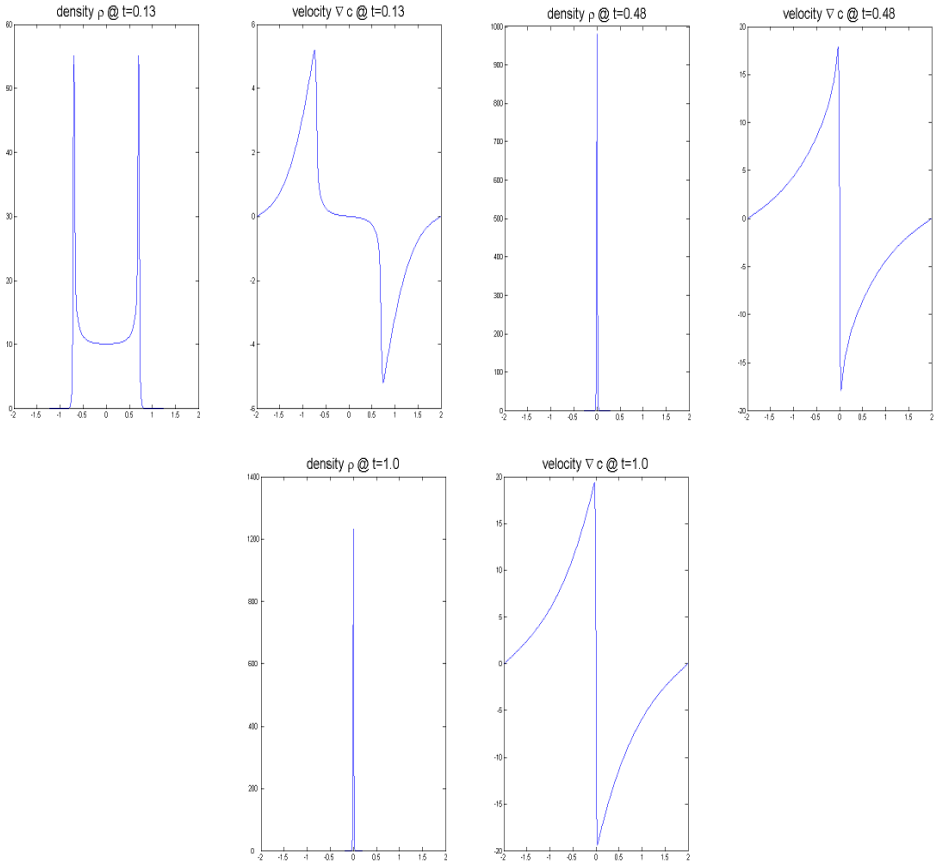

Figure 3.1 400 meshes, coefficients (3.17) are applied. Population ρ and velocity ∇c are presented at time $t = 0.13, 0.48, 1.0$ from top to bottom respectively.

- the solution ρ cannot form the blowing up profile, δ function, if the total population in Ω is less than a critical number c_Ω
- the solution ρ forms δ function singularity if the total population in Ω overwhelms the critical number

Recent studies [72, 73, 81, 140] show the existence of radially symmetric solutions for simplified system, which blows up in the center of the domain in finite time if the average of mass is greater than some critical number, i.e. $\overline{\rho_0} = \frac{1}{|\Omega|}\int_\Omega \rho_0 dx > \frac{8\pi}{\chi}$. According to our numerical simulations, we would like to stress that for original Keller-Segel equation (3.1), if the system is dominated by convection, i.e. $r = \frac{\sup|\chi|}{\inf|D|} >> 1$, then the solution will blow up

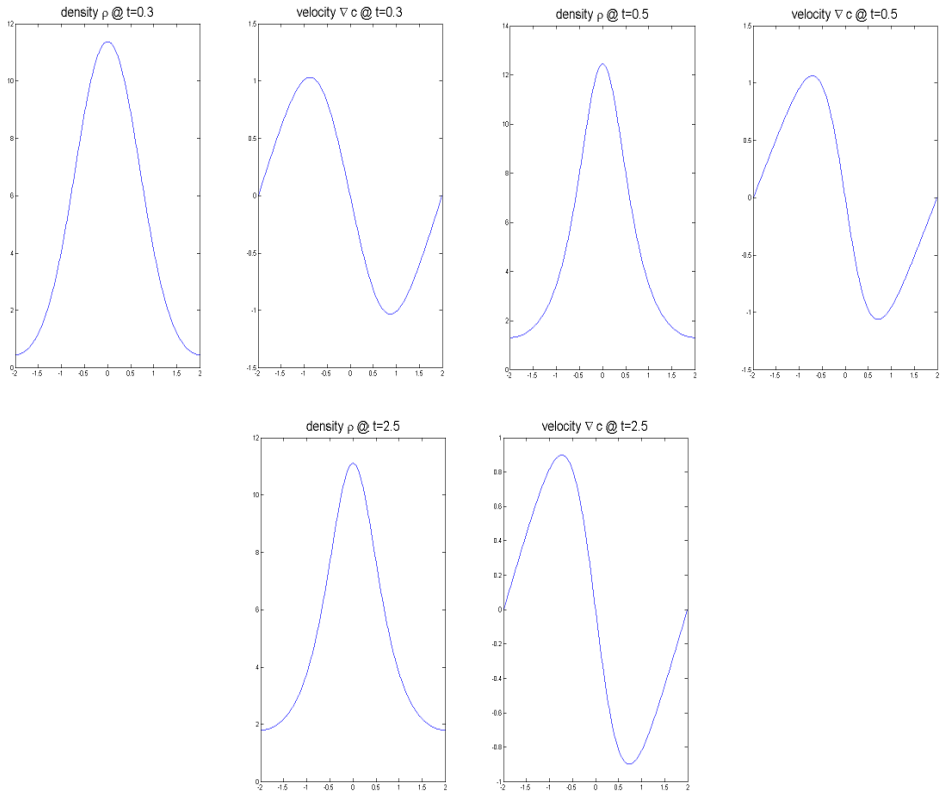

Figure 3.2 400 meshes, coefficients (3.18) are applied Population ρ and velocity ∇c are presented at time $t = 0.3, 0.5, 2.5$ from top to bottom respectively.

any way as long as $\rho_0 > 0$.

The initial condition used for experiments to verify the above conclusion is :

$$c(x, y, 0) = 0, \quad \rho_1(x, y, 0) = \begin{cases} 10, \ x^2 + y^2 \leq 1 \\ 0, \ \text{otherwise} \end{cases} \tag{3.19}$$

and the corresponding numerical domain is $[-2, 2] \times [-2, 2]$, while we uniformly partition this domain by $nx \times ny = 80 \times 80$. Two groups of constant coefficients used for simulation are:

$$\chi_\rho = 1, D_\rho = 0.05, D_c = 1, \beta = 1, \alpha = 1; \tag{3.20}$$

$$\chi_\rho = 1, D_\rho = 1.5, D_c = 1, \beta = 1, \alpha = 1 \tag{3.21}$$

where we let $g(\rho, c) = \beta\rho - \alpha c$ and $R(\rho, c) = 0$ in (3.6) as before.

We also remark that in [50, 121], the authors observe that the solution may aggregate toward boundary rather than the center of the domain given specific boundary condition or nonsymmetric initial condition. To show that our schemes can capture this phenomena well and agree with those results, we use a bias Gaussian initial condition

$$c(x,y,0)=0, \quad \rho_2(x,y,0)=\frac{\rho^0}{2\pi T}\exp\Big(-\frac{(x-x_0)^2+(y-y_0)^2}{2T}\Big) \tag{3.22}$$

where $\rho^0=10\pi$, $T=5\times 10^{-3}$ and $(x_0,y_0)=(0.1,0.1)$, and the domain is $[-\frac{1}{2},\frac{1}{2}]\times[-\frac{1}{2},\frac{1}{2}]$.

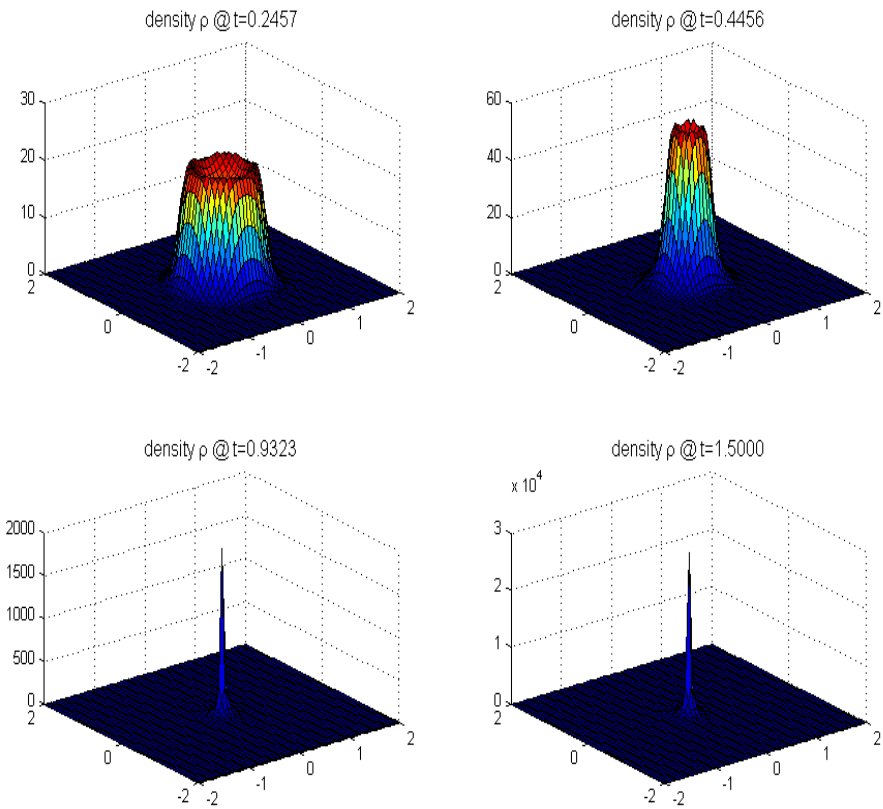

Figure 3.3 80 meshes, coefficients (3.20) are applied. Population ρ is computed subject to the initial condition (3.19). ρ is presented at time $t=0.25, 0.45, 0.9, 1.5$ from left top to right bottom respectively. Chemotactic collapse happens in the last picture.

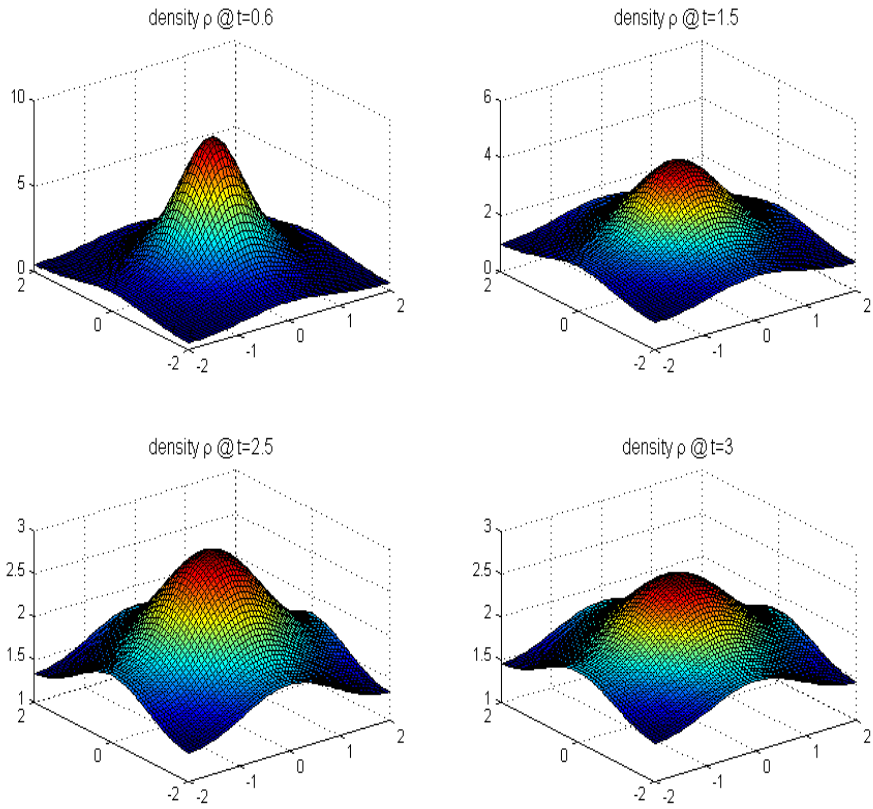

Figure 3.4 80 meshes, coefficients (3.21) are applied. Population ρ is computed subject to the initial condition (3.19). ρ is presented at time $t = 0.6, 1.5, 2.5, 3.0$ from left top to right bottom respectively. The density is under control.

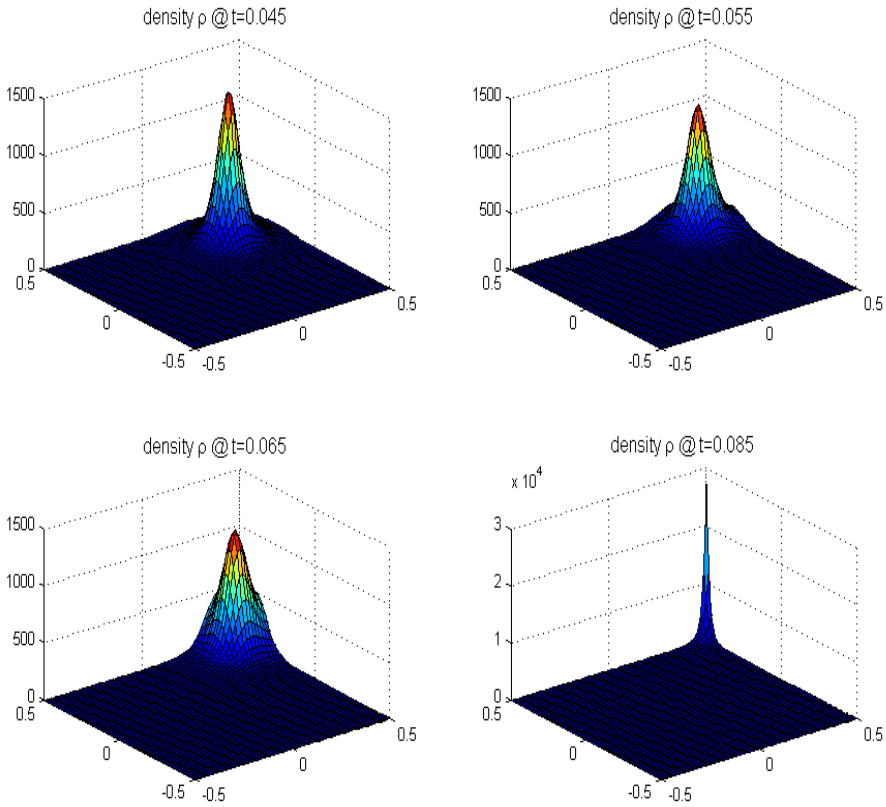

Figure 3.5 80 meshes, coefficient (3.21) are used for simulation. The initial condition used is (3.22). ρ is presented at time $t = 0.045, 0.055, 0.065, 0.085$ from left top to right bottom respectively. Nonsymmetric initial condition contributes to boundary blowing up which agrees with results in [121].

CHAPTER 4. Numerical experiments

Using the numerical scheme discussed in chapter 3, we examine the model by conducting a series of numerical experiments.

In section 4.1, we show the necessity of including regulatory T cells and DCs to recapitulate the immune stages of initiation, effector response, and resolution or equilibration. In section 4.2, we use a two-dimensional simulation to demonstrate how our T_H1 subsystem forms a persistent granuloma in response to chronic infection, whereas in the acute case the granuloma is diminished and finally eliminated. In section 4.3, we study the role of B cells and antibodies in the complete model and demonstrate that they are indispensable terms to capture a precise MHC Class II mediated responses. In section 4.4, we demonstrate that the immune response of the complete model can become highly skewed towards a T_H1 or T_H2 immune response, as well as deliver a mixed response depending upon the characteristics of the *in silico* pathogen. These results illustrate that the model is robust and can reflect appropriate MHC Class II responses to different pathogens. Finally, in section 4.5, we study the switch of subtypes of immune response during infections of *Mycobacterium avium subspecies paratuberculosis* (*Map*) in cattle based on our model and the philosophical postulate of Zinkernagel [205].

In the simulation, the experimental domain for all simulations in the one-dimensional case is the interval $[-2, 2]$, and a rectangle $[-2, 2] \times [-2, 2]$ in 2-dimensional case. For simplicity, we set that infection appears in the tissue at a radially symmetric origin with radius r such that

$$A(x, 0) = A_0(r) = A_0 \cdot 1_{\{|x| \leq r\}} \tag{4.1}$$

where constant $A_0 \geq 0$ is the initial load of particulate antigen±PAMPs. The amount of intracellular antigen and soluble antigen are naturally equal to zero at the beginning of infection. In the following experiments, we will study the local average of different immune agents at the

infection site, which is defined as

$$U_{\text{local}}(t) = \frac{1}{|\Omega_0|} \int_{\Omega_0} U(x,t)dx \tag{4.2}$$

where $\Omega_0 \subset \Omega$ is the local infection site in tissues and defined by

$$\Omega_0 = \{x \in \mathbb{R}^n \ : \ |x| \leq r_0\} \ (n = 1, 2) \tag{4.3}$$

where U represents variables in the model. Also, we investigate the temporal dynamics of immune agents in the lymph node, which is the boundary value of variables in the model.

4.1 Necessity of regulatory T cells and DCs

4.1.1 Study on T_H1 subsystem

One of our main objectives is to identify a minimal set of cells, chemical messengers, and interactions to recapitulate a functional immune system. A guiding principle is that the immune system should be robust yet tolerant of persistent infections. Furthermore, hosts should incur minimal damage, as measured by levels of inflammatory cells and cytokines, from persistent infections. It is well known that both macrophages and effector T cells play primary roles in an effective T_H1 immunity [78], thus we focus our interest on exploring the roles of the dendritic cells and regulatory T cells in this section.

For simplicity, we focus on T_H1 subsystem and temporarily exclude T_H2 cell, B cell, antibody, intracellular antigen, soluble antigen and relevant cytokines from equations (A.1)–(A.10). Furthermore, the three subsets of DCs, DE, DA, and DF, reduce to only subsets of immature and mature DCs. Instead of assuming the ability of self-replication in (A.1). we set the particulate antigen±PAMP appears at the origin in a radially symmetric region with radius r and is produced at the rate $g(x,t)$:

$$g(x,t) = \begin{cases} g_0 e^{-g_1 t}, & |x| < r \\ 0, & \text{otherwise} \end{cases} \tag{4.4}$$

where both g_0 and g_1 are non-negative constants. We distinguish chronic and acute antigen exposures by the value of g_1. If $g_1 = 0$ the particulate antigen±PAMP source is persistent,

as might be the case for a resistant, replicating pathogen; otherwise, if $g_1 > 0$ the source of antigen is transient, representing an acute infection. The subsystem is listed in the appendix A for convenience.

For the simulations in section 4.1 and 4.2, the number of meshes to partition the domain is always set as $n = 40$ for either one dimensional or two dimensional experiments.

In our first experiment, we deliver persistent antigen in the center of the one-dimensional domain by letting $g_1 = 0$, $g_0 = 8$ (units), and $r = 0.8$ in equation (4.4). Under this scenario, we investigate the temporal dynamics of the local average mass of macrophages (both resting and active), T cells (both effector T_H1 and regulatory), neutrophils and particulate antigen±PAMP.

In Figure 4.1, we plot the local average mass of neutrophils, macrophages, and T cells (both effector T_H1 and regulatory) as well as antigen load over time for the T_H1 subsystem and various further reduced models. Also, the tan dash-dot lines in the figure represent the immune response under the full model during an acute infection where $g_1 = 10$ and other conditions are as in the persistent antigen case. The complete T_H1 subsystem under persistent infection (red lines) demonstrates an early and short burst of neutrophil activity at the infection site. By 10 days after antigen delivery, there are effectively no neutrophils left. The next cell type to dominate the infection site are the macrophages, which arrive before T cells and peak five days after antigen delivery. T cell numbers peak at seven days. The cell arrival sequences agrees with that observed during *in vivo* granuloma formation [180]. Macrophages, T cells, and antigen load reach new steady state levels, also consistent with stable granuloma formation. The modeled granuloma is dominated by macrophages, which outnumber T cells by about 10:1, in agreement with *in vivo* observations [19, 141]. The newly equilibrated immune response controls antigen load 120 times lower than steady state conditions in the absence of an immune response. This outcome contrasts with acute infection, where the system approaches the initial, resting state a few days after antigen levels draw nigh zero. T cells are the slowest to disappear, likely a consequence of our failure to include an active T cell downregulation mechanism after the antigen threat has vanished.

To test the role of regulatory T cells, we remove them from the T_H1 subsystem. The dashed

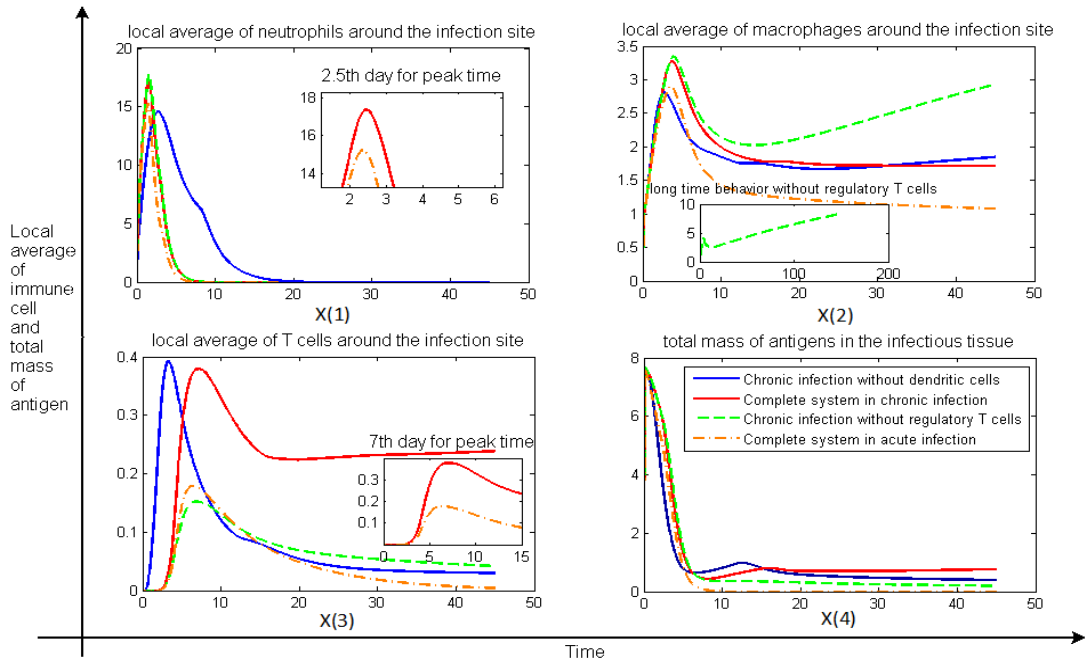

Figure 4.1 Plots X(1) to X(4) characterize the dynamics of the local mass for neutrophils, macrophages and T cells (both effector T_H1 cells and regulatory T cells) at the infection site in a T_H1 immunity during a virtual chronic infection. Inserted plots in X(1) and X(3) are highlights of peak time for neutrophils and T cells. The pathogen is defined in (4.4). This figure is from the published article [190].

green lines of Figure 4.1 display the results. Early macrophage recruitment and behavior is similar to the full model, but instead of approaching a new equilibrium, macrophage numbers increase over time. Even after 150 days, the macrophage count is still increasing (see inset plot of X(2)). This increase continues despite very low antigen loads, less than 10% of the starting conditions. The plot of antigen load over time shows that antigen clearance is efficient early in infection, but becomes increasingly inefficient, requiring more and more macrophages, as antigen levels drop. As expected, the total number of T cells at the infection site is lower because regulatory T cells are not included.

We next test the role of dendritic cells in the T_H1 subsystem. We eliminate the terms for dendritic cells and set the boundary value of effector T cells proportional to the product of total antigen mass and total macrophage mass. We justify this boundary condition by noting

that the more antigen and the more phagocytes available to transport the antigen to the lymph nodes, the more effector T cells will be primed and recruited. The results of this reduced model are shown as blue solid lines in Figure 4.1. The most important consequence of this change is the timing of macrophage and T cell recruitment to the site of infection. These two cell types now arrive simultaneously, in disagreement with the known temporal order for immune cell recruitment to granuloma [180]. The role of dendritic cells to transport antigen to the lymph nodes is a critical part of T cell recruitment, but takes time and necessarily delays T cell arrival at the infection site. Failure to capture this delay, as we have done explicitly with dendritic cells, can lead to unrealistic behavior and structure at the granuloma. Moreover, the total amount of T cells is only 2% of the macrophages when they approach equilibrium, which is lower than previously described biological system [19, 141].

With these three experiments, we conclude our modeled immune system constitutes a minimal set of immune factors that recapitulate a robust immune response, giving the dynamic behavior of both acute and chronic infections in T_H1 immunity.

4.1.2 Study on complete system

Using an artificially designed pathogen, we study the necessity of DCs and regulatory T cells for the complete model in this section. The virtual pathogen is designed to replicate and secrete antigen with the characteristics indicates in table 4.1:

Table 4.1 Characteristics of test pathogen

A_0	α_A	α_{A_p}	$\beta_{A_s\|A}$	$\beta_{A_s\|A_p}$	$p^{\text{eff}}_{A_p\|A}$	δ	$\rho_{A_p\|MA}$	n_{A_p}
10^4	0/ day	2/day	0.1/ day	0.1/ day	98%	0.12	50 / cell	1

In figure 4.2, by comparing the immune responses of a normal immune system and system without regulatory T cells up to 12 days, we notice that without regulatory T cells, the macrophage undergoes an unlimited activation even the particulate antigens has been eliminated from tissues after 5 days (figure 4.2 a(3)). As consequences of defect of regulatory T cells, the system lost the ability to inhibit the activation of macrophages and downregulation effector T cells. Without regulatory T cells: (1) activation of macrophage by T_H1 is much stronger

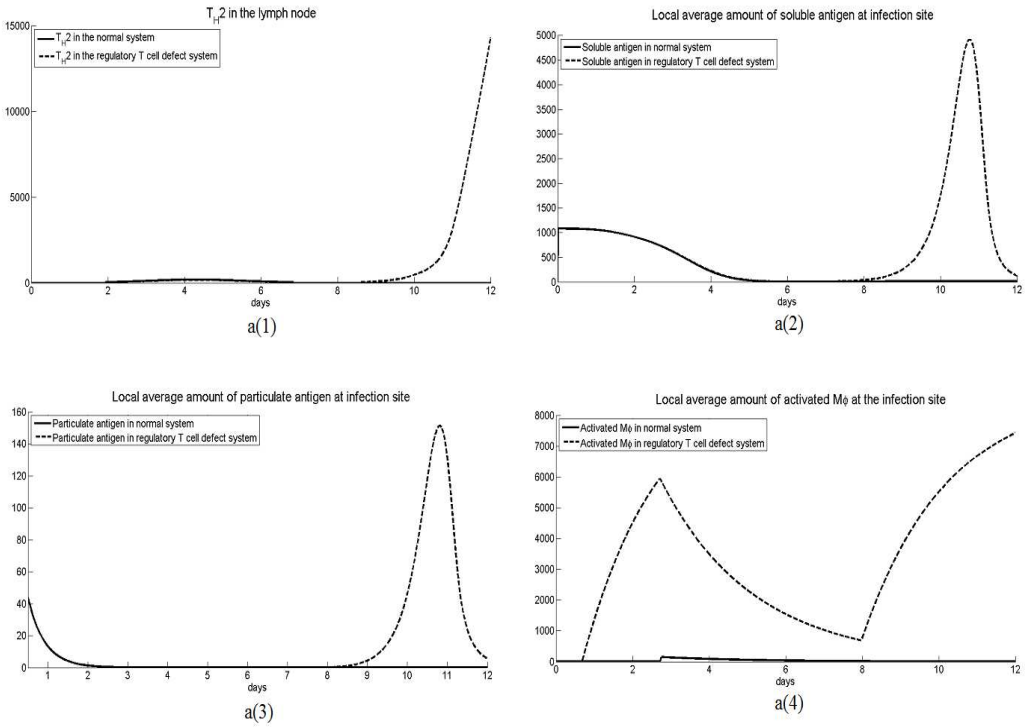

Figure 4.2 Normal immune system and system without regulatory T cells response to the pathogen described in table 4.1.

than normal system (figure 4.2 a(4)) in the sense of amount of activated macrophages; (2) as a result of cross regulation, the amount of T_H1 activated macrophages is decreasing after elimination of particulate antigens, however, macrophages are reactivated by T_H2 cells after 8 days (figure 4.2 a(1) and a(3)). The increase of the amount of intracellular antigens and subsequent rebuilt of particulate and soluble antigens in tissue (figure 4.2 a(2) and a(3)) is the result of a possible alternative activation of macrophage. Without regulatory T cells, the immune system will spontaneously induce another cycle of infections which harms the body. It concludes that regulatory T cell is necessary for a stable and self-protective MHC class II immunity.

Based on the simulations, we hypothesize that regulatory T cells may assist immune system to response against infection by intracellular pathogens through the following mechanism: on one hand, regulatory T cells suppress T_H2 cell's population by direct cell contact and therefore diminish the possibility of T_H2 cell induced alternative activation of macrophages,

and this results to a successful control of population of intracellular antigen through limiting the potential elevation of their replication rates; on the other hand, in our proposed model, regulatory T cells may deactivate the macrophages once the ratio of effector T cell cytokines and free antigens overcomes certain threshold and thus the room to contain intracellular antigen decreases, as a result, the total population of intracellular antigen will be limited and reduced. In the absence of regulatory T cells, we hypothesize that during the infection of intracellular pathogens an alternative activation of macrophage caused by T_H2 response may arrive earlier than the possible alternative activation in a T_H1 response, and therefore may lead to a poor immune response.

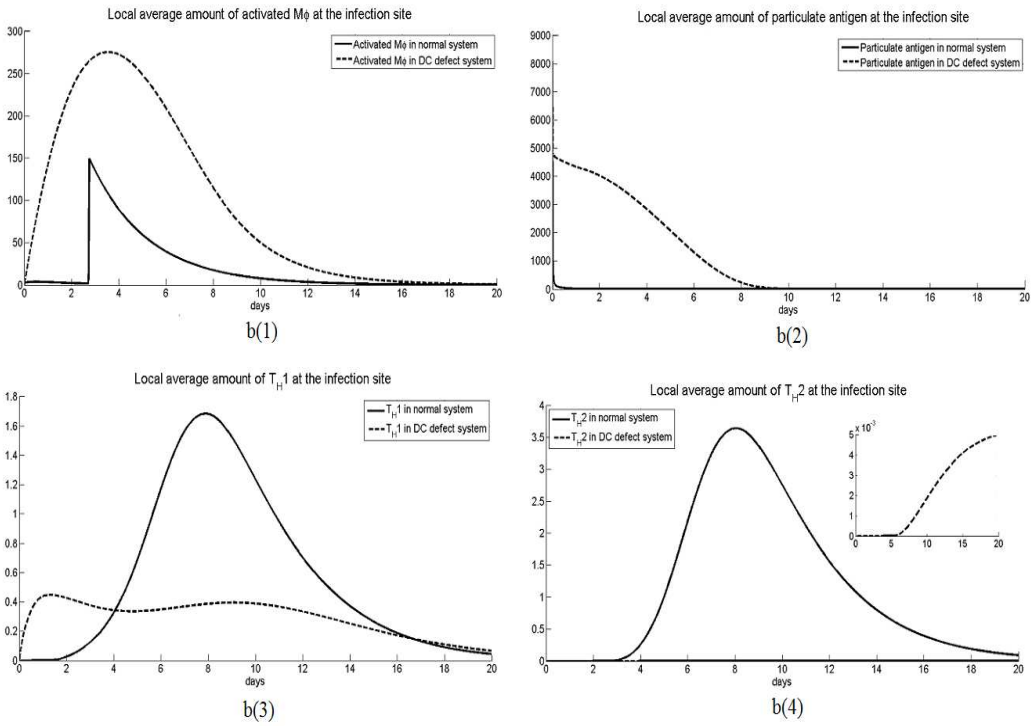

Figure 4.3 Normal immune system and system without DCs response to the pathogen described in table 4.1.

By eliminating the DCs from immune system, we observe that: (1) the timing of the immune response is disordered so that the peak in effector T cells much earlier than the activated macrophage in contrast to the normal system; (2) the amount of both T_H1 and T_H2 cells in the tissues is much less than the normal system, which results to a deficiency of antibodies; (3)

without cooperation of antibodies, the time for a broad elimination of particulate antigens in tissue is elongated. We therefore conclude that DCs is crucial for an efficient and stable MHC class II immunity.

4.2 Simulation of formation of granuloma

Granuloma formation is an outcome of a well-regulated immune response. In this section, we explore the distribution of cell types in T_H1-subset of the full model (excluding B cells, antibody, T_H2 associated immune agents) within the infection site during both chronic and acute infections. We also introduce nonsymmetric source functions for particulate antigen±PAMP and observe that granulomas form at the appropriate, now non-central location. For symmetric case, the initial antigen load is set to be

$$A(x,0) = \begin{cases} 8, & |x|^2 < 0.64 \\ 0, & \text{otherwise} \end{cases} \tag{4.5}$$

and the simulation results are shown in figure 4.4 and 4.5.

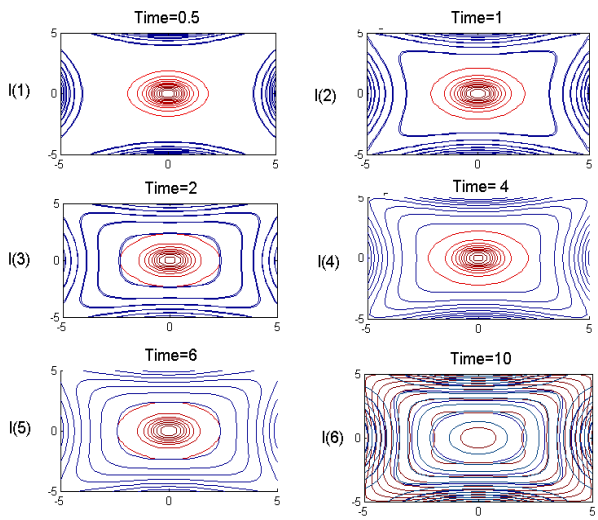

Figure 4.4 Plots l(1) to l(6) show the process of formation of the granuloma for an acute infection. The red curves represent the level sets of macrophage while the blue curves represent the level sets of total number of T cells. This figure is from the published article [190].

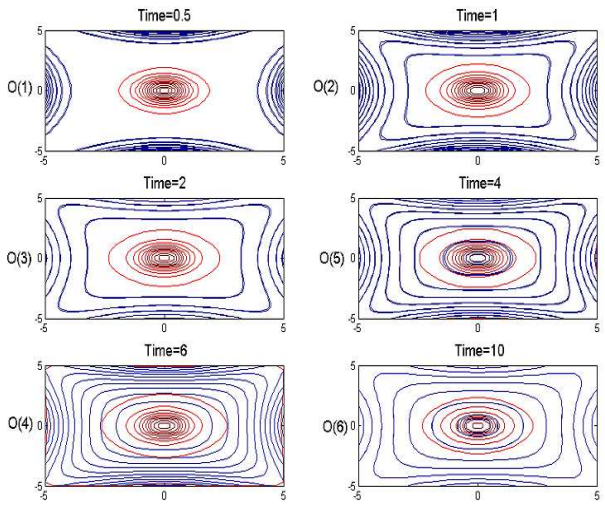

Figure 4.5 Plots o(1) to o(6) show the process of formation of the granuloma for chronic infection. This figure is from the published article [190].

A granuloma has the basic structure of macrophages surrounded by lymphocytes [78], T cells in our T_H1 subsystem. Figures 4.4 and 4.5 focus on distribution of immune cells responding to acute and chronic infection, respectively. In figure 4.4, a nascent granuloma-like structure appears during the early responses, but it quickly dissipates once antigen levels decay to zero. The disruption of structure by $t = 10$ is not merely a consequence of departing immune cells, since the density of macrophages and T cells is still high at this time.

In figure 4.5, the granuloma structure is stable. In fact, the size of the granuloma is stable from about the first time unit, although T cells will be increasing in number for several time units to come. A stable structure of macrophages and T cells is achieved by about $t = 10$.

Finally, we prescribe a non-symmetric source for particulate antigen±PAMP

$$g(x,t) = \begin{cases} k_i & x \in \Omega_i \subset \Omega \\ 0 & \text{otherwise,} \end{cases} \tag{4.6}$$

where $k_i = 2^i$ for $i = 1, 2, 3$; and Ω_i are the small disks in the tissue Ω such that

$$\begin{aligned} \Omega_1 &= B(x_0^1, r_2) = B((1, -1), 0.25), \\ \Omega_2 &= B(x_0^2, r_2) = B((-2, 2), 0.25), \\ \Omega_3 &= B(x_0^3, r_3) = B((0, 0), 0.25). \end{aligned} \tag{4.7}$$

Notice that granuloma is gradually formed in the neighborhoods of infection sites Ω_3 and Ω_2 (refer to p(3) and p(4) in figure 4.6).

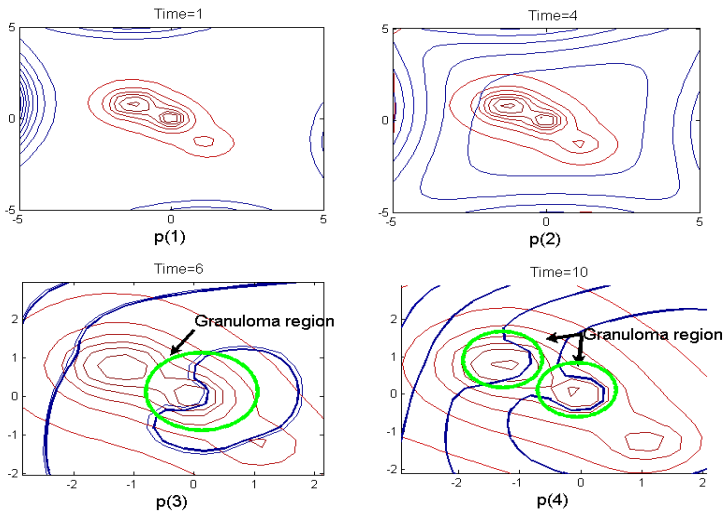

Figure 4.6 Plots p(1) to p(4) show the process of formation of the granuloma for a chronic infection with non-symmetric initial value of antigens in the infectious tissue. Green circles highlight of granuloma regions. The pathogen is defined in (4.6)-(4.7). This figure is from the published article [190].

4.3 Necessity of B cell and antibody

For the simulation in this section and section 4.4, we partition experimental domain $\Omega = [-2, 2]$ into $n = 100$ subintervals.

To appropriately respond to a pathogen that secrets large amounts of soluble antigen, antibodies and B cells are required [78]. Here we focus our interest on justifying the roles of

B cells and antibodies during the T_H2 response in our model. In numerical experiments to justify the functions of B cell and antibody, we define an intracellular pathogen that leads to a chronic infection by setting the following characteristics, whose definitions are discussed in section 2.1 in chapter 2:

Table 4.2 Characteristics of test pathogen

A_0	α_A	α_{A_p}	$\beta_{A_s\|A}$	$\beta_{A_s\|A_p}$	$p^{\text{eff}}_{A_p\|A}$	δ	$\rho_{A_p\|MA}$	n_{A_p}
10^3	0/ day	2/day	0.5/ day	0.5/ day	98%	0.12	50 / cell	1

In the context of the *in silico* pathogens that we test in the series of numerical experiments described here the pathogen defined by the characteristics in Table 4.2 replicates mildly, secretes certain amount of soluble antigens, has a low survival probability and can reach relatively high numbers within an infected cell. We expect the characteristics of this type of pathogen to trigger a mixed T_H1 and T_H2 response as result of the soluble antigen and the survival rate.

In both figures 4.7 and 4.8, the solid lines represent the results for normal system, the dash lines represent the results for a system with defect on activating B cells and the dot red lines represent results for a system with defect on producing antibodies. The results demonstrate a requirement for B cells and antibodies for an appropriate immune response.

The plot a(1) in figure 4.7, demonstrates that: (i) in the absence of activated B cells, T_H2 cells are not activated; (ii) in the absence of antibodies, the activation of T_H2 cells is dramatically weakened and delayed, and they demonstrate an abbreviated response which fails to be maintained even in the presence of large amounts of soluble antigens (figure 4.7 a(2)). Therefore, in our model antibodies are important for generating and maintaining a T_H2 response. Plot a(2) in figure 4.7 illustrates that: in the absence of either B cells or antibody, the system is not able to respond to the soluble antigen. Under these conditions particulate antigens are hard to be eliminated completely from tissue, as they are no longer removed as immune complexes (figure 4.7 a(3)). Likewise, without B cells or antibodies, the populations of mature DCs and activated macrophages reach an equilibrium at lower levels during the 3 weeks infection than normal system (figure 4.7 a(5) and 4.8 b(2)).

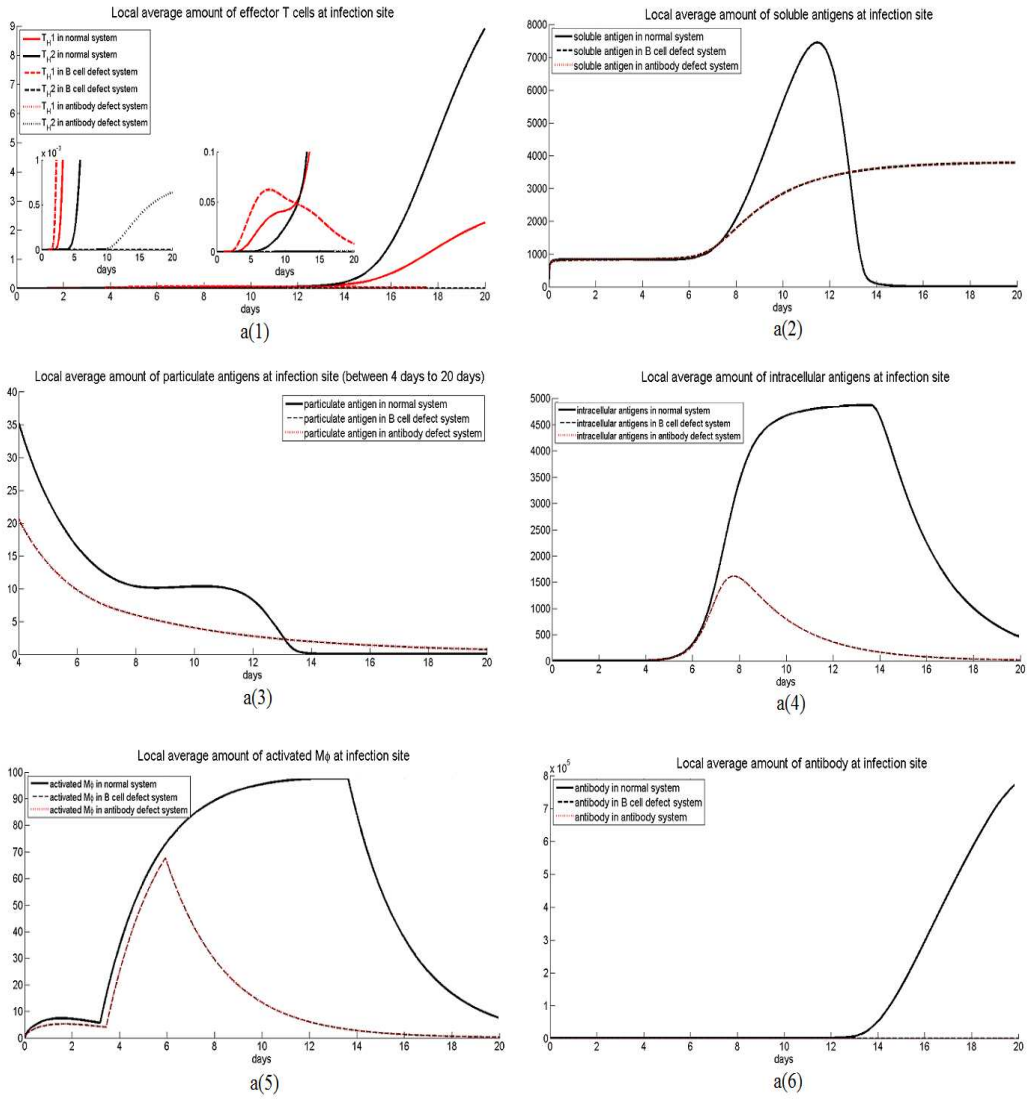

Figure 4.7 Immune model infected by the pathogen described by characteristics in table 4.2. Plot a(1) to a(6) characterize the dynamics of the local average (refer to (4.2)) for effector T cells, antigens, macrophage and antibody for the pathogen defined in table 4.2. The inserted plots in a(1) are dynamics of the effector T cells in small scales.

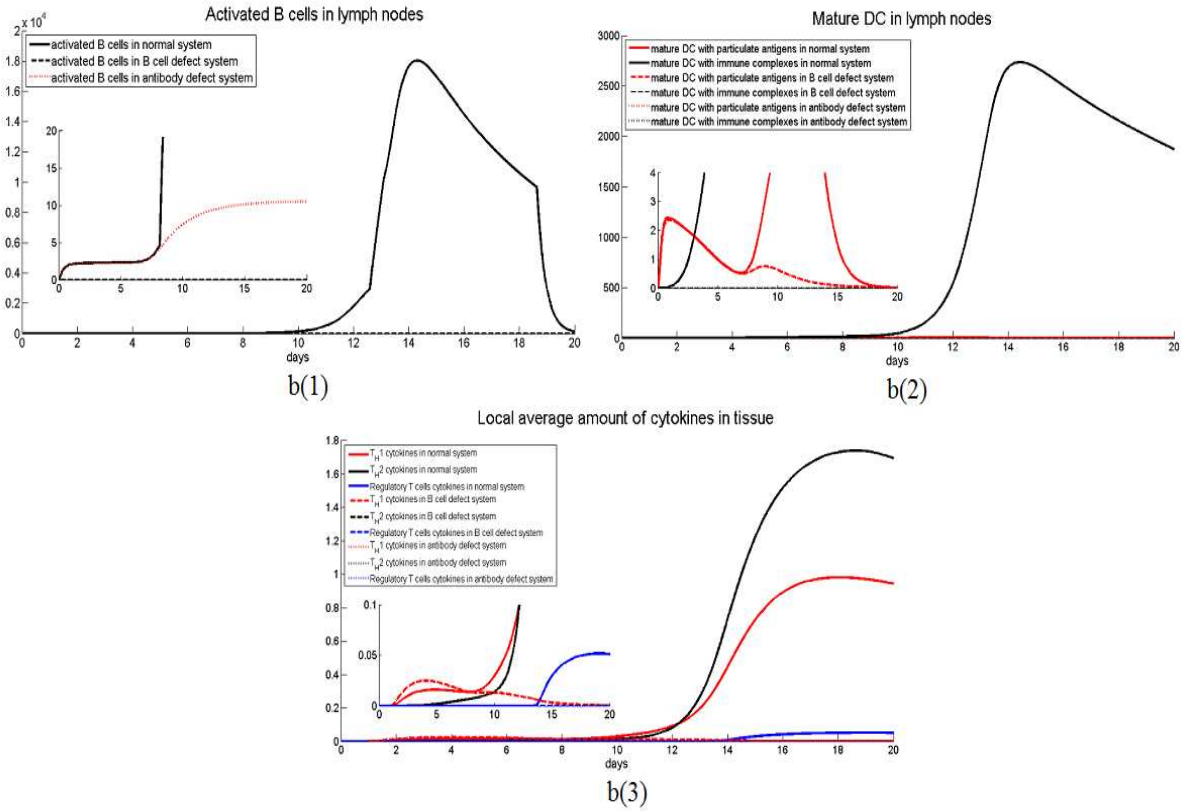

Figure 4.8 Immune model infected by the pathogen described by characteristics in table 4.2. Plot b(1) to b(3) characterize the dynamics of the level of B cells and activated B cell in the lymph nodes, and the local average for different chemicals in tissues. The inserts in b(1)-b(3) picture in small scale.

The plots b(1) and b(2) in figure 4.8, which demonstrate the level of activated B cells and mature DC in the lymph node, further illustrate that a T_H2 response is not activated or fails to function in the absence of B cells and antibodies, respectively. Furthermore, the plot b(3) reflects the dynamics of corresponding cytokines at the infection site. Deletion of B cells or antibodies both leads to altered development of regulatory T cells. Additionally, through observing a(1), a(4), and a(5), the numerical experiments show that by introducing large number of immune complexes in the system, the B cells and antibodies can constantly

support a stable T_H1 response and/or promote an even stronger T_H2 response, and therefore may contribute to the increase of the amount of intracellular antigen with this model pathogen by alternative activations. In our model antibodies and B cells limit the amount of particulate antigens and soluble antigens and promote a regulatory T cell response with lower levels of activated macrophages and mature DCs in tissue at equilibrium, as both types of antigens are processed as immune complexes during 3 weeks infection.

We conclude that B cells and antibody are necessary for our model system to generate an appropriate immune response to soluble antigens, and the effect of B cells and antibody on T_H1 responses are similar.

4.4 Complete immune response to various pathogens

In this section, we determine if the proposed model can respond appropriately to a variety of *in silico* pathogens. We model four different artificially defined pathogen "types". The first is the intracellular pathogen modeled in Table 4.2, that has a mix of $T_H1 - T_H2$ type antigens. The second has high amounts of particulate, T_H1 associated antigens and is killed with relatively high efficiency and should generate a skewed T_H1 response. The third secretes high amounts of soluble antigen and is not an intracellular pathogen and should generate a skewed T_H2 response. For completeness, we challenge the model with a pathogen that should have the characteristics of an acute infection. And finally, numerical simulation of formation of granuloma is presented. The results of these numerical experiments examine the robustness of the model to challenge with a wide array of *in silico* pathogens.

4.4.1 Mixed $T_H1 - T_H2$ responses in 3 weeks infection

The numerical experiments to demonstrate the models response to a mixed $T_H1 - T_H2$ response have been shown in the section 4.3 in figures 4.7, 4.8 (solid lines) and 4.9. For this artificially-defined pathogen there are four identifiable phases, the details of the models response in the experiment are summarized as follows:

phase 1 (up to 3 days): the innate response recognizes particulate antigen giving rise to

chemokine peak that is derived from neutrophils and activated macrophages. The activated macrophages accumulate in tissues in about $t = 3$ days (figure 4.7 a(5)); this is closely followed by early period of T_H1 cell recruitment by chemokines after their activation by mature DCs (inserts in figure 4.7 a(1) and figure 4.8 b(2)). This phase is driven by the presence of particulate antigen±PAMP and corresponding responses by neutrophils and macrophages.

phase 2 (3 days to 10 days): with the up-regulation of T_H1 cells the amount of activated macrophages increases significantly (figure 4.7 a(5) and inserted plot in a(1), insert plot in figure 4.8 b(3)) for about 7 days. During this same period, the amount of particulate antigen in the tissue keeps decreasing, as it is processed by DCs (insert in figure 4.8 b(2)). However, as a consequence of constantly increase of activated macrophages in tissue, surviving intracellular antigen ultimately increases the amount of soluble antigen in the tissue (figure 4.7 a(2) and a(4)). The load of particulate antigen in the tissue also experience a balance during this period (figure 4.7 a(3)). This phase is mediated by the continuously recruitment of mature DCs, T_H1 cells and activated macrophages. It is noted that during this phase, T_H2 cells and associated immunity are developed (insert plots in figure 4.7 a(1), figure 4.8 b(1) and b(2)).

phase 3 (10 days to 15 days): T_H2 immunity is fully developed and a mixed type of immune responses is observed. Classical and alternative activation of macrophage coexist in the system (figure 4.7 a(5) and figure 4.8 b(3)). The amount of activated macrophage and intracellular antigen reaches its maximum at about the 15th day (figure 4.7 a(4) and a(5)). As the amount of antigen reaches its highest point the T_H1 response reaches a maximal level with mature DCs and activated macrophages reaching their peaks during this phase (figure 4.7 a(5) and insert plot in figure 4.8 b(2)). Populations of T_H2 cells and B cells then experience a dramatic growth after the 11th day and a concomitant increase in antibodies (figure 4.7 a(1), a(6) and figure 4.8 b(1)). This phase is driven by the accumulation of large amounts of soluble antigens (figure 4.7 a(2)) in the presence of an established T_H1 response.

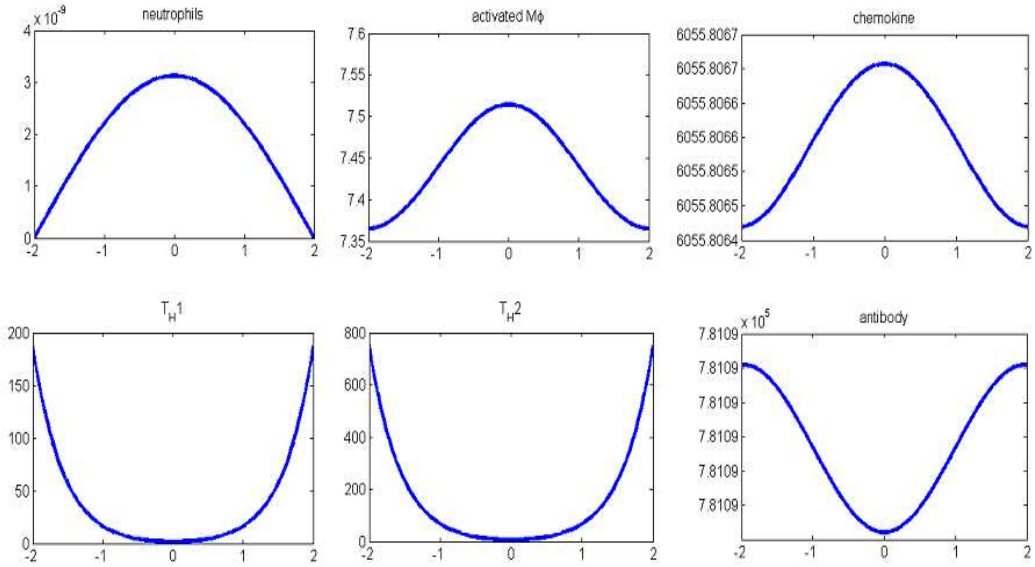

Figure 4.9 Spatial distribution of of immune agents in the mixed $T_H1 - T_H2$ response to the pathogen defined in Table 4.2 at time $t = 20$ days. Notice that few neutrophils remain in the tissue, and the macrophage, chemokine, antibody are uniformly distributed. Distributions of effector T cells are caused by mixing effect of diffusion, continuously recruitment and cross-regulation.

phase 4 (after 15 days): this last phase is dominated by a T_H2 response that is the result of increasing soluble antigens, leading to a dramatic dynamics in activated B cells (figure 4.8 b(1)), and the further activation of T_H2 cells (figure 4.7 a(1)). The number of T_H2 cells increases as T_H1 cells are subsequently suppressed (figure 4.7 a(1)) due to the cross-regulation with T_H2 cells. Similar dynamics occurs to the associated cytokines (figure 4.8 b(3)). Anti-inflammatory cytokines from regulatory T cells increases over this time as a combining result of the generation of a T_H2 response and start of the elimination of soluble antigen from the system with its conversion to immune complexes (insert in figure 4.8 b(3)). This leads to a decrease in the amount of activated macrophages, and results in the gradual decline of the average load of intracellular antigens at the infection site (figure 4.7 a(4) and a(5)). The average loads

of soluble and particulate antigens in the tissue (at the infection site) are controlled by the function of large amount of antibodies (figure 4.7 a(2), a(3) and a(6)). Therefore, with the appearance of antibodies, the immune system responds to the infection by moving towards an equilibrium dominated by an anti-inflammatory response, since persisting intracellular antigen is always able to secrete soluble antigen.

The above numerical results validate that the proposed model is able to generate a mixed $T_H1 - T_H2$ response [78, 183, 195]. It is noted that there are few neutrophils staying in the tissue as the system approaches its immunobiological equilibrium. Furthermore, spatial distribution of the immune agents in figure 4.9 implies that the mixed $T_H1 - T_H2$ response that results from this artificially defined pathogen does not support granuloma formation at equilibrium, as the activated macrophages, antibodies and chemokines are homogeneously distributed. Comparing figure 4.10 and figure 4.11 infer that antibodies, particularly, the T_H2 associated antibody (such as IgG2), function to stabilize the immune response to this tested *in silico* pathogen, in contrast to an organized granuloma (see section 4.2 and subsection below) in T_H1 immunity.

4.4.2 Skewed T_H1 responses

In figure 4.10 and 4.11, the simulation reflects the model's response against an artificial pathogen that secretes only small amounts of soluble antigen and therefore should induce a skewed T_H1 response. This *in silico* pathogen are described by characteristics listed in Table 4.3.

Table 4.3 Test pathogens' characteristics (figure 4.10) and 4.11

A_0	α_A	α_{A_p}	$\beta_{A_s\|A}$	$\beta_{A_s\|A_p}$	$p^{\text{eff}}_{A_p\|A}$	δ	$\rho_{A_p\|MA}$	n_{A_p}
1×10^4	0/ day	6/day	10^{-3}/ day	10^{-3}/ day	98%	0.12	100 / cell	2

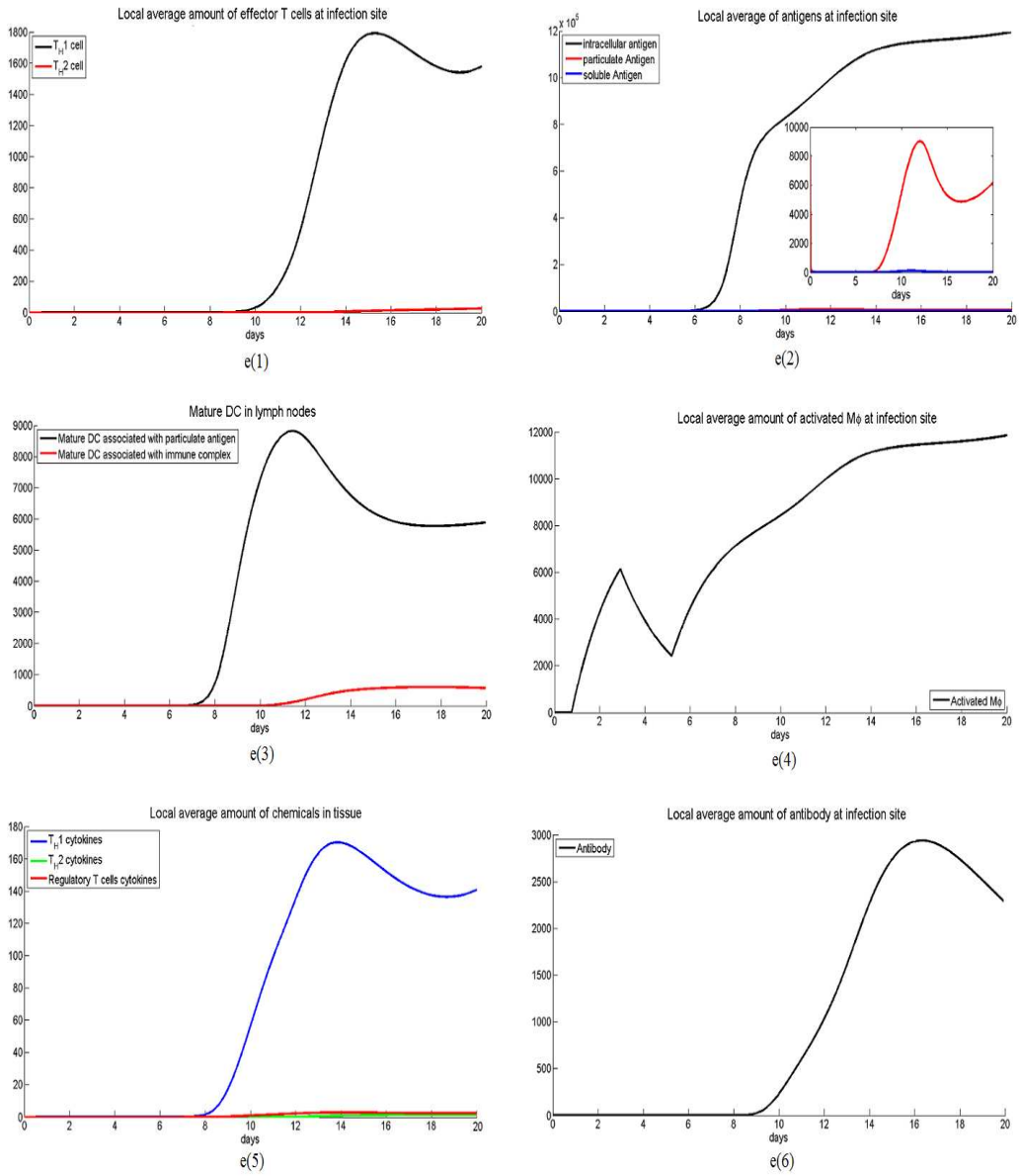

Figure 4.10 Immune model infected by the pathogen defined in Table 4.3. Plot e(1), e(2), e(4) and e(5) are the temporal dynamics of local average of effector T cells, antigens, activated macrophages and chemicals; e(3) and e(6) are the level of mature APCs (including DCs and activated B cells) in the lymph node.

The numerical experiments illustrate that a skewed T_H1 response emerges in tissue within

20 days with significantly larger numbers of T_H1 cells and their associated cytokines (figure 4.10 e(1), e(5))). In this iteration of experiment, macrophages undergo innate activation up to the 3rd day and the amount of activated macrophages decrease in the tissue as a result of elimination of most of the particulate antigens (figure 4.10 e(2) and e(4)). Dendritic cells promote the activation of effector T cells in the lymph node thoroughly after the 5th day (figure 4.10 e(3)), following which, the classical activation of macrophage by T_H1 cells is completely triggered. The amount of intracellular antigens increases rapidly along the continuously activation of macrophages. As a result of intracellular antigen increasing, an increase of particulate antigens in tissue is observed (figure 4.10 e(2)). Under the cooperation of activation macrophage and T_H1 antibodies, the level of particulate antigens in tissues is controlled after its second peak since the initial infection (figure 4.10 e(2) and e(6)). Primarily activated by mature DC with immune complexes, there are some activated B cells in the lymph node with a corresponding amount of T_H1 associated antibody present in the tissue (figure 4.10 e(6)).

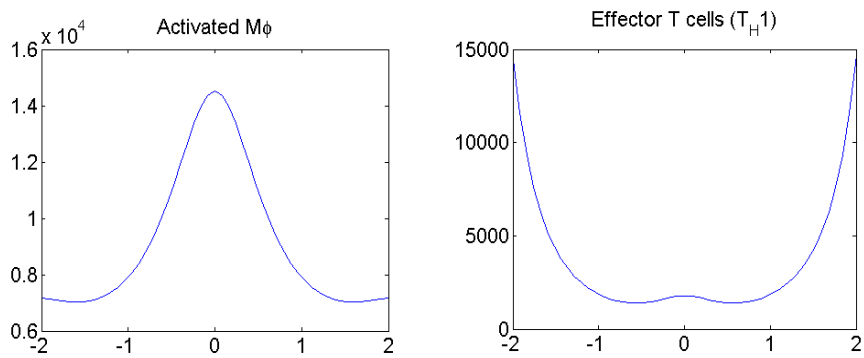

Figure 4.11 Immune model infected by the pathogen defined in Table 4.3. The plots are the spatial distribution of immune cells capturing granuloma information as the system approaching to equilibrium ($t = 20$ days).

In addition, an observable granuolma structure is formed when the immune system approaches equilibrium (figure 4.10 e(2) and e(4), 4.11). At the infection site in tissues, activated macrophages are surrounded by effector T cells, and the level of effector T cells in lymph nodes

is high. These results are broadly consistent with the immunobiological facts of a typical T_H1 response against pathogens such as *Mycobacterium* [109, 195]. These results demonstrate that the model can generate a skewed T_H1 response that stabilizes the immune system with the formation of a granuloma in response to some persistent pathogens.

4.4.3 Skewed T_H2 responses

Some pathogens, such as parasitic worms, do not replicate in the host but secrete relatively large amounts of soluble antigen that induce a dominant T_H2 response. This type of pathogen is often large and professional phagocytes or APCs are not able to engulf them or efficiently kill them through other means. Also there may not necessarily be large numbers of these types of pathogens within the host. The corresponding characteristics for such an artificially defined pathogen is listed in the Table 4.4. In addition, we assume that this type of pathogens can not be engulfed or processed by immune agents such as professional phagocyte or antibody, and the spatial movement of these pathogens are small comparing with immune agents.

Table 4.4 Test pathogens' characteristics (figure 4.12)

A_0	α_A	α_{A_p}	$\beta_{A_s\|A}$	$\beta_{A_s\|A_p}$	$p^{\text{eff}}_{A_p\|A}$	δ	$\rho_{A_p\|MA}$	n_{A_p}
1×10^4	0/ day	0/day	6/ day	6/ day	0%	0.12	NA	2

Besides the features described in table 4.4, our pathogen will not be eliminated by any professional phagocyte or antibody. Results of numerical experiments in figure 4.12 reflect several features of a skewed T_H2 response. A large number of T_H2 cells are generated (figure 4.12 f(1)) with corresponding high concentrations of T_H2 cytokines (figure 4.12 f(5)) and a large amount of antibodies (figure 4.12 f(4)). For this iteration of experiment, the persistent existing pathogen keeps secreting large amount of soluble antigens, following by successful initiation of T_H2 response at the 4th day, a very efficient clearing of soluble antigen by antibody (figure 4.12 f(2) and f(4)) is observed.

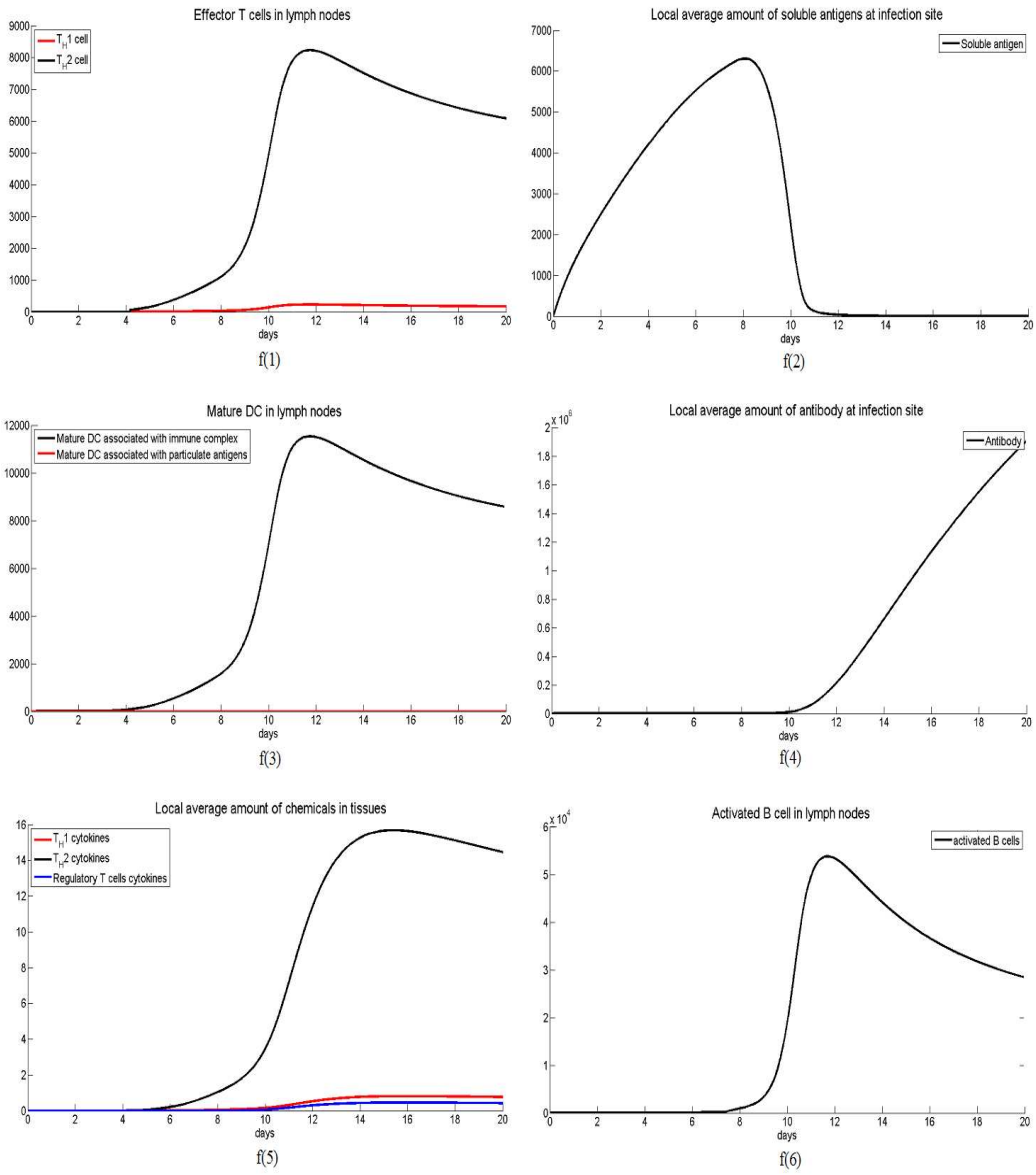

Figure 4.12 Immune model infected by the pathogen defined in Table 4.4. Plot f(1), f(2), f(4) and f(5) are the temporal dynamics of local average of the effector T cells, antigens, antibodies, and chemicals; f(3) and f(6) are the value of mature APCs (including DCs and activated B cells) in the lymph nodes.

Once produced by activated B cells, the amount of antibody stays on a stable level for long

time and leads to the inhibition of soluble antigen spreading in tissue after the 12th day (figure 4.12 f(2) and f(4)). There are some low levels of T_H1 cells that are activated by the mature DCs associated with immune complexes and their chemokines (figure 4.12 f(1), f(3) and f(5)). There is a dramatic increase in the amount of activated B cells and a gradual decrease because of the persistence of the producer of soluble antigens (figure 4.12 f(6)). These results are broadly consistent with the pathology of parasitic worms, such as *Nippostrongylus* [109, 110, 195], and demonstrate the capability of the model to mimic a T_H2 response against certain pathogens.

4.4.4 Complete system responses to acute infection

For the purpose of completeness, an acute infection with an intracellular pathogen is studied to validate that the model is robust to a wide range of artificial pathogens. To define a pathogen inducing an acute response mediated by both T_H1 and T_H2 subsystems, the characteristics listed in Table 4.5 are used. This type of antigen has a zero survival probability, in other words the immune system can readily clear the antigen successfully. The virtual pathogen used to mimic an acute infection has certain secretion rate of soluble antigens.

Table 4.5 Test pathogens' characteristics (figure 4.13)

A_0	α_A	α_{A_p}	$\beta_{A_s\|A}$	$\beta_{A_s\|A_p}$	$p^{\text{eff}}_{A_p\|A}$	δ	$\rho_{A_p\|MA}$	n_{A_p}
1×10^4	0/ day	2/day	0.1/ day	0.1/ day	100%	0.12	NA	2

From the numerical experiment, we can observe that once recognized by the immune system, particulate antigens are quickly cleared by a relatively small number of activated macrophages (and neutrophils also), and the small amount of soluble antigens are gradually cleared by mixed types of antibodies (figure 4.13 t(1)-t(2) and t(2)-t(4), respectively). Starting from the 6th day, the populations of activated macrophages in the tissue and matured APCs (including dendritic cells and activated B cells) in lymph nodes decrease exponentially along the successfully elimination of particulate antigens and soluble antigens (figure 4.13 t(1), t(3) and t(6)). T_H1 immunity dominates the early period of immune response to focus on cleaning the particulate antigens, and starting after the 3rd day T_H2 immunity quickly dominates the

immune response to clean the soluble antigens by further promoting antibody productions (figure 4.13 t(5)). Secreted by activated B cells, possible mixed types of antibodies (both T_H1 and T_H2 type) stay in the tissue to protect the body after the cycle of immune response (figure 4.13 t(4)).

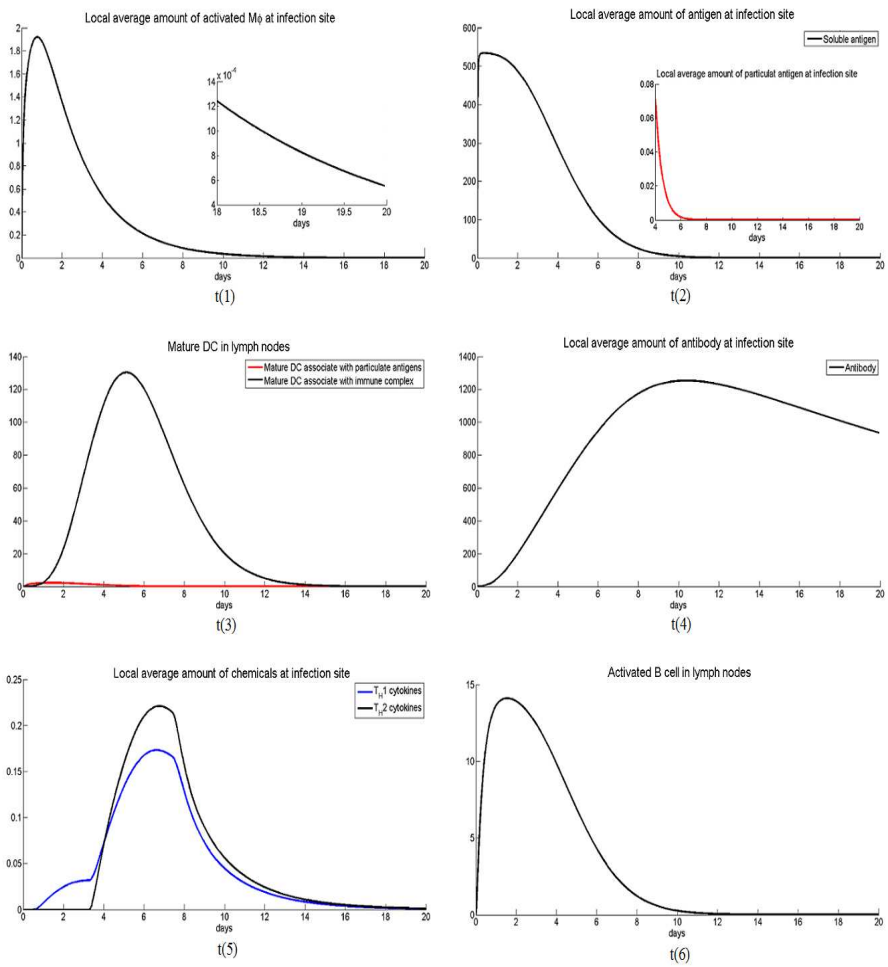

Figure 4.13 Immune model infected by the pathogen defined by table 4.5. Plot t(1), t(2), t(4) and t(5) are temporal dynamics of local average of activated macrophages, antigens, antibodies and T cell cytokines at the infection site. t(3) and (6) are the mature DC and activated B cell's dynamics in lymph nodes. Insert in t(2) is the local average amount of particulate antigens at the infection site.

Although different pathogen characteristics would undoubtedly contribute to different phenotypic immune responses during an acute infection, the numerical experiment in figure 4.13

clearly demonstrates the essential phenomena that antigen is quickly cleared by a corresponding immune response and system tends towards a resting state gradually.

By the series of numerical experiments above, we therefore validate that the proposed complete model can mimic MHC Class II mediated immune responses against diverse pathogens.

4.5 Study on *Mycobacterium avium subspecies paratuberculosis* infection

As we have already discussed in the introduction, motivated by Zinkernagel's famous postulate that the immune response is determined by the dynamics of antigen load [205], the model we proposed in chapter 2 assumes that characteristics of antigen inherently determine the phenotype of immune response and the characteristics of antigen include amount, spatial distribution, motility, replication rate, secretion rate, survivability and capacity. We attempt to use our model to generate specific hypothesis that can be evaluated by experiments. In this section, we are going to study and recapitulate the phenomena in complex immunity associated with Johne's disease based on our model.

Johne's disease, which is first described by Johne and Frothingham [88], is the clinical outcome of a chronic and progressive infection with *Mycobacterium avium subspecies paratuberculosis* (*Map*) in cattle. This infection is characterized by initial T_H1 mediated immune control, which then switches to T_H2 mediated immunity, and concomitant loss of control of the infection [169]. It is complicated and usually difficult to reproduce experimentally due to an extended post-infection interval of up to $2-3$ years before clinical signs may appear. Existing data about both the organism and the host response have been determined by *in vitro* studies, and large amount of the analysis of the immune response during experimental and natural infection provide a rough schematic picture of progression of infection of *Map*. During the early stage of infections, granulomas are very difficult to locate, which reflects a very low pathogen burden. Like *M. tuberculosis*, and *M. bovis*, *Map* persists within monocytes and macrophages through interference with phagosomal trafficking. *Map* resides, actually hides, in a phagosomal compartment that does not acidify and retains markers of early maturation stages [76, 100], and may promote secretion of anti-inflammatory cytokines, which is the regulatory T cell se-

creted cytokine in our model [200]. However, experimental facts *in vitro*, demonstrate that induction of classic activation of macrophages leads to significant *Map* killing [75], and suggest that there is sufficient local cell-mediated responses during the early period post-infection *in vivo* to maintain classic macrophage activation that limits *Map* proliferation. This is supported by strong proliferation and production of IFN$-\gamma$ from lymphocytes harvested from early *Map* infected cattle in response to *Map* antigens [129].

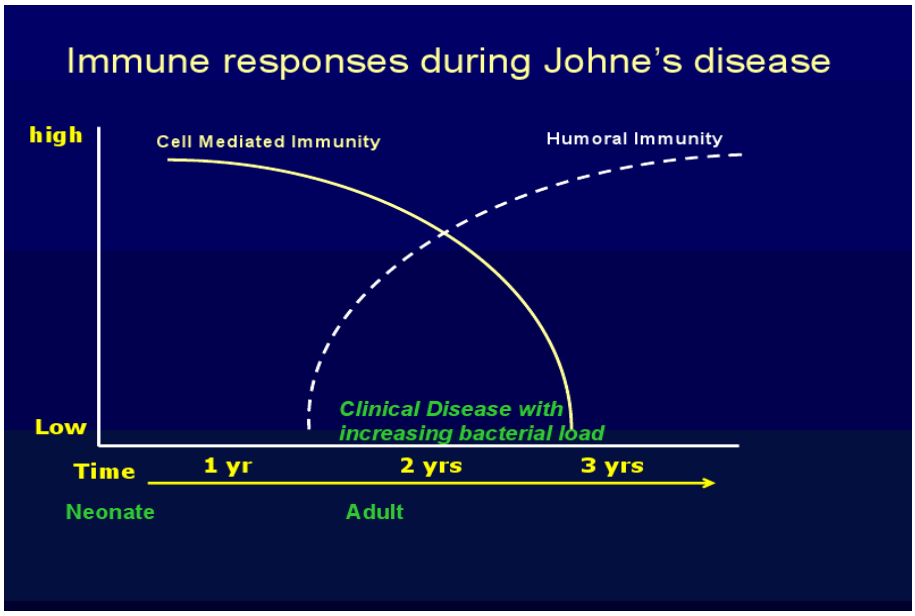

Figure 4.14 Schematic of immunity switch of Johne's disease.

Onset of clinical disease correlates with a deterioration of cell-mediated immunity leaving a dominant humoral immune response and high levels of circulating ineffectual anti-*Map* antibodies [187]. This switch is highlighted in the schematic 4.14. The mechanism of this switch has attracted much attention since it is related to the development of an immunological switch in classical TB infection in human [187, 200], however, the immune variables that lead to this switch are unknown. With limited knowledge on the mechanism, current theories focus on potential immune dysregulation through an altered balance of immune activation v.s. immune regulation and the subsequent switch of effective immunity. Recently, it is identified that *Map* p34 protein is a B cell epitope that is recognized by antibodies from *Map*-infected cattle [147], and, in addition, *Map* secretes multiple antigens that are recognized by antibodies from in-

fected cattle with clinical syndromes [163]. These suggest that T_H2 dominant epitopes and *Map* secreted antigens may influence the development of the humoral response. The switch to a humoral response is associated with progression of infected animals to multibacillary disease with very high shedding of bacteria in the feces. The pathology of this stage of disease is characterized by widespread T_H2 driven granulomatous inflammation characterized by extensive macrophages and lymphocytes infiltration into the mucosa of the intestine without clear organization. Lesional macrophages contain large numbers of intracellular bacilli. Macrophages in granulomatous inflammatory foci typically lack markers of classic macrophage activation, inducible nitric oxide synthase [77]. This suggests that these heavily infected macrophages maintain a non- or alternatively-activated phenotype.

The initial infection dose of the *in silico* pathogen designed to mimic infection of *Map* is as low as 8000 units. The pathogen have a 1% rate of survival in classically activated macrophages, an approximate doubling time of 1.5 days, a certain amount of soluble secreted antigen at 1000 units/day/pathogen and a high carrying capacity within macrophages of 300/macrophage. According to (2.2) and (2.10) within alternatively activated macrophages, the *in silico* pathogen has doubling time and secretion rate of soluble antigen increased to 3 hours and 3000 units/day/pathogen respectively, and the rate of survival increased to 50%. The infection site is numerically a small disk with diameter equal to 0.2 cm, where the pathogen is homogenously distributed.

Local amount of intracellular particulate antigen in the tissue remains low and stable at $1 - 2 \times 10^3$ units for 2 years as shown in W(1) in figure 4.15. This stable level experiences a thorough transition at 25-26 months post-infection with a 1000 fold increase in the pathogen over about 2 months (W(1) in figure 4.15). The minor B cell response and small amounts of antibody produced in phase 1 and 2 are related to the T_H1 cell response that dominates these phases (W(3) and W(4) in figure 4.15). A slowly increasing amount of soluble antigen associated in the tissue is preserved at the infection site (W(2) in figure 4.15). In the absence of a specific immune response against the soluble antigen it is limited by a natural half-life, which we have modeled as much shorter than "live" intracellular pathogen, and continuous

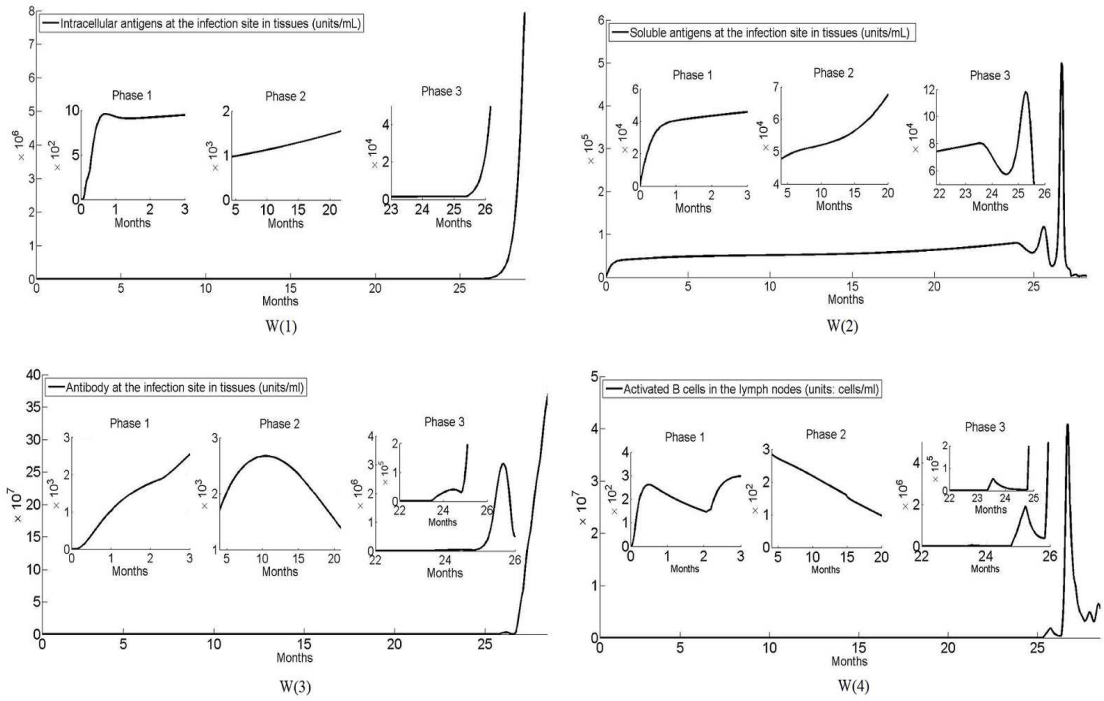

Figure 4.15 Local average amount of intracellular antigens, soluble antigens and antibodies at the infection site, and the amount of activated B cells in the lymph node over time. The inserts of phase 1 to 3 are the same results plotted on the different scales to highlight the dynamics of different phases of the infection.

processing and degradation by neighboring macrophages (W(2) in figure 4.15). Despite these immune controls, soluble antigen levels accumulate over time ultimately reaching the lymph node and promoting primary B cell activation as seen in phase 3 (W(4) in figure 4.15) resulting in a transition to several fold higher amounts of antibody and T_H2 cells that migrate to the infection site (W(3) in figure 4.15 and W(6) in figure 4.16). Antibodies consume soluble antigen and promote immune complex formation at the infection site (not shown) that is picked up by dendritic cells, which traffic to the draining lymph node (W(2) in figure 4.15 and W(5) in figure 4.16). Over the period of two months, the numbers of T_H2 cells at the infection site and the amount of immune complexes surpass a transition threshold and promote alternative activation of macrophages at the site of infection leading to enhanced pathogen survival and replication (W(1) in figure 4.15). A decline in the amount of particulate antigen during both

phase 1 and 2 leads to a concomitant decline in local T_H1 immunity that may contribute to the transition (W(5) and W(6) in figure 4.16).

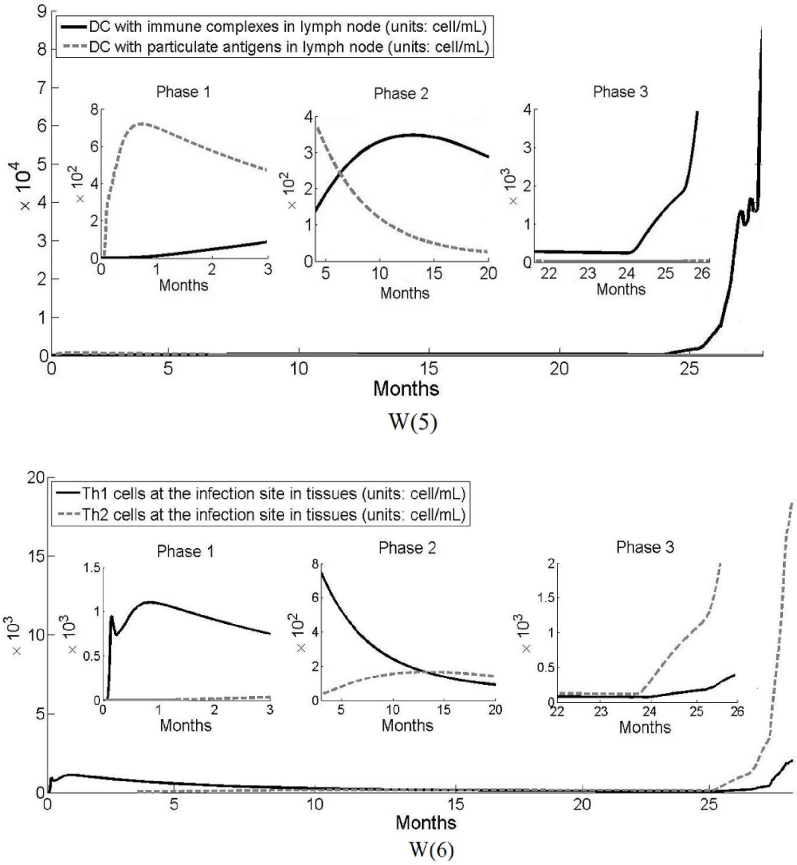

Figure 4.16 Local average population of DC associated with particulate antigen or immune complex, effector T cells at the infection site.

Our model predicts four phases of the immune response towards infection of *Map*. Phase 1 is the resolution of the initial infection. Phase 2 is a quasi-static process characterized by declining T_H1 immunity and slow accumulation of soluble antigen. Most of the variables have relatively low rates of change in this phase. Phase 3 includes the initiation of transition from a T_H1 dominated immune response to a T_H2 response. Phase 3 is the result of soluble antigen reaching threshold in the lymph node and subsequent primary B cell activation. In our model this results in T_H2 cell activation and antibody production with accompanying low levels of T_H1 immunity. None of these responses promote enhanced pathogen killing although

both particulate and soluble antigens are controlled. This stage is a relatively low level mixed response. The products of T_H2 immunity would not be readily apparent as antibodies are not in excess and they are effectively removing soluble antigen from the site of infection and antigen load remains relatively low. Phase 4 is defined by alternative activation of the local macrophage response that occurs at 26 months post-infection. At this stage antibody production and T_H2 immunity are parts of an ineffective feedback loop promoting alternative activation of macrophages and continued pathogen replication. Ultimately large amounts of accompanying soluble antigen promote a correspondingly large antibody response. Although not part of our original model, one would hypothesize that these antibodies and/or immune-complexes would significantly affect distant sites of infection leading to generalized inability to control the infection and ultimately death of the host. Interestingly, in our model, regulatory T cell function dramatically increased late in secondary to high levels of antigen interacting with the immune system.

Our model recapitulates several observations consistent with the development of clinical disease in cattle: 1) A slow decline in T_H1 immunity, 2) rapid increase in antigen load at end stage of disease, 3) a dramatic increase in antibody levels, 4) increase of regulatory type T cell response accompanying the immune phenotype switch, 5) loss of organized granuloma structure at the infection site at end stage of disease. All of the described phenomena are the result of threshold dependent transitions and determined by the driving force of antigen load in the draining lymph node and inherent immune skewing characteristics of the antigen.

It is therefore suggested by the numerical experiments that despite an initial T_H1 response, if the organism is not eliminated, continued immune activation by antigen that promotes T_H2 immunity eventually leads to immune effector response switch. Therefore, our model proposes an alternative mechanism where antigen load drives the immune phenotype switch and measured immune parameters during disease reflect a regulated immune response to antigen, albeit ultimately ineffective.

CHAPTER 5. Conclusion and discussion

Equipped with sophisticated tools, such as a highly efficient, convergent numerical scheme and the concept of homogenization, we develop a spatial -temporal mathematical model to capture various fundamental aspects of the MHC Class II immunity to antigen (foreign pathogen). System (A.1)∼(A.10) is a minimal model including only fundamental immune agents. The necessity of dendritic cells, regulatory T cells, B cells and antibodies for appropriate immune regulation are verified in numerical experiments in Sections 4.1 and 4.3 in Chapter 4. These results are consistent with our current understanding of their central roles in MHC Class II mediated immunity. Furthermore, to achieve the goal of a dynamic self-regulated model of immunity, motivated by Zinkernagel's postulate [205], we introduce the concept of a minimally defined pathogen.

The model is demonstrated to account for a series of consecutive immune responses: (1) antigen recognition, (2) an innate immune response (neutrophils and macrophages), (3) an adaptive immune response (effector T cells), and 4) the equilibrium of the immune response to the presence of a persistent antigen (chronic infection) or the elimination of the antigen and subsequent resolution of the immune response (acute infection).

Prior mathematical models of the immune system, such as classical works reviewed in Section 1.3.1 in Chapter 1, focus on temporal population dynamics. In addition to density/population dynamics, we consider the spatial motilities of the immune agents as a crucial factor. By the careful consideration of diffusion and chemotaxis (i.e., convection) rates based upon homogenization, we are able to examine particular dynamics such as regulatory and spatial-delay effects. Incorporating the spatial factor makes the arguments for some aspects of the immune response considerably clearer. For example, the delay effect on the peak time of T

cells is not a pure 'time delay function,' but is affected by the spatial diffusion and the direction switch of the maturing dendritic cells. The mathematical formulation of a switch of dendritic cells from immature to mature phased upon contact with an antigen and an accompanying change in the direction of cell movement; this is a sophisticated type of signal transduction.

One simple model of immune regulation suggests that the activation of an immune response, or its subsequent down-regulation, is primarily managed by the number of antigens that reach the secondary lymph node organs and the length of time that they remain there, which is, in part, dependent upon the success rate of the immune response towards the antigen [204, 205]. Therefore, in the model, all activation mechanisms for the various cell types are simple uni-dimensional threshold functions. For example, as discussed in Section 2.2.1, the presence of apoptotic neutrophils and activated macrophages signal the beginning of a successful immune response, after which there is an increasing reliance on the macrophage, rather than the neutrophil scavengers [141]. We use a simple threshold function that block neutrophil recruitment when macrophage-produced cytokine CM exceeds a constant threshold ϵ_N. Also, the different macrophage responses such as, innate activation, classical activation, alternative/humoral activation and down-regulation are all considered and modeled by simple threshold functions (section 2.2.2). The activation and differentiation of effector T cell and B cell are also modeled by threshold function (Section 2.4 and 2.5 in Chapter 2).

Our current results do not model a specific type of regulatory T cell, or suggest what T regulatory cell is most important, or responsible, for concrete disease. We do verify the hypothesis that regulatory T cells are important to in controlling proinflammatory events and maintaining an appropriate relationship between antigen load and the macrophage response, even in our most minimal immune model.

Acute and chronic antigen exposures are the fundamental types of antigen delivery at infection sites. Our model matches the immunological realities of these disparate conditions reasonably well. By defining pathogen characteristics, our model also successfully recapitulates various outcomes of the immune system once infected by broad class of pathogens. By applying the model, using an appropriately designed *in silico* pathogen with certain pathogen

characteristics, we are able to mimic the infection of *Map* in cattle and propose an alternative explanation of switch of T_H1 and T_H2 subtypes in immune responses. In addition, the two dimensional experiments successfully recapture the process of granuloma formation in a sole T_H1 subtype immunity.

Our current model is purposefully simplified and focused exclusively on MHC Class II mediated immune responses in tissue. In this approach, some important immune factors are excluded, such as, follicular DCs, memory T cells, and $CD8^+$ T cells. Furthermore, we simplify the process of the T_H1 and T_H2 dichotomy based solely on the characteristics of the antigen. Although this is consistent with many studies, we are aware that there are both secreted antigens that can promote T_H1 responses and particulate antigens that can promote T_H2 responses [122, 138]. However, regardless of the actual physical properties of any antigen, our model demonstrates how the amount of T_H1 or T_H2 antigens might influence the development of the immune response and the long-term consequences of persistent antigen that may be recognized as a T_H1 or T_H2 type antigen. The underlying principle that we have used to simplify the immune system is to avoid specific agents and consider instead the fundamental functions of the immune response: 1) recognition of pathogens with different phenotypic characteristics, 2) communication, 3) movement, 4) effector function (activation vs. inhibition), and 5) efficiency of eliminating the antigen. The proposed model that captures these generalities is stable. Any additional factors or specifics of the immune response, which will increase the granularity of the model, should fall into one of these five categories described mathematically in our current model.

APPENDIX A. Modeling equations for T_H1 subsystem

The modeling equations for T_H1 subsystem studied in sections 4.1.1 and 4.2 are listed below:

Equation of particulate antigens:

$$\begin{cases} \frac{\partial A}{\partial t} = \overbrace{-\mu_A A}^{\text{degradation}} \overbrace{-A(\lambda_{A|MR}MR + \lambda_{A|MA}MA + \lambda_{A|N}N + \lambda_{A|DE}DE)}^{\text{pinocytosis by phagocytes}} \overbrace{+D_A\Delta A}^{\text{diffusion}} \overbrace{+g(x,t)}^{\text{source}} \\ A(x,0) = g(x,0), \qquad A(\cdot,t)|_{\partial\Omega} = 0. \end{cases} \tag{A.1}$$

where $g(x,t)$ is the source function.

Equation of neutrophils and apoptotic neutrophils:

$$\begin{cases} \frac{\partial N}{\partial t} = \overbrace{-\mu_N N}^{\text{apoptosis}} \overbrace{-\lambda_{N|A}A \cdot N}^{\text{uptake/degranulation}} \overbrace{-\nabla(\chi_N(N \cdot \nabla CH))}^{\text{effective chemotaxis}} \overbrace{-\delta_{N|CH}CH \cdot N}^{\text{self regulation}} \\ \qquad \underbrace{+D_N\Delta N}_{\text{effective diffusion}} \\ \frac{\partial ND}{\partial t} = \underbrace{\mu_N N}_{\text{transfer from N}} \underbrace{-\lambda_{ND|MA}ND \cdot MA}_{\text{phagocytosis by macrophages}} \underbrace{-\mu_{ND}ND}_{\text{decay}} \underbrace{+D_{ND}\Delta ND}_{\text{diffusion}}, \\ N(\cdot,t)|_{\partial\Omega} = \begin{cases} N_0 & \text{if } CM \le \epsilon_N \\ 0 & \text{if } CM > \epsilon_N \end{cases}, \frac{\partial ND}{\partial n}|_{\partial\Omega} = 0,\ N(x,0) = N_0, ND(x,0) = 0. \end{cases} \tag{A.2}$$

Equations of dendritic cells:

$$\begin{cases} \frac{\partial DE}{\partial t} = \overbrace{-\mu_{DE} DE}^{\text{natural death}} \overbrace{-\gamma_{DE}(A) DE \cdot A}^{\text{activation}} \overbrace{+D_{DE}\Delta DE}^{\text{effective diffusion}} \overbrace{-\nabla(\chi_{DE}(DE \cdot \nabla CH))}^{\text{effective chemotaxis}} \\ \frac{\partial DA}{\partial t} = -\mu_{DA} DA + \gamma_{DE}(A) DE \cdot A + D_{DA}\Delta DA + \nabla(\chi_{DA}(DA \cdot \nabla CH)) \\ DE(\cdot,t)|_{\partial\Omega} = DE_0, \frac{\partial DA}{\partial n}|_{\partial\Omega} = 0, \ DE(x,0) = \begin{cases} 0, & x \in \Omega \\ DE_0, & x \in \partial\Omega \end{cases} \quad DA(x,0) = 0. \end{cases} \tag{A.3}$$

where $\gamma_{DE}(A)$ is the activation rate

$$\gamma_{DE}(A) = \begin{cases} \gamma_{DE} & A > \epsilon_{DE} \\ 0 & A \leq \epsilon_{DE} \end{cases} \tag{A.4}$$

Equation of T cells:

$$\begin{cases} \frac{\partial T}{\partial t} = \overbrace{-\mu_T T}^{\text{natural death}} \overbrace{+D_T \Delta T}^{\text{effective diffusion}} \overbrace{-\nabla(\chi_T(T \cdot \nabla CH))}^{\text{effective chemotaxis}} \overbrace{-\delta_{T|T_{reg}} T \cdot T_{reg}}^{\text{downregulation by contact with } T_{reg}} \\ \frac{\partial T_{reg}}{\partial t} = \overbrace{-\mu_{T_{reg}} T_{reg}}^{\text{natural death}} \overbrace{+D_{T_{reg}} \Delta T_{reg}}^{\text{effective diffusion}} \overbrace{-\nabla(\chi_{T_{reg}}(T_{reg} \cdot \nabla CH))}^{\text{effective chemotaxis}} \\ T(\cdot,t)|_{\partial\Omega} = \gamma_{T|DA} DA|_{\partial\Omega}, \quad T_{reg}(\cdot,t)|_{\partial\Omega} = \gamma_{T_{reg}}(CT, A) T|_{\partial\Omega} \\ T(x,0) = 0, \quad T_{reg}(x,0) = 0. \end{cases} \tag{A.5}$$

where the activation function of regulatory T cells is

$$\gamma_{T_{reg}}(CT, A) = \begin{cases} \gamma_{T_{reg}} T, & CT(\cdot,t)\Big|_{\partial\Omega} > \epsilon^1_{T_{reg}} + \epsilon^2_{T_{reg}} \int_\Omega A(x,t)dx \\ 0, & \text{otherwise} \end{cases}. \tag{A.6}$$

Equation of macrophages:

$$\begin{cases} \frac{\partial MR}{\partial t} = \overbrace{-\mu_{MR} MR}^{\text{natural death}} \overbrace{-\gamma_{MR}(CT, CT_{reg}, A) \cdot MR}^{\text{activation}} \overbrace{+D_{MR}\Delta MR}^{\text{effective diffusion}} \overbrace{-\nabla(\chi_{MR}(MR \cdot \nabla CH))}^{\text{effective chemotaxis}}, \\ \frac{\partial MA}{\partial t} = \underbrace{-\mu_{MA} MA}_{\text{degradation}} \underbrace{+\gamma_{MR}(CT, CT_{reg}, A) \cdot MR}_{\text{activation}} \underbrace{+D_{MA}\Delta MA}_{\text{diffusion}} \underbrace{-\nabla(\chi_{MA}(MA \cdot \nabla CH))}_{\text{effective chemotaxis}}, \\ MR(\cdot, t)|_{\partial\Omega} = MR_0, \frac{\partial MA}{\partial n}|_{\partial\Omega} = 0, \ MR(x, 0) = MR_0, \ MA(x, 0) = 0. \end{cases} \tag{A.7}$$

where the activation rate is

$$\gamma_{MR}(CT, CT_{reg}, A) = \begin{cases} \gamma_{MR} & CT > \epsilon^1_{MA} + \epsilon^2_{MA} A, CT_{reg} < \epsilon^3_{MA} + \epsilon^4_{MA} A \\ 0 & \text{otherwise}, \end{cases} \tag{A.8}$$

Equation of chemokines and cytokines:

$$\begin{cases} \frac{\partial CH}{\partial t} = \underbrace{(\beta_{CH|MA} MA + \beta_{CH|N} N) \cdot A}_{\text{secreted by N and MA}} \underbrace{-\mu_{CH} CH}_{\text{degradation}} \underbrace{+D_{CH}\Delta CH}_{\text{diffusion}}, \\ \frac{\partial CH}{\partial n}|_{\partial\Omega} = 0, CH(x, 0) = 0. \end{cases} \tag{A.9}$$

$$\begin{cases} \frac{\partial CT}{\partial t} = \overbrace{\beta_{CT} T}^{\text{secreted by T}} \overbrace{-\mu_{CT} CT}^{\text{natural death}} \overbrace{+D_{CT}\Delta CT}^{\text{diffusion}}, \\ \frac{\partial CM}{\partial t} = \overbrace{\beta_{CM} ND \cdot MA}^{\text{secreted by MA when engulfing ND}} \overbrace{-\mu_{CM} CM}^{\text{natural death}} \overbrace{+D_{CM}\Delta CM}^{\text{diffusion}}, \\ \frac{\partial CT_{reg}}{\partial t} = \overbrace{\beta_{CT_{reg}} T_{reg}}^{\text{secreted by regulatory T cells}} \overbrace{-\mu_{CT_{reg}} CT_{reg}}^{\text{natural death}} \overbrace{+D_{CT_{reg}}\Delta CT_{reg}}^{\text{diffusion}}, \\ \frac{\partial CT}{\partial n}|_{\partial\Omega} = \frac{\partial CT_{reg}}{\partial n}|_{\partial\Omega} = \frac{\partial CM}{\partial n}|_{\partial\Omega} = 0, \ CT_{reg}(x, 0) = CT(x, 0) = CM(x,) = 0. \end{cases} \tag{A.10}$$

APPENDIX B. Parameter estimate and discussion in the model

To simulate and study the proposed model, we must select values for all model parameters. Unfortunately, there are few direct estimates of most parameters, and *in vivo* immunological data may originate from multiple sources, for example mice or humans. We use whatever data is available, regardless of source, but acknowledge that substantial differences among species likely exist. Future calibration of model parameters against biological data will permit investigation of these differences. For parameters with no information, we have proposed what we think are reasonable values based on previously published immunological models and expert opinion. For discussion, the parameters of the system (A.1) ∼(A.10) are categorized into four groups: 1) initial conditions, 2) kinetic parameters, 3) model specific parameters, and 4) motility parameters.

Initial cell densities

Because we have used mathematical homogenization to model vascularized tissue, any immune cell that normally flows through the blood stream exists at some initial level at the modeled site of infection. Other cells, such as mature dendritic cells or antigen specific T cells that are activated in response to the infection, and all cytokines, start at zero initial concentration everywhere and are not listed in Table B.1.

There is data available on the abundance of immune cells in the blood. For simplicity, we assume the initial concentrations in the simulation area are equivalent to the concentrations in the blood. Neutrophils are the most abundant white blood cell in the vasculature, with a reported $2.5 \sim 7.5 \times 10^9$ cells per liter [19], so we choose the initial and boundary neutrophil concentration, N_0, in this range. Approximately 6% of white blood cells in humans

are monocytes. In the tissue, most of these monocytes mature into macrophages [78], leading to $MR_0 \sim 1 \times 10^8/L$ [19]. A small fraction of monocytes become dendritic cells, with initial density in lymph node at $DE_0 \sim 1 \times 10^7/L$ [28].

It is estimated that in the resting stage B cells are 23% of the total $1 \sim 5 \times 10^9/L$ lymphocytes in adults [19]. The amount of memory B cells in the lymph node is estimated to be $1 \sim 5 \times 10^3/L$.

Table B.1 Initial cell densities.

Name	Cell Type	Simulation Value (Estimated Range)	Reference
N_0	neutrophil	2.5×10^6 ($2.5 \sim 7.5 \times 10^6/mL$)	[19]
DE_0	immature dendritic cell	5×10^4 ($\sim 1 \times 10^4/mL$)	[28]
MR_0	resting macrophage	1.5×10^5 ($\sim 1 \times 10^2/mL$)	[19]
B_m	memory B cells	3 ($1 - 5/mL$)	estimate
$\sim$	comparable with		

Kinetic parameters

The kinetic parameters are those that reflect the dynamics of the immune response during the interactions of immune agents and foreign antigens. The kinetic parameters can be classified into the following classes: death/decay rates (cells/chemicals), production or secretion rates, replication or proliferation rates, activation or promotion rates, uptake or processing rates and regulation rates.

Death rates of cells and decay rates of chemicals

Apparently one of the easier quantities to experimentally measure, there is abundant data on the lifespan of immune cells as recorded in Table B.

Here, the evidence shows that neutrophils are short-lived [141], unlike macrophages, which live for months [166]. Activated or mature immune cells tend to live shorter lives than their

unactivated/immature cousins [103, 148, 149]. We model that the lifespan of different subsets of helper T cells are similar [78, 120], and according to [134], it is estimated that 3% of T cells are lost per day, so we estimate $\mu_{T_H1} \sim \mu_{T_H2} = -\ln(1-0.03) \approx 0.03$/day. The half life of neutrophils is reportedly $8 \sim 24$ hours [69, 124, 172], yielding the range of Table B. With no information for regulatory T cells, we assume effector and regulatory T cells share similar death rates. Once B cells are activated they fail to survive for a long time period, i.e. the half life is only 3 days [11], unless there are abundant growth and survival factors present. In our model, without the effect of affinity maturation or germinal center formation the half-life of plasma B cells is set to be 4 weeks. The half life of antibody ranges from 7 to 24 days [106].

The other entities in the model are not living cells, and most have high decay rates typical of proteins. Particularly, the decay rate of T_H2 cytokines is relatively larger than the decay rate of T_H1 cytokines [120]. Apoptotic neutrophils, however, are large objects, cleared through phagocytosis by macrophages, not through decay, so we assign them a small decay rate. Particulate antigen±PAMPs, soluble antigen and intracellular antigen, which are all proteins, represent a pathogen that actively avoids its own decay, so we have also assigned them small decay rates. Immune complexes usually have a stable structure so that we estimate their decay rate to be relatively small.

Table B.2 Death rates of cells and decay rates of proteins (unit: /day)

Name	Rate of death of $\cdots$	Simulation Value (Estimated Range)	Reference
μ_N	neutrophil apoptosis	1 $(0.69-2.08)$	[69, 124, 172]
μ_{DE}	immature dendritic cell	0.25 $(0.23-0.35)$	[103]
μ_{DA}	mature DC with A	1.00 $(0.69-1.39)$	[103]
μ_{DF}	mature DC with IC	1.00 $(\sim \mu_{DA})$	estimate
μ_{T_H1}	effector T_H1 cell	0.33 $(0.03-0.333)$	[97, 134, 185]

Table B.2 (Continued)

	Death rates of cells and decay rates of proteins (unit: /day)		
μ_{T_H2}	effector T_H2 cell	0.33 ($\sim \mu_{T_H1}$)	[120]
$\mu_{T_{\text{reg}}}$	regulatory T cell	0.33 ($\sim \mu_{T_H1}$)	[97]
μ_{MR}	resting macrophage	0.0033 ($0.0033 - 0.007$)	[148, 149]
μ_{MA}	activated macrophage	0.4 ($0.01 - 0.4$)	[57, 148, 149]
$\mu_{MA\|A_p}$	MA due to bursting	2	estimate
μ_{B_a}	activated B cell	0.23 ($0.05 - 0.23$)	[78, 117, 183]
μ_{B_p}	plasma B cell	0.45 ($0.33 - 0.5$)	[117], estimate
	Rate of decay of $\cdots$		
μ_{ND}	apoptotic neutrophil	10^{-4}	estimate
μ_{CH}	chemokine	10^{-3}	[57]
μ_A	particulate antigen±PAMPs	$\sharp$	
μ_{A_s}	soluble antigen	$\sharp$	
μ_{A_p}	intracellular antigen	$\sharp$	
μ_{IC}	immune complexes	10^{-5}	estimate
μ_{CM}	activated macrophage cytokine	2	[8, 186]
μ_{CT1}	T_H1 cytokine	2.16 ($2.16 - 33.2$)	[35, 60]
μ_{CT2}	T_H2 cytokine	3.7 ($3.7 - 7.23$)	[120], estimate
$\mu_{CT_{\text{reg}}}$	regulatory T cell cytokine	3.70 ($3.6969 - 7.23$)	[201]

Production and secretion rates

There are data available on the rates of chemokine and cytokine production by immune cells, however since the chemical messengers of our model perform the functions of multiple biological molecules, our secretion rates, reported in Table B.3, can only approximate true secretion rates.

In our model, there is only one generic chemokine secreted by neutrophils and activated macrophages at distinct rates. Taken into account the opsonization of antibody, after engulfing immune complexes, professional phagocyte secretes chemokine more rapidly than solely

Table B.2 (Continued)

Death rates of cells and decay rates of proteins (unit: /day)			
μ_F	antibody	0.03 $(0.1 - 0.043)$	[106, 117]
$\sharp$	pathogen dependent		

engulfing particulate antigens. There are three cytokines $CT1, CT2$ and CT_{reg} secreted by effector T_H1, T_H2 cells and regulatory T cells respectively; and T_H2 cytokines are secreted at a relatively slower rate than the secretion rate of T_H1 cytokines [120]. The secretion rate of antibody is estimated mainly based on the information in [66, 160]. The secretion rate of soluble antigen is pathogen dependent, for example, parasitic worms may secrete large amounts of soluble antigen in short time period [78] while *Mycobacterium*, although not well described *in vivo*, presumably secrete less at a slower rate.

Table B.3 Production and secretion rates (Unit: pg/(cell·day) and pg/(cell·(pg/ml)·day))

Symbol	Rate of Secretion of ...	Simulation Value (Estimated Range)	Reference
β_{CT1}	cytokine by effector T_H1 cell	0.1 $(2.0 \times 10^{-4} - 0.1)$	[59, 201]
β_{CT2}	cytokine by effector T_H2 cell	0.09 $(2.0 \times 10^{-4} - 9.12 \times 10^{-2})$	[120]
$\beta_{CT_{\text{reg}}}$	cytokine by regulatory T cell	0.06 $(\sim \beta_{CT1})$	[201], estimate
β_{CM}	cytokine by activated macrophage	3×10^{-2}	[8, 9], estimate
$\beta_{F\|B_p}$	antibody by plasma B cell	2-4 $(0.25 - 12.5)$	[43, 66, 117, 160]
$\beta^1_{CH\|MA}$	chemokine by MA with A	3×10^{-6} $(3 \times 10^{-5} - 15 \times 10^{-3})$	[5]
$\beta^2_{CH\|MA}$	chemokine by MA with IC	6×10^{-7}	estimate
$\beta^1_{CH\|N}$	chemokine by N with A	3×10^{-6} $(\sim \beta^1_{CH\|MA})$	estimate
$\beta^2_{CH\|N}$	chemokine by N with IC	6×10^{-7} $\sim \beta^2_{CH\|MA}$	estimate
$\beta_{A_s\|A}$	soluble antigen by A	$\sharp$	
$\beta_{A_s\|A_p}$	soluble antigen by A_p	$\sharp$	
$\sharp$	pathogen dependent		

Replication or proliferation rates

In our model, foreign antigen can replicate and mature B cells in the lymph node can proliferate. Moreover, for simplicity, in contrast to how we model the generation of subsets of effector T cells and mature dendritic cells, activated B cells experience intrinsic differentiation. In this work, we model that particulate antigen does not replicate while intracellular antigen replicates. The differentiation rate for plasma B cells in Table B.4 is estimated based on [2, 26, 27, 117]. The proliferation rate of activated B cells is estimated in a similar way to our estimate of the natural death rate above.

Table B.4 Replication and proliferation rates (Unit: /(cell· day))

Symbol	Rate of replication	Simulation Value (Estimated Range)	Reference
α_A	particulate antigen	$\sharp$	
α_{A_p}	intracellular antigen	$\sharp$	
	Rate of proliferation		
$\alpha_{B_p\|B_a}$	plasma B cells	3 $(2-5)$	[117]
α_{B_a}	activated B cells	0.3 $(0.2-1.44)$	[2, 10, 33, 117]
$\sharp$	pathogen dependent		

Activation and promotion rates

The maturation of immature dendritic cells, activation of resting macrophages, and the recruitment of regulatory T cells by activation in the lymph nodes, the activation/promotion rate of effector T cells and B cells are estimated in our model. Subsets of mature dendritic cells can activate effector helper T cells by presenting antigens at comparable rates [125]. The activation rate of dendritic cells by immune complex is estimated based on the opsonization effect of antibody. The rate of co-stimulation of B cells due to helper T cells is estimated partially based on [117]. The parameters reported in the Table B.5 are considered as maximum activation rates.

Table B.5 Activation and promotion rates (Unit: /(cell·day) or /(cell·pg/ml·day))

Symbol	Activation/recruitment /stimulation rate of ...	Simulation Value (Estimated Range)	Reference
$\gamma_{MA\|MR}$	macrophage	0.025 $(0.02 - 0.4)$	estimate, [201]
$\gamma_{T_H1\|DA}$	effector T_H1 cell by DA	2.5	estimate, [97]
$\gamma_{T_H1\|DF}$	effector T_H1 cell by DF	0.2	estimate
$\gamma_{T_H2\|B_a}$	effector T_H2 cell by B_a	0.004 $(0.004 - 3)$	estimate, [117]
$\gamma_{T_H2\|DF}$	effector T_H2 cell by DF	0.8 $(> \gamma_{T_H1\|DF})$	estiamte
$\gamma_{T_{\text{reg}}}$	regulatory T cell recruitment	0.5	estimate
γ^1_{DE}	DC maturation recognizing A	4×10^{-4} $(1 \times 10^{-4} - 6.5 \times 10^{-3})$	[190]
γ^2_{DE}	DC maturation recognizing IC	1×10^{-4} $(\sim \gamma^1_{DE})$	estiamte
$\gamma_{B_a\|T_H1}$	B cells by T_H1	1×10^{-6}	estimate
$\gamma_{B_a\|T_H2}$	B cells by T_H2	7×10^{-5} $(7 \times 10^{-5} - 0.1)$	[117]
$\gamma_{B_m\|A_s,IC}$	memory B cells with antigens	3×10^{-2}	estimate

Uptake or processing rates

The processing (uptake / phagocytosis / pinocytosis) rates for particulate antigen±PAMP in equation (A.1), vary by immune agents. Activated macrophages are three times more efficient antigen processors than resting macrophages [167], but immature dendritic cells are the most efficient antigen processors of all immune cells[173]. We expect, among all immune cells, most particulate antigen±PAMP to be consumed by phagocytic cells, so the decay rate μ_A is a lower bound on processing rates. These claims yield

$$\lambda_{A|DE} > \lambda_{A|MA} > \lambda_{A|N} > \lambda_{A|MR}. \tag{B.1}$$

Concrete data suggests antigen processing rates for activated macrophage are in the range $10^{-7} \sim 10^{-5}$ per second [57, 148, 149].

To estimate the processing rates of antibody listed in Table B.6, we use the facts that antibody binds with antigen in an efficient way [183] and that the association rate of immune

complexes with other immune agents (a type of processing rate) is relatively large [61, 78, 123].

Table B.6 Uptake or processing rates (Unit: /(cell·day) or /(pg/ml·day))

Symbol	Uptake Rate of ...	Simulation Value (Estimated Range)	Reference
$\lambda_{A\|MA}$	A by activated macrophage	0.8×10^{-4}	[57, 148, 149]
$\lambda_{A\|MR}$	A by resting macrophage	0.25×10^{-6}	estimate, [167]
$\lambda_{A\|N}$	A by neutrophil	0.55×10^{-6}	estimate
$\lambda_{A\|DE}$	A by immature dendritic cell	1.50×10^{-4}	estimate, [173]
$\lambda_{A_s\|F}$	A_s by antibody	5×10^{-4} $(5 \times 10^{-4} - 5 \times 10^{-2})$	[55, 61, 117, 123]
$\lambda_{A\|F}$	A by antibody	1×10^{-4} $\sim \lambda_{A_s\|F}$	estimate
$\lambda_{IC\|MA}$	IC by activated macrophage	1×10^{-3}	estimate
$\lambda_{IC\|DE}$	IC by immature dendritic cell	2×10^{-4}	estimate
$\lambda_{IC\|N}$	IC by neutrophils	1.1×10^{-5}	estimate

Regulation rates

Very little is known about immune self-regulation, so the functions and parameters of Table B.9 are our simple proposals. It is known that neutrophils invading the site of an infection produce auto-inhibitory factors [150, 202]. Since neutrophils produce the vast majority of infection site chemokine early in infection, we let the concentration of chemokine stand in for all such factors. Then $\delta_{N|CH}$ is the rate of neutrophil degradation due to this feedback loop.

Besides the regulation of effector T cell by regulatory T cell through direct cell-cell contact [190], cross regulation of T_H1 and T_H2 effector T cell development is included in our model. In [52, 53, 54], effective reaction rate is used for the model, based on which cross-regulation rate is estimated in our model.

Model specific parameters

The adaptive immune response functions through a variety of different regulatory mechanisms. As a comprehensive approach to regulation we use a series of threshold functions for

Table B.7 Regulation rates (Unit: /(cell·day))

Symbol	Rate of ...	Simulation (Estimated range)	Reference
$\delta_{N\|CH}$	auto-regulation of neutrophil	1.0×10^{-5}	estimate
$\delta_{T_H1\|T_{\mathrm{reg}}}$	downregulation of effector T_H1 cells	0.5×10^{-4}	estimate, [97]
$\delta_{T_H2\|T_{\mathrm{reg}}}$	downregulation of effector T_H2 cells	0.5×10^{-4} ($\sim \delta_{T_H1\|T_{\mathrm{reg}}}$)	estimate
$\delta_{T_H1\|T_H2}$	crossregulation of effector T_H2 cells	0.6×10^{-4}	estimate
$\delta_{T_H2\|T_H1}$	crossregulation of effector T_H1 cells	0.6×10^{-4}	estimate

both immune agents and antigen load [206].

Most immune actions are tightly regulated such that they are promoted in certain environments and blocked in others. Immune actions typically exist on a continuous scale, for example phagocytosis can occur at a continuum of rates. Cytokines, other molecular signals, and even cells in the environment are sensed via cell surface receptors, and processed via signal transduction networks inside the cell to output the cellular activity level. One can think of cells and their networks as functions that map environmental states to cellular actions. In most cases, the explicit expressions of the functions are unknown. In our simple model, we assume these functions are step functions that map the relevant environmental quantities to an on/off state of activity. As a consequence, we specify two activity levels: maximal (on) and off. We also assume that the space of environmental conditions can be simply partitioned between those environments that turn activity on and those that turn it off. As discussed in chapter 2, immune activities that are modeled in this way are neutrophil recruitment, activation of effector T cell, regulatory T cell recruitment, B cell activation, and macrophage activation.

To model different types of pathogens, as discussed in section 2.1, we use a limited number of characteristics to capture how pathogens interact with the immune system. To establish a chronic infection, the continuous presence of pathogens or associated antigens is necessary and plays important role in triggering immune responses constantly. The pathogen dependent generic term $1 - p^{\mathrm{eff}}_{A_p|A}$ captures the probability (percentage) for an intracellular antigen to remain or recruit during an ongoing immune response. If $p^{\mathrm{eff}}_{A_p|A} = 1$ the immune response is fully successful and it is considered as an acute infection, and $p^{\mathrm{eff}}_{A_p|A} < 1$ for chronic infections.

Table B.8 Threshold parameters (Unit: pg/ml or scalar)

Name	Threshold for $\cdots$	Simulation range	Reference
ϵ_N	neutrophil recruitment	$(0.1 - 1 \times 10^3)$	estimate
$\epsilon^1_{T_{\text{reg}}}$	regulatory T cell recruitment	$(0.3 - 3)$	estimate
$\epsilon^2_{T_{\text{reg}}}$		$(0.01 - 0.1)$	estimate
$\epsilon^1_{MA\|T_H1}$	classical macrophage activation	$(0.02 - 3)$	estimate
$\epsilon^2_{MA\|T_H1}$		$(1.0 \times 10^{-3} - 0.1)$	estimate
$\epsilon^1_{MA\|T_{\text{reg}}}$	downregulation of macrophage	$(0.1 - 3)$	estimate
$\epsilon^2_{MA\|T_{\text{reg}}}$		$(-0.1 - (-0.01))$	estimate
$\epsilon_{MA\|T_H2}$	alternative macrophage activation	$(0.1 - 200)$	estimate
θ_{IC}	alternative macrophage activation	1.0×10^6	estimate
θ_F	huomral/alternative activation	1.0×10^6	estimate
θ_{T_H1}	activation of T_H1	$(0.1 - 10)$	estimate
θ_{T_H2}	activation of T_H2	$(0.1 - 100)$	estimate, [177]
$\theta_{B_a\|A_s}$	activating B cell by soluble antigen	$(100 - 5000)$	estimate
$\theta_{B_a\|DA,DF}$	activating B cell by antigen-bond on DC	$(1 - 50)$	estimate
$\theta_{B_a\|A}$	activating B cell by particulate antigens	$(1 - 500)$	estimate
$\theta_{B_a\|IC}$	activating B cell by immune complexes	$(1 - 5000)$	estimate

Capacity and escaping probability are also pathogen dependent. Constant $\delta \in (0, 1]$ is an artificial parameter modeled to capture how the alternative/humoral activation may influence the immune responses ability to activate macrophages and eliminate the pathogen (refer to section 2.1.2 and 2.2.2).

Motility parameters

The chemotaxis and diffusion rates for immune cells in Table B are larger than those measured *in vitro* because the circulation of immune cells in the microvasculature, governed by Stoke's equation, has been approximated by effective chemotaxis and diffusion [30, 191, 193] as discussed in section 2.2.1. Apoptotic neutrophils created in the extravascular tissue do not re-enter the vascular space. They diffuse at real rate 10^{-4} μm^2/min, substantially slower than proteins like antigen/PAMP, chemokines and cytokines.

According to the similar cellular structures of subsets of effector T cells and mature DCs

Table B.9 Model related parameters

Symbol	Description	Simulation range	Reference
$p^{\text{eff}}_{A_p\|A}$	immune efficiency	$\sharp$	
$\rho_{A_p\|MA}$	capacity of intracellular antigen in MA	$\sharp$	
$k_{A\|A_p}$	escaping rate of intracellular antigen	$\sharp$	
n_{A_p}	switch of alternative activation	$\sharp$	
δ	effective alternative activation parameter	$[0, 1]$	
δ_{B_a}	proliferation constant of activated B cells	$(0.05 - 5.0) \times 10^6$	estimate
ρ_{DE}	MHC class II presented on the surface of DC	$(5.0 - 500) \times 10^2$/cell	estiamte
τ_0	time lag of activation of effector T cell	12 hrs	[78]
$p_{B\|DE}$	fraction of available bond for naive B cell	$[0, 1]$	
$\sharp$	pathogen dependent		

[183], we set the effective motility coefficients of DF and T_H2 similar to the chemotaxis rates of DA and T_H1, respectively. Soluble antigen, antibody and immune complex are small molecules that diffuse relatively fast in comparison to other quantities [78].

Table B.10 Chemotaxis and Diffusion rates (Unit: $c\text{m}^2$/(pg/ml·day), $c\text{m}^2$/day)

Name	Chemotaxis coefficient of $\cdots$	Simulation Value (Estimated Range)	Reference
χ_{DE}	immature dendritic cells	3.5×10^{-3}	estimate
χ_{DA}	mature dendritic cells with A	5×10^{-3}	estimate
χ_{DF}	mature dendritic cells with IC	5×10^{-3}	estimate
χ_{T_H1}	effector T_H1 cells	6.5×10^{-3}	estimate, [146]
χ_{T_H2}	effector T_H2 cells	6.5×10^{-3}	estimate
$\chi_{T_{\text{reg}}}$	regulatory T cells	6.5×10^{-3}	estimate
χ_N	neutrophils	8×10^{-3}	estimate, [57, 133]
χ_{MR}	resting macrophages	2.5×10^{-3}	estimate

Table B.10 (Continued)

χ_{MA}	activated macrophages	3×10^{-3}	estimate, [104, 184, 194]
		$(0.16 \times 10^{-6} - 0.48)$	
χ_{A_p}	intracellular antigen	3×10^{-3}	estimate
		$(\sim \chi_{MA})$	
	Diffusion coefficient of $\cdots$		
D_A	particulate antigen±PAMPs	$\sharp$	estimate
D_{A_p}	intracellular antigen	5×10^{-2}	estimate
		$(\sim D_{MA})$	
D_{A_s}	soluble antigen	$\sharp$	estimate
D_{IC}	immune complex	$\sharp$	estimate
D_{CH}	chemokine	1	estimate, [57, 149]
D_{CT1}	effector T_H1 cell cytokine	1	estimate, [130]
D_{CT2}	effector T_H2 cell cytokine	1	estimate
		$(\sim D_{CT1})$	
$D_{CT_{\mathrm{reg}}}$	regulatory T cell cytokine	1	estimate
		$(\sim D_{CT1})$	
D_F	antibody	2	estimate
D_{DE}	immature dendritic cell	7×10^{-2}	estimate
D_{DA}	mature dendritic cell with A	7×10^{-2}	[125, 126]
D_{DF}	mature dendritic cell with IC	7×10^{-2}	estimate
		$(\sim D_{DF})$	
D_{T_H1}	effector T_H1 cell	5×10^{-2}	[130]
D_{T_H2}	effector T_H2 cell	5×10^{-2}	estimate
		$(\sim D_{T_H1})$	
$D_{T_{\mathrm{reg}}}$	regulatory T cell	4×10^{-2}	estimate
		$(\sim D_{T_H1})$	
D_N	neutrophil	0.8	estimate, [45]
		$(0.002 - 0.8)$	
D_{ND}	apoptotic neutrophil	1.0×10^{-5}	estimate
D_{MR}	resting macrophage	8×10^{-2}	estimate
D_{MA}	activated macrophage	5×10^{-2}	estimate, [57, 148]
$\sharp$	pathogen dependent		

BIBLIOGRAPHY

[1] Z. A. Agur, *Theoretical analysis of the immune response to antigenically varying pathogens*, Mathematics Applied to Biology and Medicine, Eds. J. Demongeot, V. Capasso, Mathematica Biology Ser. Winnipeg, Canada: Wuerz Publishing Ltd., 1993, pp. 237-242.

[2] F. Agenès, *B lymphocyte life span, rate of division and differentiation are regulated by total cell number*, European Journal of Immunology, *33*(4) (2003), pp. 1063-1069.

[3] S. Akira, *TLR signaling*, Curr. Top. Microbiol. Immunol., *311* (2006), pp. 1-16.

[4] J. Alexander, A. R. Satoskar, and D. G. Russell, *Leishmania species: models of intracellular parasitism*, J. Cell Sci., *112* (1999), pp. 2993-3002.

[5] A. Andoh, H. Takaya, T. Saotome, M. Shimada, K. Hata, Y. Araki, F. Nakamura, Y. Shintani, Y. Fujiyama, and T. Bamba, *Cytokine regulation of chemokine (IL-8, MCP-1, and RANTES) gene expression in human pancreatic periacinar myofibroblasts*, Gastroenterology, *119*(1) (2000), pp. 211-219.

[6] C. Asseman, S. Mauze, M. W. Leach, R. L. Coffman, and F. Powrie, *An essential role for interleukin 10 in the function of regulatory T cells that inhibit intestinal inflammation*, J. Exp. Med., *190*(7) (1999), pp. 995-1004.

[7] A. Ariel, and N. C. Serhan, *Resolvins and protectins in the termination program of actue inflammation*, Trends in Immu., *28*(4) (2007), pp. 176-183.

[8] A. Aderem, and D. M. Underhill, *Mechanisms of phagocytosis in macrophages*, Ann. Rev. Immun., *17* (1999), pp. 593-623.

[9] A. K. Bahl, and J.C. Foreman, *Stimulation and release of interleukin-1 from peritoneal macrophages of the mouse*, Inflam. Research, *42* (1994), pp. 154-158.

[10] J. Barker, and C. M. Verfaillie, *A novel in vitro model of early human adult B lymphopoiesis that allows proliferation of pro-B cells and differentiation to mature B lymphocytes*, Leukemia, *14* (2000), pp. 1614-1620.

[11] F. D. Batista, and M. S. Neuberger, *Affinity dependence of the B cell response to antigen: a threshold, a ceiling, and the importance of off-rate*, Immunity, *8*(6) (1998), pp. 751-759.

[12] H. Bashyam, *Th1/Th2 cross-regulation and the discovery of IL-10*, J. Exp. Med., *204*(2) (2007), pp. 237.

[13] F. D. Batista, and N. E. Harwood, *The who, how and where of antigen presentation to B cells*, Nature Rev. Immunology, *9* (2009), pp. 15-27.

[14] G. Bell, *Mathematical model of clonal selection and antibody production. I*, J. Theor. Biol., *29* (1970), pp. 191-232.

[15] G. Bell, *Mathematical model of clonal selection and antibody production. II*, J. Theor. Biol., *33* (1971), pp. 339-378.

[16] G. Bell, *Mathematical model of clonal selection. III. The cellular basis of immunological paralysis*, J. Theor. Biol., *33* (1971), pp. 379-398.

[17] G. Bell, *Lymphocyte traffic patterns and cell-cell interactions*, Theoretical Immunology, Ed. G. Bell, A. Perelson, G. Pimbley. N.Y., 1978. pp. 341-375.

[18] A. Bergtold, D. D. Desai, A. Gavhane, and R. Clynes, *Cell surface recycling of internalized antigen permits dendritic cell priming of B cells*, Immunity., *23*(5) (2005), pp. 503-514.

[19] M. H. Beers, R. S. Porter, and T. V. Jones, *The Merck Manual*, 18th edition, Merck & Co., Inc., 2006

[20] Y. Belkaid, C. A. Piccirillo, S. Mendez, E. M. Shevach, and D. L. Sacks, *CD4+CD25+ regulatory T cells control Leishmania major persistence and immunity*, Nature, *420* (2002), pp. 502-507.

[21] E. J. Blink, A. Light, A. Kallies, S. L. Nutt, P. D. Hodgkin, and D. M. Tarlinton, *Early appearance of germinal center-derived memory B cells and plasma cells in blood after primary immunization*, J. E. M., *201*(4) (2005), pp. 545-554.

[22] G. A. Bocharov, and A. A. Romanyukha, *Mathematical model of antiviral immune response. III. Influenza A Virus Infection*, J. Theor. Biol., *167* (1994), pp. 323-360.

[23] S. B. Brown, and J. Savill, *Phagocytosis triggers macrophage release of fas ligand and induces apoptosis of bystander leukocytes*, J. Immunol., *162* (1999), pp. 480-485.

[24] C. Bruni, M. Giovenco, G. Koch, and R. Strom, *A dynamical model of humoral immune response*, Math. Biosci., *27* (1975), pp. 191-212.

[25] F. M. Burnet, *The clonal selection theory of acquired immunity*, The University Press, Cambridge, 1959.

[26] K. L. Calame, *Plasma cells: finding new light at the end of B cell development*, Nat. Immunol., *2*(12) (2001), pp. 1103-1108.

[27] K. L. Calame, K. I. Lin, and C. Tunyaplin, *Regulatory mechanisms that determine the development and function of plasma cells*, Annu. Rev. Immunol., *21* (2003), pp. 205-230.

[28] D. M. Catron, A. A. Itano, K. A. Pape, D. L. Mueller, and M. K. Jenkins, *Visualizing the first 50 hr of the primary immune response to a soluble antigen*, Immunity, **21**(3) (2004), pp. 341-347.

[29] A. Chertock, and A. Kurganov, *A second-order positivity preserving central-upwind scheme for chemotaxis and haptotaxis models*, Numer. Math., *111*(2) (2008), pp. 169-205.

[30] D. Cioranescu, and J. S. J. Paulin, *Homogenization of reticulated structures*, Springer-Verlag, New York, 1999.

[31] S. Childress, and J. K. Percus, *Nonlinear aspects of chemotaxis*, Math. Biosci., *56* (1981), pp. 217-237.

[32] S. L. Constant, and K. Bottomly, *Induction of Th1 and Th2 CD4C T-cell responses: the alternative approaches*, Ann. Rev. Immunol., *15* (1997), pp. 297-322.

[33] J. Coopermana, R. Neelya, D. T. Teachey, S. Gruppc. and J.K. Choia, *Cell Division Rates of Primary Human Precursor B Cells in Culture Reflect In Vivo Rates*, Stem Cells, *22* (2004), pp. 1111-1120.

[34] L. da Fontoura Costa, L. C. Cintra, and D. Schubert, *An integrated approach to the characterization of cell movement*, Cytometry Part A, *68A* (2005), pp. 92-100.

[35] C. D'Amico, G. Frascaroli, G. Bianchi, P. Transidico, A. Doni, A. Vecchi, S. Sozzani, P. Allavena, and A. Mantovani, *Uncoupling of inflammatory chemokine receptors by IL-10: generation of functional decoys*, Nat. Immunol., *1* (2000), pp. 387-391.

[36] C. De Lisi, and A. S. Perelson, *The kinetics of aggregation phenomena*, J. Theor. Biol., *62* (1976), pp. 159-210.

[37] C. De Lisi, *Detection and analysis of recognition and selection in the immune response*, Bull. Math. Biol., *39* (1977), pp. 705-719.

[38] C. De Lisi, *Some mathematical problems in the initiation and regulation of the immune response*, Math. Biosci., *35* (1977), pp. 1-26.

[39] C. De Lisi, and A. Rescigno, *Immune surveillance and neoplasia. I. Minimal mathematical model*, Bull. Math. Biol., *39* (1977), pp. 204-221.

[40] C. De Lisi, and A. Rescigno, *Immune surveillance and neoplasia. II. Two-stage mathematical model*, Bull. Math. Biol., *39* (1977), pp. 487-497.

[41] P. C. Doherty, *Some problem areas in the interaction between viruses and the immune system*, Immunol. Cell. Biol., *65* (1986), pp. 279-286.

[42] T. Dörner, and A. Radbruch, *Selecting B cells and plasma cells to memory*, J. E. M., *201*(4) (2005), pp. 497-499.

[43] H. M. Dosch, P. Lam, and D. Guerin, *Differential regulation of activation, clonal expansion, and antibody secretion in human B cells*, J. Immuno., *135*(6) (1985), pp. 3808-3816.

[44] E. J. Ehlert, A. Ludwig, A. T. Grimm, B. Lindner, H. D. Flad, and E. Brandt, *Down-regulation of neutrophil functions by the ELR1 CXC chemokine platelet basic protein*, Blood, *96*(9) (2000), pp. 2965-2972.

[45] S. Felder, and Z. Kam, *Human neutrophil motility: Time-dependent three-dimensional shape and granule diffusion*, Cell Motility and the Cytoskeleton, *28*(4) (1994), pp. 285-302.

[46] R. Fernandez-Botran, V. M. Sanders, T. R. Mosmann, and E. S.Vitetta, *Lymphokine-mediated regulation of the proliferative response of clones of T helper 1 and T helper 2 cells*, J. Exp. Med., *168* (1988), pp. 543-558.

[47] D. F. Fiorentino, M. W. Bond, and T. R. Mosmann, *Two types of mouse helper T cells. IV. Th2 clones secrete a factor that inhibits cytokine production by Th1 clones*, J. Exp. Med., *170* (1989), pp. 2081-2095.

[48] D. F. Fiorentino, A. Zlotnik, P. Vieira, T. R. Mosmann, M. Howard, K. W. Moore, and A. OGarra, *IL-10 acts on the antigen-presenting cell to inhibit cytokine production by Th1 cells*, J. Immunol., *146* (1991), pp. 3444-3451.

[49] S. Fillatreau, and A. Radbruch, *IRF4-a factor for class switching and antibody secretion*, Nat. Immunol., *7*(7) (2006), pp. 704-706.

[50] F. Filbet, *A Finite Volume Scheme for the Patlak-Keller-Segel Chemotaxis Model*, Numerische Mathematik, *104* (2006), pp. 457-488.

[51] F. Filbet, and C. W. Shu, *Approximation of Hyperbolic Models for Chemosensitive Movement, SIAM Journal on Scientific Computing archive*, *27* (2005), pp. 850-872.

[52] M. A. Fishman, and A. S. Perelson, *Modeling T Cell-Antigen Presenting Cell Interactions*, J. Theor. Biol., *160* (1993), pp. 331-342.

[53] M. A. Fishman, and A. S. Perelson, *Th1/Th2 cross regulation*, J. Theor. Biol., *170* (1994), pp. 25-56.

[54] M. A. Fishman, and A. S. Perelson, *Th1/Th2 differentiation and cross-regulation*, Bulletin of Mathematical Biology, *61*(3) (1999), pp. 403-436.

[55] G. A. Funk, A. D. Barbour, H. Hengartner, and U. Kalinke, *Mathematical Model of a Virus-neutralizing Immunglobulin Response*, J. Theor. Biol., *195*(1) (1998), pp. 41-52.

[56] T. F. Gajewski, and F. W. Fitch, *Anti-proliferative effect of IFN-gamma in immune regulation. I. IFN-gamma inhibits the proliferation of Th2 but not Th1 murine helper T lymphocyte clones*, J. Immunol., *130* (1988), pp. 4225-4252.

[57] D. Gammack, C. R. Doering, and D. E. Kirschner, *Macrophage response to Mycobacterium tuberculosis infection*, J. Math. Biol., *48* (2004), pp. 218-242.

[58] R. N. Germain, and M. K. Jenkins, *In vivo antigen presentation*, Curr. Opin. Immunol., 16 (2004), pp. 120-125.

[59] A. V. Gett, and P. D. Hodgkin, *Cell division regulates the T cell cytokine repertoire, revealing a mechanism underlying immune class regulation*, Immunol., **95**(16) (1998), pp. 9488-9493.

[60] B. Gilbertson, J. Zhong, and C. Cheers, *Anergy, IFN-α production, and apoptosis in terminal infection of mice with Mycobacterium avium*, J. Immunol., *163* (1999), pp. 2073-2080.

[61] R. W. Glaser, *Antigen-Antibody Binding and Mass Transport by Convection and Diffusion to a Surface: A Two-Dimensional Computer Model of Binding and Dissociation Kinetics*, Analytical Biochemistry, *213*(1) (1993), pp. 152-161.

[62] S. Gordon, *Alternative activation of macrophages*, Nature Rev. Immunol., *3*(1) (2003), pp. 23-35.

[63] Z. Grossman, B. Min, M. Meier-Schellersheim, and E. W. Paul, *Concomitant regulation of T cell activation and homeostasis*, Nature Rev. Immunol., *4* (2004), pp. 387-395.

[64] J. C. Gury, F. Ria, F. Galbiati, S. Smiroldo, and L. Adorini, *The mode of protein antigen administration determines preferential presentation of peptide-class II complexes by lymph node dendritic or B cells*, Int. Immunol., *9*(1) (1997), pp. 9-15.

[65] A. T. Haase, *Population Biology Of Hiv-1 Infection: Viral and CD4+ T Cell Demographics and Dynamics in Lymphatic Tissues*, Annual Review of Immunology, *17* (1999), pp. 625-656.

[66] E. G. Hanania, A. Fieck, J. Stevens, L. J. Bodzin, B. Ø. Palsson, and M. R. Koller, *Automated in situ measurement of cell-specific antibody secretion and laser-mediated purification for rapid cloning of highly-secreting producers*, Biotechnology and Bioengineering, *91*(7) (2005), pp. 872-876.

[67] C. Haslett, *Granulocyte apoptosis and its role in the resolution and control of lung inflammation*, Am. J. Respir. Crit. Care. Med., *160*(5)pt2 (1999), pp. 5-11.

[68] B. O. Haglund, D. E. Wurster, L. O. Sundel, and S. M. Upadrashta, *Effect of SDS micelles on rhodamine-B diffusion in hydrogels*, J. Chem. Educ., *73* (1996), pp. 889-893.

[69] C. Haurie, C. D. Dale, and C. M. Mackey, *Cyclical neutropenia and other periodic hematological disorders: a review of mechanisms and mathematical models*, Blood, *92*(8) (1998), pp. 2629-2640.

[70] J. S. Hege, and G. Cole, *A mathematical model relating circulating antibody and antibody forming cells*, J. Immunol., *97* (1966), pp. 34-40.

[71] B. Hellriegel, *Modelling the immune response to malaria with ecological concepts: short-term behavior against long-term equilibrium*, Proc. R. Soc. Lond. B., *250* (1992), pp. 249-256.

[72] M. A. Herrero, M.A., E. Medina, and J. J. L. Velazquez, *Finite-time aggregation into a single point in a reaction-diffusion system*, Nonlinearity, *10* (1997), pp. 1739-1754.

[73] M. A. Herrero, and J. L. L. Velazquez, *A blow up mechanism for a chemotaxis model*, Ann. Scuola Normale Superiore, *24* (1997), pp. 633-683.

[74] G. A, Hoffman, *A theory of regulation and self-nonself discrimination in an immune network*, Eur. J. Immunol., *5* (1975), pp. 638-647.

[75] J. M. Hostetter, E. M. Steadham, J. S. Haynes, T. B. Bailey, and N. F. Cheville, *Cytokine effects on maturation of the phagosomes containing Mycobacteria avium subspecies paratuberculosis in J774 cells*, FEMS Immunol. Med. Microbiol., *34* (2002), pp. 127-134.

[76] J. M. Hostetter, E. M. Steadham, J. S. Haynes, T. B. Bailey, and N. F. Cheville, *Phagosomal maturation and intracellular survival of Mycobacterium avium subspecies paratuberculosis in J774 cells*, Comp. Immunol. Microbiol. Infect. Diseases, *26* (2003), pp. 269-283.

[77] J. M. Hostetter, E. Huffman, K. Byl, and E. Steadham, *Inducible nitric oxide synthase immunoreactivity in the granulomatous intestinal lesions of naturally occurring bovine Johne's disease*, Vet. Pathol., *42* (2005), pp. 241-249.

[78] C. A. Janeway, P. Travers, M. Walport, and M. J. Shlomchik, *Immunobiology : the immune system in health and disease*, Garland Science Publishing, New York, 2005.

[79] N. K. Jerne, *The immune system*, Scientific American, *229* (1973), pp. 52-60.

[80] N. Jerne, *Towards a network theory of the immune system*, Ann. Immunol., *125C*(1-2) (1974), pp. 373C389.

[81] W. Jager, and S. Luckhaus, *On Explosions of Solutions to a System of Partial Differential Equations Modeling Chemotaxis*, Trans. AMS, *329* (1992), pp. 819-824.

[82] H. Jiang, and L. Chess, *An integrated view of suppressor T cell subsets in immunoregulation*, J. Clin. Invest., *114*(9) (2004), pp. 1198-1208.

[83] Y. Jiang, A. H. Liu, and K. S. Zhao, *Studies on the flow and distribution of leukocytes in mesentery microcirculation of rats*, W. J. Gastroenterology, *5*(3) (1999), pp. 231-234.

[84] M. Jilek, and Z. Ursinova, *The probability of a contact between immunocompetent cell and antigen*, Folia Microbiol., *15* (1970), pp. 294-302.

[85] M. Jilek, and Z. Ursinova *On the distribution of the first contact of immunocompetent cell with antigen*, Folia Microbiol., *15* (1970), pp. 492-299.

[86] M. Jilek, *The number of immunologically activated cells after repeated immunization (a mathematical model)*, Folia Microbiol., *16* (1971), pp. 12-23.

[87] M. Jilek, *On contact of immunocompetent cells with antigen (Note on probability model)*, Folia Microbiol., *16* (1971), pp. 83-87.

[88] H. A. Johne, and J. Frothingham, *Ein eigenthuemlicher fall von tuberculosis beim rind*, Dtsch. Z. Tiermed. Pathol., *21* (1895), pp. 438-454.

[89] E. Y. Jones, L. Fugger, J. L. Strominger, and C. Siebold, *MHC class II proteins and disease: a structural perspective*, Nature Reviews Immunology, *6* (2006), pp. 271-282.

[90] D. E. Jones, W. Zhou, J. M. Hostetter, and B. Su, *A threshold/transition model of class II immunity using antigen load as the driving force predicts a delayed Th1 to Th2 switch during Mycobacterium avium subspecies paratuberculosis*, under preparation.

[91] P. Kalinski, and M. Moser, *Consensual immunity: success-driven development of T-helper-1 and T-helper-2 responses*, Nat. Rev. Immunol., *5*(3) (2005), pp. 251-260.

[92] A. T. Kamath, J. Pooley, M. A. OKeeffe, D. Vremec, Y. F. Zhan, A. M. Lew, A. DAmico, L. Wu, D. F. Tough, and K. Shortman, *The development, maturation, and turnover rate of mouse spleen dendritic cell populations*, J. Immunol., *165* (2000), pp. 6762-6770.

[93] A. V. Karpov, and A. A. Romanyukha, *Mathematical modelling of destructive pneumonia*, Immunological and Metabolic Systems Mathematical Models and Methods of Investigations, Eds. G. I. Marchuk, A. Werynski, Lecture Notes of the ICB Seminars, Biosystems, Warsaw: ICB, 1992, pp. 50-67.

[94] M. T. Kasaian, K. A. Leite-Morris, and C. A. Biron, *The role of CD4+ cells in sustaining lymphocyte proliferation during lymphocytic choriomeningitis virus infection*, J. Immunol., *146*(6) (1991), pp. 1955-1963.

[95] K. F. Keller, and L. A. Segel, *Intiation of slime mold aggregation viewed as an instability*, J. Theor. Biol., *26* (1970), pp. 399-415.

[96] C. Kemir, and R. J. De Boer, *A Mathematical Model on Germinal Center Kinetics and Termination*, J. Immunol., *163* (1999), pp. 2463-2469.

[97] O. Kim, D. Levy, and P. Lee, *Modeling Regulatory Mechanisms in the Immune System*, J. Theor. Biol., *246* (2007), pp. 33-69.

[98] B. Knoechel, J. Lohr, E. Kahn, J. A. Bluestone, and A. K. Abbas, *Sequential development of interleukin 2-dependent effector and regulatory T cells in response to endogenous systemic antigen*, J. Exp. Med., *202* (2005), pp. 1375-1386.

[99] A. Kurganov, and E. Tadmor, *New high-resolution central schemes for nonlinear conservation laws and convection-diffusion equations*, J. Comput. Phys. *160*, (2000), pp. 1461-1488.

[100] M. P. Kuehnel, R. Goethe, A. Habermann, E. Mueller, M. Rohde, G. Griffiths, and P. Valentin- Weigand, *Characterization of the intracellular survival of Mycobacterium avium ssp. paratuberculosis: phagosomal pH and fusogenicity in J774 macrophages compared with other mycobacteria*, Cell Microbiol., *3* (2001), pp. 551-566.

[101] A. Lanzavecchia, *Mechanisms of antigen uptake for presentation*, Curr. Opin. Immunol., *8*(3) (1996), pp. 348-354.

[102] R. E. Langman, and M. Cohn, *The E-T (elephant-tadpole) paradox necessitates the conept of a unit of B-cell function: the Protection*, Molecular Immunology, *24* (1987), pp. 675-697.

[103] A. Lanzavecchia and F. Sallusto, *Regulation of T cell immunity by dendritic cells*, Cell, *106* (2001), pp. 263-266.

[104] D. A. Lauffenburger, and J. J. Linderman, *Receptors: models for binding, trafficking, and signaling*, Oxford University Press, New York, 1993.

[105] B. van Leer, *Towards the Ultimate Conservative Difference Scheme: IV. A New Approach to Numerical Convection*, J. Comp. Phys., *23* (1977), pp. 276-299.

[106] M. S. Leffell, A. D. Donnenberg, and N. R. Rose, *Handbook of Human Immunology*, CRC Press, Boca Raton, 1997.

[107] Y. J. Liu, *Central schemes on overlapping cells*, J. Comput. Phys., *209* (2005), pp. 82-104.

[108] Y. J. Liu, P. E. Sacks, B. Su, and W. Zhou, *Parameter identification and numerical simulation of chemotaxis equations in Patlak-Keller-Segel Model*, under preparation.

[109] D. V. Lim, *Microbiology*, Kendall Hunt, 2003.

[110] Q. Liu, Z. Liu, C. T. Rozo, H. A. Hamed, F. Alem, J. F. Jr Urban, and W. C. Gause, *The role of B cells in the development of CD4 effector T cells during a polarized Th2 immune response*, J. Immunol., *179*(6) (2007), pp. 3821-3830.

[111] J. R. Lumb, *Lymphocyte differentiation, repertoire development and migration: The need for mathematical models*, Computers and Mathematics with Applications, *14* (1987), pp. 657-697.

[112] J. Ma, T. Chen, J. Mandelin, A. Ceponis, N. E. Miller, M. Hukkanen, G. F. Ma, and Y. T. Konttinen, *Regulation of macrophage activation*, Cell. Mol. Life Sci., *60* (2003), pp. 2334-2346.

[113] A. S. MacDonald, and R. M. Maizels, *Alarming dendritic cells for Th2 induction*, The Journal of Experimental Medicine, *205*(1) (2008), pp. 13-17.

[114] C. A. Macken, and A. S. Perelson, *A multistage model for the action of cytotoxis T lymphocytes in multicellular conjuates*, J. Immunol., *132* (1984), pp. 1614-1624.

[115] G. I. Marchuk, *Mathematical immune response models and their interpreation*, Proc. of the IFIP Working Conference on Modelling and Optimization of Complex Systems. Berlin a.o.: Springer-Verlag, 1979, pp. 114-129.

[116] G. I. Marchuk, R. V. Petrov, A. A. Romanyukha, and G. A. Bocharov, *Mathematical model of antiviral immune response. I. Data analysis, generalized picture construction and parameters evaluation for hepatitis B*, J. Theor. Biol., *151* (1991), pp. 1-40.

[117] G. I. Marchuk, *Mathematical modelling of immune responses in infectious diseases*, Kluewer Academic Publishers, 1997.

[118] F. O. Martinez, L. Helming, and S. Gordon, *Alternative Activation of Macrophages: An Immunologic Functional Perspective*, Annu. Rev. Immunol., *27* (2009), pp. 451-483.

[119] S. Marino, and D. E. Kirschner, *The human immune responses to Mycobacterium tuberculosis in lung and lymph node*, J. Theor. Biol., *227* (2004), pp. 463-486.

[120] S. Marino, D. Sud, H. Plessner, P. L. Lin, J. Chan, J. L. Flynn, and D. E. Kirschner, *Differences in reactivation of tuberculosis induced from anti-TNF treatments are based on bioavailability in granulomatous tissue*, PLoS Comput. Biol., *3*(10) (2007), pp. 1909-1924.

[121] A. Marrocco, *Numerical simulation of chemotactic bacteria aggregation via mixed finite elements*, M.2.A.N., *37* (2003), pp. 617-630.

[122] F. A. Marshall, and E. J. Pearce, *Uncoupling of induced protein processing from maturation in dendritic cells exposed to a highly antigenic preparation from a helminth parasite*, J. Immunol., *181*(11) (2008), pp. 7562-7570.

[123] D. W. Mason, and A. F. Williams, *The Kinetics of Antibody Binding to Membrane Antigens in Solution and at the Cell Surface*, Biochem. J., *187* (1980), pp. 1-20.

[124] L. C. Meagher, J. M. Cousin, J. R. Seckl, and C. Haslett, *Opposing effects of glucocorticoids on the rate of apoptosis in neutrophilic and eosinophilic granulocytes*, J. Immunol., *156*(11) (1996), pp. 4422-4428.

[125] T. R. Mempel, S. E. Henrickson, and U. H. von Andrian, *T-cell priming by dendritic cells in lymph nodes occurs in three distinct phases*, Nature, *427* (2004), pp. 154-159.

[126] T. R. Mempel, M. L. Scimone, J. R. Mora, and U. H. von Andrian, *In vivo imaging of leukocyte trafficing in blood vessels and tissues*, Curr. Opin. Immunol., *16* (2004), pp. 406-417.

[127] S. Merrill, *Mathematical model of humoral immune response*, Techn. Rep. of the Univ. of Iowa, 1976, 40 p.

[128] S. Merrill, *A mathematical model of B cell stimulation and humoral immune response*, Techn. Rep. of the Univ. of Iowa, 1976, 70 p.

[129] H. Mikkelsen, G. Jungersen, and S. S. Nielsen, *Association between milk antibody and interferon-gamma responses in cattle from Mycobacterium avium subsp. paratuberculosis infected herds*, Vet. Immunol. Immunopathol., *127* (2009), pp. 235-241.

[130] M. J. Miller, S. H. Wei, M. D. Cahalan, and I. Parker, *Autonomous T cell trafficking examined in vivo with intravital two-photon microscopy*, J. Immunol., *100*(5) (2003), pp. 2604-2609.

[131] D. M. Mosser, *The many faces of macrophage activation,* J. Leukocyte Biol., *73* (2003), pp. 209-212.

[132] R. R. Mohler, C. Bruni, and A. Gandolfi *A systems approach to immunology*, Proc. IEEE., *68* (1980), pp. 964-990.

[133] P. V. Moghe, R. D. Nelson, and R. T. Tranquillo, *Cytokine-stimulated chemotaxis of human neutrophils in a 3-D conjoined fibrin gel assay*, J. Immunol. Methods., *180* (1995), pp. 193-211.

[134] H. Mohri, A. S. Perelson, K. Tung, R. M. Ribeiro, B. Ramratnam, M. Markowitz, R. Kosst, A. Hurley, L. Weinberger, D. Cesar, M. K. Hellerstein, and D. D. Ho, *Increased turnover of T lymphocytes in HIV-1 infection and its reduction by antiretroviral therapy*, J. Exp. Med., *194*(09) (2001), pp. 1277-1287.

[135] T. R. Mosmann, and K. W. Moore, *The role of IL-10 in crossregulation of Th1 and Th2 responses*, Immunology Today, *12* (1991), pp. 49-53.

[136] T. R. Mosmann, *Properties and functions of interleukin-10*, Adv. Immunol., *56* (1994), pp. 1-26.

[137] M. Moser, and K. M. Murphy, *Dendritic cell regulation of TH1-TH2 development*, Nat. Immunol., *1*(3) (2000), pp.199-205.

[138] A. S. Mustafa, H. A. Amoudy, H. G. Wiker, A. T. Abal, P. Ravn, F. Oftung, and P. Andersen, *Comparison of Antigen-Specific T-Cell Responses of Tuberculosis Patients using Complex or Single Antigens of Mycobacterium tuberculosis*, Scand. J. Immunol., *48*(5) (1998), pp. 535-543.

[139] K. M. Murphy, W. Ouyang, J. D. Farrar, J. Yang, S. Ranganath, H. Asnagli, M. Afkarian, and T. L. Murphy, *Signaling and transcription in T helper development*, Annu. Rev. Immunol., *18* (2000), pp. 451-494.

[140] T. Nagai, *Blow-up of radially symmetric solutions to a chemotaxis system*, Adv. Math. Sci. Appl., *5* (1995), pp. 581-601.

[141] C. Nathan, *Neutrophils and immunity: challenges and opportunities*, Nat. Rev. Immunol., *6* (2006), pp. 173-182.

[142] H. Nessyahu, and E. Tadmor, *Nonoscillatory central differencing for hyperbolic conservation law*, J. Comput. Phys., *87* (1990), pp. 408-463.

[143] M. A. Nowak, and R. M. May, *Mathematical biology of HIV infection: antigenic variation. and diversity threshold*, Math. Biosci., *106* (1991), pp. 1-21.

[144] M. A. Nowak, S. Bonhoeffer, A. M. Hill, R. Boehme, H. C. Thomas, and H. McDade, *Viral dynamics in hepatitis B virus infection*, Proc. Natl. Acad. Sci. U.S.A., *93* (1996), pp. 4398-4402.

[145] M. A. Nowak, and R.M. May, *Virus Dynamics: Mathematical Principles of Immunology and Virology*, Oxford University Press, 2000.

[146] T. Okada, M. J. Miller, I. Parker, M. F. Krummel, M. Neighbors, S. B. Hartley, A. O'Garra, M. D. Cahalan, and J. G. Cyster, *Antigen-engaged B cells undergo chemotaxis toward the T zone and form motile conjugates with helper T cells*, PLoS Biology, *3*(6) (2005), pp. 1047-1061.

[147] M. Ostrowski, S. L. Mundo, N. B. Harris, R. G. Barletta, and O. J. Lopez, *B-cell epitopes in the immunodominant p34 antigen of mycobacterium avium ssp. paratuberculosis recognized by antibodies from infected cattle*, Scand. J. Immunol., *58* (2003), pp. 511-521.

[148] M. R. Owen, and J. A. Sherratt, *Pattern formation and spatiotemporal irregularity in a model for macrophage-tumor interactions*, J. Theor. Biol., *189* (1997), pp. 63-80.

[149] M. R. Owen, and J. A. Sherratt, *Mathematical modeling of macrophage dynamics in tumours*, Math. Models. Methods. Appl., *9* (1999), pp. 513-539.

[150] G. Pap, J. Fursz, J. Fennt, G. C. Kovcs, L. Nagy, and J. Hamar, *Self-regulation of neutrophils during phagocytosis is modified after severe tissue injury*, Int. J. Mol. Med., *17*(24) (2006), pp. 649-654.

[151] W. E. Paul, *Between two centuries: Specificity and regulation in immunology*, J. Immunol., *139*(1) (1987), pp. 1-6.

[152] R. J. H. Payne, M. A. Nowak, and B. S. Blumberg, *Analysis of a cellular model to account for the natural history of infection by Hepatitis B Virus and its role in the development of Primary Hepatocellular Carcinoma*, J. Theor. Biol., *159* (1992), pp. 215-240.

[153] A. S. Perelson, *The IgM-IgG switch looked at from a control theoretic viewpoint*, Proc. of the 8th IFIP Conference on Optimization Techniques, Heidelberg: Springer-Verlag, 1978, pp. 431-440.

[154] A. S. Perelson, M. Mirmirani, and G. Oster, *Optimal strategies in immunolgy. I. B cell differentiation and proliferation*, J. Math. Biol., *5* (1978), pp. 213-256.

[155] A. S. Perelson, *Towards a realistic model of the immune network*, Theoretical Immunology Part Two, SFI Studies in the Science of Complexity, Ed. Perelson A. S., Addison-Wesley, Redwood CA, 1988, Volume III, pp. 337-401.

[156] A. S. Perelson, *Modeling the interaction of the immune system with HIV*, Mathematical and statistical approaches to AIDS epidemiology (Lecture Notes In Biomathematics), Ed. C. Castillo-Chavez, Springer-Verlag, New York, 1989, pp. 350-370.

[157] A. S. Perelson, and G. Weisbuch, *Immunology for Physicists*, Review in Modern Physics, *69*(4) (1997), pp. 1219-1267.

[158] A. S. Perelson, and P. W. Nelson, *Mathematical analysis of HIV-1 dynamics in vivo*, SIAM Rev., *41* (1999), pp. 3-44.

[159] A. S. Perelson, *Modelling viral and immune system dynamics*, Nature Review, *2* (2002), pp. 28-36.

[160] L. Perez, J. C. Alvarez-Cermeno, C. Rodriguez, E. Roldán, and J. A. Brieva, *B cells capable of spontaneous IgG secretion in cerebrospinal fluid from patients with multiple sclerosis: dependency on local IL-6 production*, Clin. Exp. Immunol., *101*(3) (1995), pp. 449-452.

[161] C. Pfeiffer, J. Stein, S. Southwood, H. Ketelaar, A. Sette, and K. Bottomly, *Altered peptide ligand can control CD4 T lymphocyte differentiation in vivo*, J. Exp. Med., *181* (1995), pp. 1569-1574.

[162] F. Powrie, S. Menon, and R. L. Coffman, *Interleukin-4 and interleukin-10 synergize to inhibit cell-mediated immunity in vivo*, Eur. J. Immunol., *23* (1993), pp. 3043-3049.

[163] M. Pradenas, M. C. Jara, N. Hernandez, A. Zambrano, M. T. Collins, and J. Kruze, *Antibody recognition to secreted proteins of Mycobacterium avium subsp. paratuberculosis in sera from infected ruminants*, Vet. Microbiol., *138* (2009), pp. 378-383.

[164] H. Qi, J. L. Cannons, F. Klauschen, P. L. Schwartzberg, and R. N. Germain, *SAP-controlled TCB cell interactions underlie germinal centre formation*, Nature, *455* (2008), pp. 764-769.

[165] H. Qi, G. E. Jackson, A. Y. C. Huang, and R. N. Germain, *Extrafollicular activation of lymph node B cells by antigen-bearing dendritic cells*, Science, *312* (2006), pp. 1672-1676.

[166] M. Rabinovitch, *Professional and non-professional phagocytes: an introduction*, Trends in Cell Biology, *5* (1995), pp. 85-87.

[167] L. E. Racoosin, and A. J. Swanson, *M-CSF-induced macropinocytosis increases solute endocytosis but not receptor-mediated endocytosis in mouse macrophages*, J. Cell Sci., *102* (1992), pp. 867-880.

[168] P. Richter, *A network theory of the immune system*, Eur. J. Immunol., *5* (1975), pp. 350-354.

[169] B. A.-C. Rideout, S. T. Brown, W. C. Davis, J. M. Gay, R. A. Gianella, M. E. Hines II, W. D. Hueston, and L. J. Hutchinson, *Committee on diagnosis and control of Johne's disease*, National Academies Press, 2003.

[170] L. Rong, and A. S. Perelson, *Modeling latently infected cell activation: viral and latent reservoir persistence, and viral blips in HIV-infected patients on potent therapy* PLoS Comput. Biol., *5*(10) (2009), pp. 1-18.

[171] A. Rot, and U.H. von Andrian, *Chemokines in innate and adaptive host defense: basic chemokinese grammar for immune cells*, Annu. Rev. Immunol., *22* (2004), pp. 891-928.

[172] S. I. Rubinow, and J. L. Lebowitz, *A mathematical model of neutrophil production and control in normal man*, J. Math. Biol., *1*(3) (1975), pp. 187-225.

[173] F. Sallusto, M. Cella, C. Danieli, and A. Lanzavecchina, *Dendritic cells use macropinocytosis and the mannose receptor to concentrate macromolecules in the major histocompatibility complex class II compartment: downregulation by cytokines and bacterial products*, J. Exp. Med., *182* (1995), pp. 389-400.

[174] S. Sakaguchi, *Naturally Arising CD4+ Regulatory T Cells for Immunologic Self-Tolerance and Negative Control of Immune Responses* Annual Review of Immunology, *22* (2004), pp. 531-562.

[175] S. Sakaguchi, N. Sakaguchi, M. Asano, M. Itoh, and M. Toda, *Immunologic self- tolerance maintained by activated T cells expressing IL-2 receptor a-chains (CD25). Breakdown of a single mechanism of self-tolerance causes various autoimmune diseases*, J. Immunol., *155*(3) (1995), pp. 1151-1164.

[176] N. Saito, *Conservative upwind finite-element method for a simplified Keller-Segel system modelling chemotaxis*, IMA J. Numer. Anal., *27* (2007), pp. 332-365.

[177] A. Scherer, M. Salathé, and S. Bonhoeffer, *High Epitope Expression Levels Increase Competition between T Cells*, PLoS Computational Biology, *2*(8) (2006), pp. 948-958.

[178] H. Scott, J. Chan, and J. Flynn, *Chemokines and tuberculosis*, Cytokine. Growth. Factor. Rev., *14* (2003), pp. 467-477.

[179] L. A. Segel, and A. S. Perelson, *Exploiting the diversity of time scales in the immune system: A B-cell antibody model*, Journal of Statistical Physics, *63* (1991), pp. 1113-1131.

[180] N. C. Serhan, D. S. Brain, D. C. Buckley, W. D. Gilroy, C. Haslett, A. J. L. O'Neill, M. Perretti, G. A. Rossi, and L. J. Wallace, *Resolution of inflammation: state of the art, definitions and terms*, FASEB J., *21* (2007), pp. 325-332.

[181] C. W. Shu, *Essentially non-oscillatory and weighted essentially non-oscillatory schemes for hyperbolic conservation laws*, In Advanced Numerical Approximation of Nonlinear Hyperbolic Equations, Eds. B. Cockburn, C. Johnson, C. W. Shu and E. Tadmor, Lecture Notes in Mathematics, Berlin, Springer, 1998.

[182] D. J. Smith, S. Forrest, D. H. Ackley, and A. S. Perelson, *Variable efficacy of repeated annual influenza vaccination*, Proc. Natl. Acad. Sci. U.S.A., *96* (1999), pp. 14001-14006.

[183] L. Sompayrac, *How the Immune System Works*, Blackwell Publishing, 2002

[184] S. Sozzani, W. Luini, M. Molino, P. Jlek, B. Bottazzi, C. Cerletti, K. Matsushima, and A. Mantovani, *The signal transduction pathway involved in the migration induced by a monocyte chemotactic cytokine*, J. Immunol., *147* (1991), pp. 2215-2221.

[185] J. Sprent, *Lifespans of naïve, memory and effector lymphocytes.*, Curr. Opin. Immunol., *5* (1993), pp. 433-438.

[186] D. Sredni-Kenigsbuch, T. Kambayashi, and G. Strassmann, *Neutrophils augment the release of TNF-α from LPS-stimulated macrophages via hydrogen peroxide*, Immunol. Lett., *71*(2) (2000), pp. 97-102.

[187] J. R. Stabel, *Transitions in immune responses to Mycobacterium paratuberculosis*, Vet. Microbiol., *77* (2000), pp. 465-473.

[188] C. C. Stempin, and F. M. Cerban, *Macrophages and arginase induction as a mechanism for parasite escape*, Medicina (B Aires), *67*(6) (2007), pp. 737-746.

[189] N. E. Street, and T. R. Mosmann, *Functional diversity of T lymphocytes due to secretion of different cytokine patterns*, FASEB. J., *5* (1991), pp. 171-177.

[190] B. Su, W. Zhou, K. Dorman, and D. E. Jones, *Mathematical modeling of immune responses in tissues*, Comput. Math. Methods Med., *10*(1) (2009), pp. 9-38.

[191] B. Su, *Homogenization in the diffusion of IP3 from cell membrane to rndoplasmic reticulum*, preprint.

[192] S. Suvas, and T. B. Rouse, *Treg control of antimicrobial T cell responses*, Curr. Opin. Immunol., *18* (2006), pp. 344-348.

[193] L. Tartar, *Nonhomogeneous media and vibration theory*, Ed. E. Sanchez-Palencia, Springer-Verlag, Berlin, 1980, Appendix

[194] R. T. Tranquillo, and D. A. Lauffenburger, *Definition and measurement of cell migration coefficients* in *Biological Motion (Lecture Notes in Biomathematics 89)*, Eds. W. Alt and G. Hoffmann, Springer-Verlag, New York, 1990, pp. 475-486.

[195] J. C. E. Underwood, *General and Systematic Pathology*, Churchill Livingstone, 2000.

[196] H. von Boehmer, *Mechanisms of suppression by suppressor T cells*, Nature. Immunol., *6* (2005), pp. 338-344.

[197] Y. Vanloubbeeck, J. Hostetter, and D. E. Jones, *The biology of dendritic cells and their potential use in veterinary medicine*, Anim. Hea. Res. Rev., *4* (2003), pp. 131-142.

[198] U. H. von Andrian, and T. R. Mempel, *Homing and cellular traffic in lymph nodes*, Nat. Rev. Immunol., *3* (2003), pp. 867-878.

[199] P. Waltman, and E. Butz *A threshold model of antigen-antibody dynamics*, J. Theor. Biol., *65* (1977), pp. 499-512.

[200] D. J. Weiss, and C. D. Souza, *Review paper: modulation of mononuclear phagocyte function by Mycobacterium avium subsp. paratuberculosis*, Vet. Pathol., *45* (2008), pp. 829-841.

[201] J. E. Wigginton, and D. E. Kirschner, *A model to predict cell-mediated immune regulatory mechanisms during human infection with mycobacterium tuberculosis*, J. Immunol., *166* (2001), pp. 1951-1967.

[202] A. M. Williams, M. C. Cave, G. Quaid, and S. J. Solomkin, *Chemokine regulation of neutrophil function in surgical inflammation*, Archives of Surgery, *134*(12) (1999), pp. 1360-1366.

[203] M. Zanetti, *T for two: When helpers need help*, Autoimmunity Reviews, *4*(8) (2005), pp. 571-578.

[204] R. M. Zinkernagel, *Immunity to viruses, Fundamental immunology*, Third Edition, Ed. W. Paul, Raven Press, New York, 1993, pp. 1211-1250.

[205] R. M. Zinkernagel, *Localization dose and time of antigens determine immune reactivity*, Seminars in Immunology, *12* (2000), pp. 163-171.

[206] R. M. Zinkernagel, and H. Hengartner, *Regulation of the immune respones by antigen*, Science, *293* (2001), pp. 251-253.

[207] W. Zhou, D. E. Jones, and B. Su, *Modeling of MHC class II mediated immune responses in tissues*, under preparation.

[208] J. Zhu, and W. E. Paul, *CD4 T cells: fates, functions, and faults*, Blood, *112*(5) (2008), pp. 1557-1569.

ACKNOWLEDGEMENTS

It is my pleasure to take this opportunity to express my thanks to those who made this thesis possible.

First and foremost, I would like to express my gratitude to my advisor Professor Bo Su. His guidance, patience and support throughout my stay at ISU made this work possible. His insights and helpful discussions often inspired me and renewed my hopes for completing my graduate education. I would like to thank my co-advisor, Professor Sacks, for his long time supports, helps and generous guidance.

I also would like to appreciate Professor Douglas Jones, without whom the whole work can not even be done. His generous supports and patient guidance encourage me a lot, and most of my knowledge on immunobiology are directly from him. Discussion with him inspires me for the whole work and my life. It is difficult to overstate my gratitude to him. I would appreciate him with all my best.

I would also like to thank my committee members for their efforts and contributions to this work: Professor Lisheng Hou and Professor Gary Lieberman. I also would like to express my gratitude to Professor Yingjie Liu from Georgia Institute of Technology for his generous supports and advices for a long time.

I also want to thank my family for their support. Though my parents were far from me during my graduate education at ISU, their support and love were always with me. I would also like to thank my wife and daughter for their love.

Last but not least, I want to thank all the colleagues, friends and staffs here in Mathematics Department of Iowa State University.